Safety Investigation of Partially Filled Railway Tank Cars

Iman Hazrati Ashtiani

A Thesis

in

The Department

of

Mechanical, Industrial and Aerospace Engineering

Presented in Partial Fulfillment of the Requirements

For the Degree of

Doctor of Philosophy (Mechanical Engineering) at

Concordia University

Montreal, Quebec, Canada

May 2018

CONCORDIA UNIVERSITY
SCHOOL OF GRADUATE STUDIES

This is to certify that the thesis prepared

By: **Iman Hazrati Ashtiani**

Entitled: **Safety Investigation of Partially Filled Railway Tank Cars**

and submitted in partial fulfillment of the requirements for the degree of

Doctor of Philosophy (Mechanical Engineering)

complies with the regulations of the University and meets the accepted standards with respect to originality and quality.

Signed by the final examining committee:

Chair
Dr. Tiberiu Popa

External Examiner
Dr. Moustafa El-Gindy

External to Program
Dr. Khaled E. Galal

Examiner
Dr. Youmin Zhang

Examiner
Dr. Ashok Kaushal

Thesis Supervisor
Dr. Subhash Rakheja

Thesis Supervisor
Dr. A.K.W. Ahmed

Approved by
Dr. Ali Dolatabadi Chair of Department or Graduate Program Director

June 22, 2018
Date of Defense

Dr. Amir Asif Dean, Faculty of Engineering and Computer Science

ABSTRACT

Safety investigation of partially filled railway tank cars

Iman Hazrati Ashtiani, Ph.D.

Concordia University, 2018

The adverse effects of liquid cargo slosh on dynamic responses and safety performance of partially filled road vehicles are well known. The general-purpose railway tank car may also encounter partial fill conditions due to variations in density of the liquid cargo and track load limit. The additional slosh forces and moments from the partially filled state of the tank may further affect the wheel-rail forces, dynamic response, and safety of the rail vehicles. The coupled sloshing cargo and vehicle system dynamics have been investigated in only a few studies because of complexity and high computation demand. The objective of this study is to investigate the influence of liquid cargo sloshing on the dynamic performance of railway tank cars. Other than detail modelling, the topics of lateral dynamics, curving performance and switch passing responses of partially filled railway tank cars through a co-simulation approach have been addressed in this dissertation.

The nonlinear damping characteristics of friction wedges in the secondary suspension of a freight wagon are investigated considering non-smooth unilateral contact, multi-axis motions, slip-stick conditions, and geometry of the wedges. The parameters of the contact pairs within the suspension were identified to achieve smooth and efficient numerical solutions while ensuring adequate accuracy. The friction wedge model was integrated into the multibody dynamic model of a three-piece bogie to study the effects of wedge properties on hunting characteristics. The resulting 114-degrees-of-freedom wagon model incorporated constraints due to side bearings, axle boxes, and the centre plates, while the wheel-rail contact forces were obtained using the *FastSim* algorithm. The simulation results were obtained to study hunting characteristics of the wagon in terms of critical speed and the predominant oscillation frequency. The study also examined the effects of wedge friction and geometry on lateral stability characteristics of the freight car. The results showed subcritical *Hopf* bifurcation of dynamic responses of the wagon. The parametric

study showed an increase in the wedge angle, friction coefficient, and springs free length to yield higher critical speed. The validated dynamic model of the wagon is further used to investigate the effects of liquid sloshing on hunting speed of partly filled tank car. An analytical liquid slosh model is used to capture dynamic response of the liquid cargo in a horizontal cylindrical tank using up to five fundamental modes in the roll plane under lateral as well as yaw motions of the tank car. The liquid slosh model is co-simulated with the comprehensive nonlinear model of a railway tank car to evaluate the lateral dynamic response of the tank car. The results suggest that fill levels and the corresponding slosh forces can adversely affect the lateral stability performance and yield lower critical hunting speed of railway tank car.

The influence of liquid cargo sloshing on the dynamic performance of railway tanker in a typical curve negotiation is further examined using the proposed coupled co-simulation model. The performance measures include car roll angle, unloading of the wheelset and derailment quotient. The results clearly demonstrate that partial state of the tank car and resulting slosh could lead to a significantly larger dynamic response of the system and may result in separation of wheel and rail contact at lower forward speed in comparison to the rigid cargo assumption. Dynamic simulations of partially filled railway tank cars without fluid slosh consideration will thus lead to underestimation of overturning critical conditions on the curving manoeuvres. Above performance measures in a switch-passing manoeuvre is finally examined for different fill ratios and switch geometries. The results obtained for the coupled vehicle and liquid slosh model clearly showed strong interactions between the switch-induced transient liquid slosh and vehicle dynamics for the partial-fill ratio of 60% and less. The effect of fluid slosh on the car body roll angle and wheelset unloading ratio was observed to diminish with fill ratio above 90%. Neglecting the contributions due to dynamic slosh force and roll moment may lead to overestimation of the critical speed in switch-passing manoeuvres if the car is partially filled.

ACKNOWLEDGEMENTS

I wish to express my sincere appreciation to my thesis supervisors, Dr. Subhash Rakheja and Dr. A.K. Waizuddin Ahmed, for their great support and continued guidance and efforts through the thesis work. It was not possible to survive this undertaking without the discussions and valuable comments I had with them. I appreciate their time and consideration for reviewing my works several times. They were always supportive and gave me the opportunity to try.

I would also acknowledge Canadian National Railway for their financial support provided in the form of Railway Dynamics Fellowship and Concordia University for International Tuition Fee Remission and Accelerator Awards. Moreover, I should appreciate the Canadian Transportation Research Forum (CTRF) for granting me one of their prestigious Scholarships for Graduate Study in Transportation in 2018.

I would like to express appreciation to Dr. Amir Kolaei, who immensely helped me with developing the liquid slosh code and improving the method. His time and support are highly appreciated.

I would like to express my special thanks to my family. My parents for their love and encouragements, for teaching my siblings and me what to avoid but permitting us to pursue our way of life. I wish I could be a better son!

Finally, I want to acknowledge Mehrnoosh Abedi, my true friend and the wonderful wife. In past ten years of our companionship, she made immense sacrifices and managed unbearable situations.

Dear Merhnoosh, you are my champion and your smile is my joy of life!

This dissertation is dedicated to

Mehrnoosh

My lifetime friend, supporter and love.

Contents

LIST OF FIGURES

LIST OF TABLES

NOMENCLATURE

SYMBOL	DESCRIPTION
α_w	Friction wedge angle
k^w	Springs of wedge
k^b	Springs of the bolster
μ_s	Friction coefficients between wedge-side frame
μ_b	Friction coefficients between wedge-bolster
γ_w	Toe condition of side frame
G	Modulus of rigidity
v	Poisson's ratio
μ	Friction coefficient on the flange
μ_t	Friction coefficient in tread region
Y/Q	Nadal derailment coefficient
Y	Transverse wheel-rail force
Q	Vertical wheel-rail force
F_n	Normal force of wheel
F_T	Tangential friction work
k_{xx}	Effective stiffness in longitudinal (x)
k_{yy}	Effective stiffness in longitudinal (y)
k_{zz}	Effective stiffness in longitudinal (z)
k_θ	Bending stiffness of the springs corresponding to angular deformations about x
k_β	Bending stiffness of the springs corresponding to angular deformations about y
k_ψ	Bending stiffness of the springs corresponding to angular deformations about z
Δ	Penetration of contact point
K_c	Contact stiffness
C_c	Damping coefficient of contact point in point-plan model
$\overrightarrow{F_s}$	Friction Force in point-plane contact model
μ_0	Static friction coefficient
μ_s	Dynamic friction coefficient
$\vec{v}_s$	Sliding velocity vector

v_{str}	Stribeck velocity
μ_∞	Friction Coefficient at high sliding velocity
δ	Empirical exponent of transition in friction coefficient
$\dot{y}_w$	Lateral displacement of leading wheelset *c.g.*
$\dot{y}_w$	Lateral velocity of leading wheelset at *c.g.*
O	Geometric center of Tank
$z_{c.g.}$	Vertical coordinate of the liquid cargo mass center for a given fill ratio
g	Acceleration of gravity
R	Cylindrical tank radius
H	Liquid fill height
Oyz	Tank-fixed coordinate system
y_0	Coordinates of the free-surface at the intersection of the tank wall
z_0	Coordinates of the free-surface at the intersection of the tank wall
τ	Fluid domain
S_f	Liquid free surface
S_w	Wetted surface of the tank wall
Φ	Potential function
Φ_R	Velocity potential of rigid body motion of liquid
Φ_S	Velocity potential of relative motion of liquid
$\dot{Y}(t)$	Lateral velocity of the container
$\dot{Z}(t)$	Vertical velocity of the container
$\theta(t)$	Roll angle of the container
Φ_{st}	Stokes-Joukowski potential
φ_i	Natural mode liquid movements
γ_i	Generalized coordinates
σ_i	Circular frequency of free surface oscillations
λ_i	Time-invariable hydrodynamic coefficient
ξ_i	Time-invariable damping coefficient
ν_s	Liquid cargo kinematic viscosity
ρ	Fluid density

m	Fluid mass per unit length
L	Length of the tank
$\bar{\psi}_i$	Normalized damping ratio of liquid cargo
$P(y,z,t)$	Hydrodynamic pressure distribution
$F_z(t)$	The vertical force of liquid cargo acting on the container
Ω_i	Normalized Frequency

ACRONYM	**DESCRIPTION**
UM	Universal Mechanism
FRA	Federal Railway Association
TC	Transportation Canada
DOT	Department of Transportation
DoF	Degree of Freedom
FE	Finite Element
CFD	Computational Fluid Dynamic
VoF	Volume of Fluid
ANCF	Absolute nodal coordinate formulation
FFT	Fast Fourier Transform
PSD	Power Spectral Density
AoA	Angle of attack
UIC	Union Internationale des Chemins de fer (International Union of Railway)
c.g.	Center of gravity
MBD	Multibody dynamics
MBS	Multibody system
EN	European Norms
AAR	Association of American Railroad
ECP	Electronically Controlled Pneumatic

CHAPTER 1

Literature review and scopes of the dissertation

1.1 Introduction

Directional stability and dynamics of railway wagons have been extensively investigated over the past many decades. These have particularly focused on lateral and longitudinal dynamics that are known to relate to derailment risks. Among the reported 1067 rail accidents in Canada in 2013, 70% involved freight trains. Moreover, 58% of the reported accidents resulted in derailments, although 48% of these were non-main-track derailments (such as those in the yards) occurring at low speeds [1]. Main-track derailments could be catastrophic, particularly, when dangerous goods are involved considering the associated risks to public safety, property in commerce and the environment. In North America, railway tank cars are the primary movers of hazardous materials, including petrochemicals, accounting for nearly 20% of the total US fleet (281,923 tank cars) [2].

The curving stability and derailment potential of a railway freight car are strongly influenced by a number of design and operational factors such as the axle loads, bogie and coupling designs, track geometry and the travelling speed. For tank cars, liquid free surface movement and thus the cargo load shift and associated interactions with the car constitute an additional important factor leading to higher derailment potential, when the tank car is partially-filled [3]. Railway tank cars, similar to road tankers, in many situations, are known to transport liquid cargos in the partial-fill state due to variations in density of the liquid cargo and the regulatory load limits. The liquid cargo movement in a tank car during curve negotiation and/or barking maneuvers can lead to more crucial lateral/longitudinal and rotational motions of the container, which may adversely affect the wheel-rail contact forces leading to reduced curving instability and higher derailment potentials [*e.g.*, 4, 5].

Transverse baffles are widely used in highway tanks to limit the liquid cargo free surface motion, also denoted as fluid slosh, and thus the cargo shift in the longitudinal plane so as to preserve the braking performance of the vehicle. Such baffles, however, offer only minimal resistance to cargo slosh in the roll plane caused by a steering maneuver [6]. The use of baffles in railway tank cars, however, is extremely limited since these tend to increase tare weight of the car and interfere with cleaning, drain and inspection. A partial fill condition in a tank, however, yields relatively lower centre of gravity (*c.g.*) height compared to a completely filled tank, which may be

expected to be beneficial in the context of the curving stability in the absence of load shift due to cargo slosh. For highway tankers, however, it has been shown a lower fill volume yields higher load shift and magnitudes of slosh forces, which affects the roll stability of the vehicle in a highly adverse manner [7, 8].

While the handling, cornering and jack-knifing potential of partially-filled road tankers have been widely investigated, the effect of cargo movement on the dynamics of railway tank cars has been addressed in only a few studies [3]. The load shift across the wheelsets and the bogies of a railway wagon could lead to excessive roll and/or loss of contact between the rail and the wheel, reduced curving performance and lower critical speeds, which have not yet been investigated in the presence of fluid slosh. Lateral dynamics (hunting oscillations) of a freight car on a tangent track is also a critical performance measure that limits the operating speed. An in-depth study on the influence of fluid slosh on the hunting stability would thus also be of significant interest as none has been reported to date.

This dissertation research focuses on analyses of effects liquid cargo slosh in the roll plane on the hunting, curving and switch-passing response characteristics of a partially-filled tank car. Owing to the important effects of secondary suspensions and various friction pairs on dynamics of the car, a comprehensive multi-body dynamic model of the vehicle model was formulated considering multi-dimensional suspension properties and nonlinear subsystem models. An analytical fluid slosh model was formulated using the mode summation approach to evaluate the lateral slosh force and roll moment due to lateral acceleration, and roll and yaw motions of the car body. The model, owing to its superior computational efficiency, was integrated to the multibody dynamic vehicle model via co-simulations in order to investigate the interactions of the moving cargo with the wagon. The effects of forces and moments arising from the free surface movements are investigated on the hunting and curving performance, and wagon's responses during a switch-passing maneuver. The simulation results are obtained for different fill volumes of the tank, and results are further analyzed in terms of measures like critical hunting speed, unloading ratio, different derailment quotient, car body roll angle and lateral wheelset loads.

1.2 Literature review

Safety dynamic analyses of a partly filled tank car encompasses various challenges involving modelling the railway tank car with inherent nonlinearities of various subsystems, modelling of dynamic wheel-rail interactions, modelling for liquid cargo dynamics, simulation methodologies for hunting and curving responses, and more. The reported relevant studies are reviewed and discussed in a systematic manner so as to build essential knowledge on the challenges and methods of analysis. The reported studies grouped under relevant subjects are briefly discussed below in order to develop the scope of the investigation.

1.2.1 Dynamics of railway tank cars

With growing demands for high load capacity and higher speeds for railway freight cars, the stability of railway vehicles has been widely investigated to establish safe operating limits and to seek improved designs [9, 10]. The hunting properties of railway cars, in particular, have been extensively studied using widely different methods [11, 12]. These have reported the critical hunting speeds as the lowest running speed at which a constant amplitude limit cycle motion of a wheelset occurs. Standardized guidelines have also been developed for assessing the lateral stability limits of railway vehicles [13-15]. Early studies employing linear or linearized wheel/rail contact and suspension component models, invariably, revealed zero lateral mode damping, when a critical speed was reached [9, 10]. The kinematic and constitutive relations for the wheel-rail contact as well as the truck and suspension components, however, are strongly nonlinear. A number of studies have conducted nonlinear hunting analyses by defining quasi-linear component characteristics using the describing functions for the nonlinear subsystems [12, 16]. In the quasi-linear approach, the motion of the system is approximated by a harmonic function at a particular frequency. Further studies, however, have shown weak correlations between the measured critical speeds and those obtained from the quasi-linear analyses [17].

Huilgol [18] was the first to show the presence of *Hopf* bifurcation in the responses of a wheelset model with nonlinear wheel/rail contact forces. Subsequently, some studies investigated bifurcations in the lateral responses of different rail truck models, incorporating nonlinear creep-creep force relationship and wheel/rail contact geometry [11]. These have concluded that the subcritical *Hopf* bifurcation is common in railway vehicles' responses [19], and thus raised significant concerns about the validity of the concept of critical speed derived from the linear

theories. The nonlinear stability of the freight cars has also been reported using the continuation-based bifurcation analysis [20]. Yang and Chen [21] also studied the *Hopf* bifurcation in a railway truck with suspension nonlinearities and concluded that the suspension hysteresis can lead to supercritical bifurcations. The study also reported the influence of system parameters on the amplitude of the limit cycle motion. Wickens [22] conducted nonlinear stability analyses of four different bogie configurations and illustrated important effects of wheel-rail contact friction coefficient and traction ratio. It was shown that the stability of a passive bogie is generally very robust under varying traction and braking conditions as well as with variations in the friction coefficient. In case of an actively controlled bogie with rigid wheelsets, it was shown that the creep saturation could reduce the stability limit significantly. Through analyses of both the linear and non-linear wheel/rail creep and geometry models, Polach [12, 20] showed that the linearized analysis coupled with the tuning of the suspension damping and contact parameters could lead to lower critical speeds compared to the those predicted from the non-linear models.

An accurate estimation of the critical speed is vital for the complex railway system such as a three-piece railway bogie, since it provides essential information leading to designs of components and wheel/rail profiles. Accurate predictions of the critical speeds and dynamic responses, however, necessitate in-depth nonlinear component modelling and analysis. The vast majority of the reported nonlinear analyses utilize simplified representations of the friction damping in the secondary suspension [*e.g.*, 23, 24]. The friction wedges in the secondary suspension of a three-piece truck exhibit strongly nonlinear damping property, which is attributed to complex variations in the contact forces, contacting surfaces geometry and the friction coefficient [25]. Moreover, the friction wedge design yields variable multi-directional and highly nonlinear damping properties of the secondary suspension, which could enhance the performance limits over a wide range of loading conditions. The reported studies, however, generally represent the friction wedges by simplified kinematic constraints and equivalent linear vertical/lateral damping [23], which may not represent the secondary suspension components accurately over the probable ranges of loading and operating conditions.

Accurate analyses of hunting and curving performance characteristics of a railway car necessitate comprehensive modelling of the subsystems such as the bogie, primary and secondary suspension, wheel-rail contact geometry, and normal and creep contact forces. These invariably exhibit strong nonlinear properties. Widely different component models with varying complexities

have been reported. Furthermore, the reported studies have employed widely different analyses methodologies and performance measures for assessing the lateral/yaw dynamic responses. The reported component models, analyses methods and performance measures are discussed in the following sub-sections.

1.2.2 Modeling of the railway wagon

The heavy-haul freight cars used in North America, Australia and Russia generally employ three-piece bogies. The structure of a three-piece bogie comprises a bolster interfaced with two side frames with spring nests and wedges, which provide nonlinear friction damping for the suspension. Such highly nonlinear frictional suspensions are common in freight railway cars due to their low maintenance and production costs. The modelling of strongly nonlinear and multi-dimensional properties of the suspension, however, continues to be most challenging. Damping in this bogie design is due to dry friction in multiple interfaces formed by the wedges, center plate, side bearings and the adapters. Although the general concept of the bogie design has not changed over the past many decades, different generations of this bogie have included modifications in the springs as well as side bearings and wedges to achieve more safe and efficient operations [26, 27].

The highly complex designs of friction wedges provide variable multi-directional damping in the secondary suspension to enhance performance limits of the vehicle over a wide range of loading condition. Different combination of wedges and the suspension systems employed in three-piece bogies can be classified as variable and constant frictional damping on the bases of the design, as shown in Figure 1.1 [28]. In the variable damping design, the resultant normal forces in the contacting faces of wedges can be expressed as functions of relative deflections of the wedge and bolster springs (k^w and k^b,respectively) in addition to the wedge angle, α_w. On the other hand, in the constant damping design presented in Figure 1.1(b), the preloaded wedge spring generates constant normal forces in wedge-side frame and wedge-bolster contact faces. The resulting friction forces are further related to friction coefficients between wedge and side frame, μ_s, and wedge and bolster, μ_b faces. Toe condition of the side frame, γ_w, shown in Figure 1.1(a), is another design parameter that can be divided into no-toe (γ_w=0), toe-out (γ_w>0) and toe-in (γ_w<0) designs. The toe angle is a significant parameter since it affects not only relative movements of the components but also the forces developed within the wedge suspensions [28].

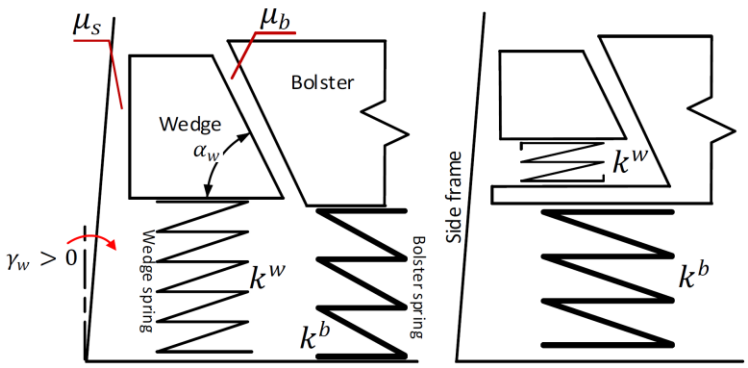

Figure 1.1: Different configurations of the wedges employed in three piece-bogies: (a) variable damping and (b) constant damping [28].

The friction wedges in the secondary suspension of a three-piece bogie exhibit strongly nonlinear damping property, which is attributed to complex variations in the contact forces, contacting surfaces geometry and the friction coefficient [29, 30]. Moreover, the friction wedge design yields variable multi-directional damping of the secondary suspension, which is considered vital for enhancing performance limits of the wagon, including vertical acceleration, hunting and curving stability, over a wide range of loading conditions.

An extensive review of different approaches considered for modelling of frictional wedges of three-piece bogies has been presented by Wu *et al.* [23]. The reported mathematical models of a friction wedge suspension can be classified into three types: Combination models [*e.g.*, 29, 30], quasi-static models [*e.g.*, 31, 32] and multi-body system (*MBS*) models [33, 34]. The combination models represent the directional properties of wedges by a combination of the stiffness and damping elements. While this modelling approach is quite simple and computationally efficient, it cannot be applied for parametric analysis of the wedge suspension design, especially the geometric parameters [23]. Moreover, such models do not consider the potential loss of contact between the contacting surfaces. Quasi-static models have been reported for quasi-static or dynamic analysis of the wedge system considering the geometry of the wedge in addition to wedge-bolster separation. The *MBS* modelling approach, on another hand, considers the complex geometry and distributing contact to describe the dynamic phenomena more accurately that the combination or quasi-static models are not able to represent. Simulation of curved surfaces of wedge or warp stiffness of the bogie are some of these conditions. Moreover, implementations of the penetration contact and friction contact models are only possible in the *MBS* models. Xia [31] considered the effects of

wedge mass and described the system damping by a two-dimensional dry friction model. The numerical analyses challenge associated with discontinuity of the state inherent in the dry friction model has been addressed via smoothing different functions for numerical techniques, which has been treated by a smoothing [28, 34, 35]. In *MBS* wedge model, the coordinates of the different corner points of the wedge define the contact domains of wedge with side frame and bolster. The contact forces are thus obtained using a point-plane model when the instantaneous positions of the corner points approach interference. Despite this, Wu *et al.* [23] stated that *MBS* wedge models are not yet suitable for stability analysis in the train system due to their complexity and high computational demand. Tune adjustment of contact models could avoid the extreme interpenetration of contacting components while it is not needed to define small integration time steps and error tolerance. The resulting normal forces are thus obtained as a function of the penetration depth and its time derivative. The method also accounts for the possible separations of the wedges from the bolster/side frame under extreme unloading. Jamming and warping in addition to stick and slip conditions of the relative movement of the wedge with respect to side frame and bolster are also possible in *MBS* method.

1.2.3 Wheel-rail contact forces

The wheel-rail contact forces directly influence the curving and hunting performance and derailment potential of a railway wagon. The forces developed at the contact interface are related to the wheel-rail contact geometry. The determination of the contact region and geometry is known to be quite challenging considering the complex geometry of the wheel and the rail. A number of algorithms have been developed to determine the instantaneous contact region of the wheel rolling on the rail. The reported studies focus on both the contact geometry and contact locations of the wheel with the rail, which are generally obtained using two methods: (i) solutions of kinematic algebraic equations describing the wheel and rail profiles [36]; and (ii) the nodal search method [37]. In the algebraic approach, functions describing the wheel and rail geometries are used to identify the coordinates of the contact points using the minimum distance between the two continuous functions. In the nodal approach, the wheel and rail profiles are parameterized by discrete nodal points and the minimum distances between the nodes on the wheel and rail profiles are used to determine the contact points. The nodal method is considered meritorious compared to the algebraic approach since it can be applied to non-smooth surfaces [9].

Both the methods generally assume constant rail and wheel profiles along the track to generate a lookup table of coordinates, which is subsequently applied to identify coordinates of the contact points [9, 36, 38]. The lookup table is generally formulated for a defined span covering a range of wheel/rail motions. It would thus be possible to encounter contact scenarios that are not accurately described by the lookup table [37]. In dynamic analyses, pre-generated lookup table is used to estimate coordinates of the contact locations through interpolations of instantaneous wheel responses (vertical and lateral displacements, and roll and yaw rotations) and the outputs (contact point coordinates). This method, referred to as "off-line" method, may lead to inaccuracies in predicted locations of the contact points, particularly under severe contact scenarios [9, 37]. Alternatively, the coordinates of contact points are computed by locating the nearest points between the two profiles at every instant during the dynamic simulations [39]. A hybrid method, employing the lookup table for the tread contact and the direct method for the flange contact has also been proposed to enhance the computational efficiency [40, 41].

The aforementioned studies reporting methodologies for mapping of the wheel-rail contact surfaces have been derived for rigid wheel and rail surfaces assuming negligible deformations of the wheel and the rail. The normal contact problem of elastic wheel and rail was addressed on the basis of the Hertz contact theory by Carter [42], assuming continuous and frictionless contact surfaces, small deformations of the contacting bodies, and diminishing contact stress in regions away from the primary contact area (half-space assumption). Although the Hertz's contact theory has been widely accepted for analysis of wheel-rail contact problem, a few studies have suggested several limitations of the theory, particularly in cases involving flange contact, contact with rails with short pitch irregularities and plastic rail or wheel deformations under excessive loads [40, 43].

Apart from the normal forces, the wheel-rail contact yields substantial creep forces that directly affect the longitudinal and curving dynamics of the vehicle. Carter [42] presented analytical formulations for deriving forces developed in a two-dimensional rolling cylinder contact with a thick plate. Applications of these solutions to the wheel-rail contact have shown notable differences in the circumferential and longitudinal velocities of the driven wheels, which directly relate to longitudinal creep force developed at the wheel-rail interface.

Vermeulen and Johnson [44] developed a three-dimensional model of the wheel-rail rolling contact problem to determine the lateral and longitudinal contact forces attributed to creepage. The non-dimensional creep factors were used to define deviations from the pure rolling condition in

terms of ratios of slip velocities to the nominal velocities along in longitudinal and lateral directions. The contact patch in this model was divided into two axisymmetric elliptical regions corresponding to slip and stick. The contact forces were obtained as functions of the creepage, normal loads, modulus of rigidity G, Poisson's ratio v, friction coefficient μ, and coefficients related to the contact geometry, particularly the minor and major radii of the elliptical contact patch [9]. The creep forces in this method are limited to no-spin and smooth half spaces contact, and may yield errors in estimating wheel/rail forces during curving or interactions with irregular tracks [9, 40]. Alternatively, Kalker's linear contact theory has been widely used under steady-state rolling conditions assuming negligibly small slip within the contact area to obtain estimates of contact forces and spin moment developed at the contact patch [45]. The '*CONTACT*' simulation program, developed by Kalker [45] on the basis of theory of elasticity, provides forces developed between the two contacting bodies considered as half spaces, as well as stick and slip regions within the contact patch. The applications of the program to railway vehicle dynamic simulations, however, have been limited due to its excessive computational demands. The linear Kalker's theory under small creepage and spin is reported to yield less than 5% difference when compared to the *CONTACT* simulation results [9, 40].

The *FastSim* simulation program, based on the simplified Kalker's theory, is generally used in multi-body railway dynamic simulation platforms, which yields estimates of contact forces in a highly efficient manner [45]. In this method, the contact patch is discretized into several small regions and the local strain for each region is determined. The tangential force distributed over the contact surface is subsequently computed from the longitudinal, lateral, and rotational creepages. The geometry of contact zone described by the Hertzian function and the maximum tangential force is limited to the wheel-rail adhesion using the Coulomb's dry friction relationship. This method has been reported to yield up to 5% estimation error in the normal condition, 10% error for pure spin and 20% error for the combined translational and spin creepages, when compared with the results obtained from the *CONTACT* benchmark method [40, 45]. Owing to the discretization of the contact patch, the *FastSim* delivers detailed insight into the traction distribution and slip-stick regions as predicted by the simplified theory. Many studies have refined the method by incorporating non-Hertzian contact (non-elliptical) geometry [43], more elaborate friction laws [46, 47] and unsteady contact conditions [48, 49]. A number of other methods have also been

proposed to study the rolling contact problem such as, Kalker's USETAB [9], multi-Herzian and non-Hertzian [38] methods.

1.2.4 Performance measures of railway tank cars

Reported studies have defined widely different performance measures for evaluating critical speeds corresponding to instability conditions of a railway vehicle configuration, derailment potential, lateral load transfer, and more. The reported measures invariably derive from the dynamic motion and/or force responses under defined inputs or maneuvers. The magnitudes of lateral and yaw displacements of the wheelset under a given input have been used as the key performance measures in some of the reported studies [11, 20]. Alternatively, the forces transmitted to the track by the axle as well as the lateral acceleration of the bogie frame or a wheelset have been used as a measure for reaching the critical hunting speed, which are also defined in the standards and regulations for acceptance tests [14, 15]. These responses are generated either due to an input of short duration followed by an ideal track, or irregularity representing a measured track profile. Testing of the wagon in straight track with measured irregularities is the most common method used for assessment of railway vehicle stability in the industry. The standards, UIC 518 [14] and EN 14 363 [15], define two different measurement methods: (i) the "normal measuring method" involving the measurements of sum of guiding forces for applications to standardized new vehicles; and (ii) the "simplified measuring method" based on acceleration responses of the bogie frame is an extension of the standardized method for applications to existing modified vehicles.

It has been reported that applications of each of these methods lead to different critical speeds for a similar wagon [12]. The application of a lateral excitation can lead to nearly 20 *km/h* higher critical speeds than those predicted from simulations of the wagon running on a track with measured irregularities [12]. Moreover, the normal measuring method based on sum of guiding forces, as defined in UIC 518 [14] yields higher critical speeds than those obtained from the simplified measuring method based on measurements of acceleration responses of the bogie frame). The greatest deviations among the different methods for identifying the critical speeds have been reported when supercritical bifurcations attributed to small limit cycles occur [20]. Although the challenges in establishing the critical speeds accurately using a nonlinear model have been widely recognized [11, 50], the existing methods with certain extensions have generally been

accepted for identifying the stability limits from the vehicle responses to a defined disturbance at different speeds.

Derailment risk of a railway wagon is the most critical measure, which has been the focus of many studies. Widely different methods have been reported for assessing the derailment potential of a railway car. A number of studies have investigated correlations between the wheel-rail contact forces and derailment potential of the railway vehicles using widely different criteria [4, 51]. The wheelset derailment is frequently described in terms of wheel flange climb on the rail and separation of wheel-rail contact. The lateral wheelset dynamics is thus considered as the primary contributory factor, while the gauge widening, rail roll/deflection and track-plane shift are reported as the secondary contributory factors [38]. The reported studies have shown that flange climb generally occurs under large positive angle of attack (AoA) induced on a curved track or due to yaw motion of a bogie [38, 52]. The loss of wheel-rail contact, on the other hand, is attributed to excessive wheelset/bogie roll or hunting leading to high lateral velocity. The wheelset derailment can also be caused by a large magnitude of impact force that may occur at relatively higher speeds [53, 54].

The flange-climb is considered as a primary indicator of an impending derailment. Different flange-climb derailment safety criteria have evolved since the early criterion of Nadal [38, 52]. The flange climb criterion assumes initial two-point wheel-rail contact condition with flange contact point leading the tread contact point, as shown in Figure 1.2 [4]. In this condition, the wheel surface at flange contact moves (slides) downwards relative to the rail, as the wheel flange climbs over the rail. The onset of a derailment is considered to occur when an upward motion of the wheel flange is initiated, and the contact force approaches the maximum friction force.

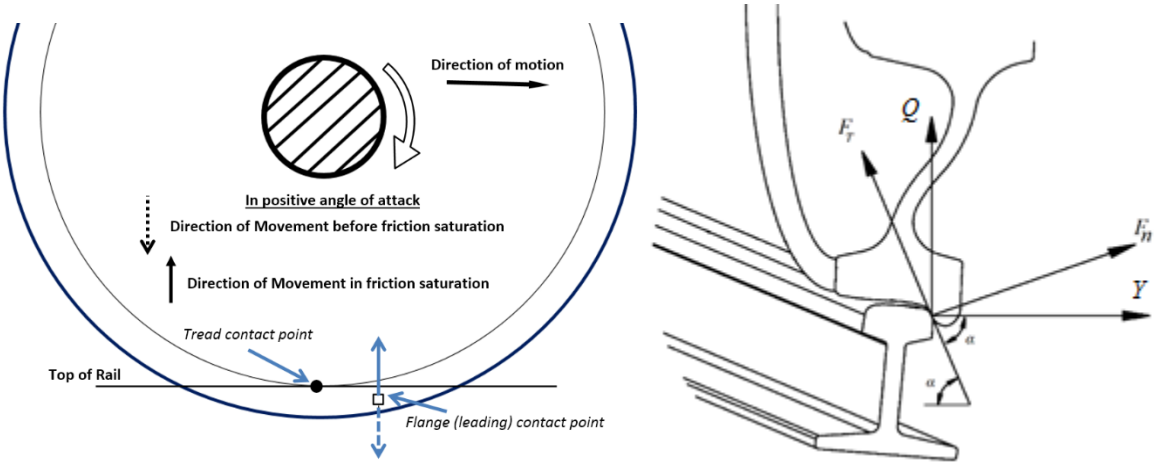

(a) (b)

Figure 1.2: Illustration of the Nadal's wheel-flange contact: (a) two wheel-rail contact points under a positive angle of attack; and (b) wheel-rail contact corresponding to onset of a potential derailment [4, 38].

Nadal [4] proposed a critical derailment coefficient, Y/Q, on the basis of the observed correlations between the normal F_n and tangential friction F_T forces and the transverse Y and vertical Q wheel-rail forces under zero longitudinal creep force (no braking or traction). The equilibrium of wheel-rail contact forces at the single flange contact point, assuming loss of tread contact due to upward motion of the wheel, yields the Y/Q relationship. The relationships among the different forces are expressed as a function of the wheel flange angle α, as [52]:

$$F_T = Q\sin\alpha - Y\cos\alpha; \qquad F_n = Q\cos\alpha + Y\sin\alpha \tag{1.1}$$

When the tangential force approaches the wheel-rail adhesion limit, $F_T = \mu F_n$, the critical derailment coefficient is obtained as:

$$\frac{Y}{Q} = \frac{\tan\alpha - \mu}{1 + \mu\tan\alpha} \tag{1.2}$$

Considering typical wheel flange angle, $\alpha = 60°$, and wheel-rail friction coefficient, $\mu = 0.3$, the above relation yields the critical derailment coefficient, $Y/\mathrm{Q} = 0.95$. A safety factor of 1.2, is generally assumed, which yields the critical derailment coefficient of 0.8 that relates to the onset of a potential derailment [14]. Many subsequent analytical and experimental studies have been

conducted, which recommend widely different values of the critical derailment coefficient [51, 52, 55]. It has been reported that Nadal's criterion is applicable when the angle of attack exceeds 0.5 degree, while it yields a conservative derailment prediction under a small or negative angle of attack [4, 52, 56]. Nadal's criterion, however, does not consider the effects of variations in the friction between the rail and non-flanging wheel of the wheelset. Moreover, flange climb happens instantaneously, when the Y/Q limit is exceeded. Despite these limitations, the derailment criterion based on Y/Q continues to be widely used as an initial design guidance and as primary acceptance criterion [14].

Weinstock proposed a less conservative wheel flange climb criterion for predicting incipient derailment by summing the absolute values of Y/Q of the two wheels of the same wheelset, known as the 'axle sum Y/Q' ratio [38, 52]. The method considers different friction coefficients for the flange and the tread contact regions. While the Y/Q ratio of the flanging wheel is evaluated using Nadal's equation, the Y/Q ratio of the non-flange wheel or tread contact is described by the friction coefficient between the tread-rail crown regions with a lower contact angle in the 0 to 3° range. It was suggested that sum of the Nadal's Y/Q values on the flanging wheel considering the coefficient of friction for the non-flanging wheel region (tread, μ_t) can provide a more accurate indication of the impending derailment for small or negative angles of attack, such that:

$$\frac{Y}{Q} = \frac{\tan\alpha - \mu}{1 + \tan\alpha} + \mu_t \tag{1.3}$$

The proposed method not only retains the simplicity of the originally proposed Nadal's criterion but it also yields a more accurate prediction in terms of directly measurable quantities of an instrumented wheelset.

The derailment potential is also strongly related to lateral load shift across a wheelset encountered during curving or due to excessive super-elevation or track irregularity. Some studies have established a relation between the load shift and the wheelset derailment [3, 10]. A critical value of the load shift, defined as the change in the wheel load normalized by the static load, of 0.6 has been identified for a single wheelset derailment [54]. Another study suggested a critical value of dynamic wheel load ratio in the order of 0.8 [14].

Owing to the grave implications of a railway vehicle, the derailment limits are invariably defined with a safety margin. Different standards, however, recommend varying values of the derailment safety margin, which are mostly based on Nadal's criterion. Jun and Qingyuan [54] suggested that Y/Q ratio exceeding 0.8 for a duration of more than 15 *ms* as the critical value, while Garg and Dukkipati [10] suggested the consideration of a longer duration of 50 *ms*. In Western Europe, $Y/\mathrm{Q} > 0.8$ over a moving distance of 2 *m* is considered as the critical. In China, the safety margin is based on both the Y/Q ratio and the wheel load shift ($Y/\mathrm{Q} < 1.0$ and $\Delta Q/Q_0 < 0.60$) as the safe margin, while $Y/\mathrm{Q} > 1.2$ and $\Delta \mathrm{Q}/Q_0 > 0.65$ are considered critical. In North America, the benchmark values for safety evaluation are considered as, $Y/\mathrm{Q} > 1.0$ and $\Delta Q/Q_0 > 0.9$ [54]. The UIC 518 [14] and EN 14 363 [57] recommend that the Y/Q for each wheel over a distance of 2 *m* must not exceed 0.8 *m* on a curved track with radius equal to or greater than 250 *m*. Using the data obtained from a single wheelset derailment tests on a rolling rig, it has been shown that a derailment would occur when the magnitude of wheel lift approaches $25\ mm$ coupled with relative transverse displacement of $70\ mm$ [55].

The wheelset responses in the presence of rail defects, particularly the roll deflections, and the gauge widening could also cause wheelset derailment. Rail rollover criteria can vary from Y/Q above 0.6 for the inside flange contact to approximately 0.2 when the contact lies on the outside of the track [38, 56]. This criterion, defined in AAR M1001 Recommendation Practices [58], assumes negligible effect of torsional stiffness of the rail and single contact condition for each wheel.

Apart from the above, it has been reported that the lateral shift of the track plane can cause one of the wheel to drop between the rails leading to wheelset derailment [38, 56]. Lateral track shift is known as a general phenomenon caused by repeated excessive lateral forces at the wheel-rail interface. A few studies have shown higher rates of track shift in poorly laid, newly laid and newly maintained tracks [38, 56]. Concert ties tend to limit the track shift compared to the other ties. A generalized limiting value of the critical lateral load, L_c, has been proposed as a linear function of the vertical wheel load, as [56]:

$$L_c = a_v Q_{axle} + b_l \tag{1.4}$$

where Q_{axle} is vertical axle load, and a_v and b_l are empirical constants that depend on the type of ballast and ties used in the track.

Despite the developments in various derailment criteria, a generally applicable criterion does not yet exist. Some of the proposed derailment criteria are considered conservative for some applications, while accurate physical interpretations of the derailment phenomena are lacking for many situations [4, 59].

1.2.5 Liquid slosh models

The dynamic forces and moments arising from movement of liquid cargo within partly-filled moving containers are known to affect directional performance and stability limits of road, rail as well as marine vehicles [3, 7]. In railway vehicles, the additional forces induced by the liquid free surface oscillations in a partly-filled tank, may alter the wheel-rail contact forces and the coupling forces. The liquid slosh dynamics and the fluid-structure interactions have thus been widely investigated to study movements of liquid fuels within automobile tanks and spacecraft [60], liquid cargo in tank trucks [8], rail tank cars [3] and ocean vessels [61, 62]. These studies have focused on analysis of slosh forces, moments, load shift and natural frequencies of the free surface oscillations using different liquid slosh models, which are briefly discussed below.

Different numerical and analytical methods have been developed to study fluid slosh within fixed or moving containers. The most widely used numerical methods involve solutions of the Navier-Stokes and continuity equations in conjunction with appropriate boundary conditions. These methods, however, are known to impose excessive computational demands for applications in moving vehicles' dynamic analyses [63-65].

Simplified quasi-static slosh models have been widely used to study the effects of liquid cargo slosh on steady-state roll stability limits and directional performance of road tank vehicles [66, 67]. The quasi-static methods have been used to derive relative rollover threshold limits of articulated road tank vehicle with various tank cross-sections such as circular, modified-oval, elliptical and modified square tanks [7, 8, 68, 69]. Kang *et al.* [70] proposed an optimal tank cross-section using the quasi-static approach. The study converged to a tank-cross section similar to a '*Reuleaux triangle*', which resulted in substantially higher rollover threshold of the vehicle compared to the circular and modified oval tanks. Quasi-static fluid slosh models, however, do not describe the transient slosh effect, which has been shown to yield substantially greater forces and moments compared to the steady-state values predicted from the quasi-static approach [64, 71, 72].

Alternatively, a number of studies have proposed linear slosh models assuming in-viscid fluid and irrotational flows, thereby permitting the use of the potential flow theory [73, 74]. It has been shown that the linear slosh theory can effectively predict the slosh forces and moments under low amplitude excitations, while the method yields substantial errors in the vicinity of the slosh resonant frequencies [64]. The linear slosh analyses have been widely used to compute slosh resonance frequencies [75], free surface movements [76, 77], and slosh forces and moments [78]. Early studies on linear slosh analysis focused on upright cylindrical or rectangular stationary tanks [65]. Conformal mapping techniques have been applied to study slosh problems in horizontal cylindrical tanks with and without baffles [76, 77]. Multi-modal methods have also been proposed to study linear slosh in horizontal tanks [78]. The boundary element methods (*BEM*), yield linear slosh solutions with relatively greater computational efficiency, particularly for arbitrary cross-section tanks with partition walls or baffles [79]. Low amplitude liquid sloshing of inviscid and incompressible fluids in a 3-D arbitrary shape baffled tankers has been investigated by Firouz-Abadi *et al.* [80] using BEM coupled with the subdivision of the fluid domains.

A range of numerical methods based on finite difference, finite element, finite volume and boundary element methods have been developed and applied to study nonlinear slosh dynamics for different tank cross sections. Rebouillat and Liksonov [81] presented a comprehensive review of numerical nonlinear slosh analysis methods. Numerical methods of nonlinear slosh have been categorized by D'Alessandro [63] as Lagrangian, Eulerian, Smoothed Arbitrary Lagrangian-Eulerian (*ALE*) and Particle Hydrodynamics (*SPH*) methods. Lagrangian method tracks the free surface movement considering that the nodes moves with the fluid. In contrast, the fixed domain nodes are used in Eulerian method, where the free surface movement does not alter the element's shape. The computational cost of moving mesh used in the Lagrangian method is thus higher than the Eulerian method. The SPH method is a Lagrangian method, where the fluid is divided into a set of particles. The finite-element, finite-difference and SPH models could be integrated to the multi-body vehicle dynamics models, although with very high computational demand. As an example, Fleissner *et al*. [82] coupled a three-dimensional fluid/granule model based on SPH method with a 17-DoF model of a truck to study the effects of liquid and grain movements on braking and steering dynamics of the truck.

Popov *et al.* [83] used a finite-difference method for numerical integration of Navier-Stokes, continuity and free surface equations for analysis of two-dimensional nonlinear slosh in a

horizontal cylindrical container assuming incompressible flows with zero surface tension in the free boundary. A number of recent studies have employed volume of fluid (*VoF*) and finite difference methods for analysis of two- and three-dimensional slosh in road tankers of different cross sections using FLUENT software [71, 72, 84]. These have shown that magnitudes of dynamics slosh forces and moments are substantially greater than those predicted from the quasi-static models. Moreover, it is shown that transverse baffles can effectively limit the magnitudes of longitudinal slosh forces.

Owing to the complexities associated with integration of the dynamic slosh models with the multi-body dynamic vehicle models, a few studies have proposed mechanical analogous of fluid slosh [85, 86]. These models provide estimates of liquid slosh characteristics by simple equivalent mechanical models [74, 87]. The analogy is based on the assumption that liquid in a container can be divided into stationary (with respect to container structure) and moving components, while the free surface oscillations can be described by the motion of a simple spring-mass-damper or a pendulum system. The parameters of the mechanical equivalent models are invariably identified from the slosh responses obtained from linear slosh analysis [87].

Abramson [88] conducted a series of experimental and analytical studies on forced responses of liquids in upright cylindrical, spherical and rectangular tanks with separating walls. The data were used to identify parameters of an equivalent mechanical model. A detailed formulation of an equivalent model of fluid slosh under translational and pitching movement has been presented by Roberts *et al.* [89]. Comprehensive formulations of mechanical equivalent slosh models for some tank geometries have also been presented by Ibrahim [65]. Considering that, the parameters of equivalent mechanical models are obtained based on linear slosh theory, such models are considered valid under low amplitude slosh and when the excitation frequency is not close to the slosh resonant frequencies, which tends to cause flow separation.

Bauer *et al.* [60] proposed a mass-spring analogy with a non-linear spring obtained from tests conducted on a vertical cylindrical tank. Ranganathan *et al.* [85] employed the pendulum analogy to describe lateral oscillations of fluid within a two-dimensional circular road tanker. The natural frequencies of pendulum model were compared with those reported by Budiansky [90]. Ranganathan *et al.* [86] also proposed an equivalent mass-spring mechanism to simulate longitudinal movement of fluid in a three-dimensional circular road tanker, which was validated in terms of fundamental slosh frequencies reported by McCarty *et al.* [75].

An equivalent trammel pendulum was proposed by Salem *et al.* [87] to study the lateral fluid sloshing in a two-dimensional partly-filled elliptical container. The parameters of the equivalent pendulum model including arms of trammel pendulum, fixed and pendulum masses, and the height of the fixed mass with respect to the tank base. These were estimated from the fundamental slosh frequency, horizontal force and roll moment around the tank's base, obtained from a finite element fluid slosh model in LS-Dyna. A set of proposed trammel pendulum could be considered to represent the mechanics of low amplitude slosh and can be integrated for coupling with multi-body vehicle model without much difficulty. Applications of such methodology, however, have been limited due to challenges associated with parameters identifications, which generally involve either experiments or analyses using linear slosh theory or numerical simulations.

1.2.6 Liquid slosh analysis in railway vehicle

While the effects of fluid slosh on roll and yaw dynamics of road tank vehicles have been investigated in a number of reported studies, only a few studies have explored the effects on the dynamics of railway vehicles. Furthermore, these studies have mostly employed simple pendulum slosh models considering only the fundamental slosh mode. Khandelwal and Nigam [91] employed a pendulum model of liquid slosh considering a rectangular railway wagon moving on an irregular track with constant longitudinal acceleration. The slosh model parameters were estimated based on the data reported by Abramson [88] assuming low amplitude free surface motion. The effect of damping was also considered by introducing a viscous damper with the pendulum. The study considered bounce and bounce/pitch models of a single wagon tank car permitting slosh due to track irregularity and longitudinal acceleration/deceleration. The study showed that fluid slosh serves as an effective damper, when excitation frequencies are distant from the fundamental slosh frequency.

Bogomaz *et al.* [92] developed roll, pitch and yaw plane models of a partly-filled tank car using the equivalent pendulum models of fluid slosh. The pendulum parameters were obtained through solutions of the boundary value problem over the liquid domain coupled with modal solution of the free surface. The simulation model in the pitch plane alone was validated from the tests conducted on a tank car subject to longitudinal impacts at different speeds. The simulation results revealed notable contributions of fluid slosh to lateral and vertical accelerations under excitations

caused by rail irregularities and curving. The study employed simplified models of tank car incorporating suspension and wheel/rail contact with linear properties.

A three-dimensional model of a partly-filled tank car developed by Younesian *et al.* [3] integrated a two-dimensional mechanical equivalent model of fluid slosh along the longitudinal axis. The fluid slosh parameters were estimated by representing the cylindrical tank by a rectangular cross-section in order to utilize the data reported by Abramson [88]. The simulations were performed under braking in a curve with super-elevation. The results obtained under different speeds, fill volume and track irregularity showed greater unloading of the inside track wheels in the presence of fluid slosh. It was concluded that neglecting fluid slosh in a partly-filled tank car could lead to underestimation of the derailment potential and wheel unloading by 18 and 25 percent, respectively. Transportation of dense liquid cargo in high capacity railway tanks was also reported to be more critical, as it has been reported for road tankers [8, 93].

In a recent study, Di Gialleonardo *et al.* [94] investigated the wheel unloading and thus the derailment of a partly-filled railway tank car subject to 'S'-curve maneuvers at different speeds. The liquid slosh was characterized by multiple equivalent lateral mass-spring models distributed along the length of tank car to account for yaw motion of the tank. The fluid in the tank was represented by nine identical equi-spaced but uncoupled spring-mass systems to track the fluid mass motion under lateral and yaw excitations. The parameters of mechanical equivalent model were identified through minimization of error between the model response and responses obtained from two-dimensional Computational Fluid Dynamic (*CFD*) analysis for 25, 50 and 75 % fill ratios (ratio of the fill height to the tank diameter). The distributed mechanical-equivalent fluid slosh model was integrated to a 35-DoF model of a 4-axle tank car. The simulation results obtained for an 'S'-curve track revealed relatively higher wheel unloading in the presence of fluid slosh, as reported by Younesian *et al.* [3]. During the trailing portion of the curve higher wheel unloading was reported for the third wheelset, while first wheelset revealed higher derailment (Y/Q) ratio. The results also showed greater shift in the liquid load, caused by centrifugal acceleration, which has been widely reported for the road tankers [8, 65, 72]. The study also showed greater load shift when the 'S'-curve frequency was close to the natural frequency of the mechanical-equivalent model.

The effects of longitudinal and lateral fluid slosh on the oscillatory motions of the coupling screws were investigated by Vera *et al.* [95] considering a model of four partly-filled tank cars with

two-axles each. The fluid slosh along the lateral axis was described by a pendulum model, proposed by Ranganathan [86]. The slosh along the longitudinal axis was modeled by the mass-spring system proposed by Abramson [88], assuming five compartments for each tank car. The results attained for the 85% filled wagons under curving showed lateral load shift ratio of 0.6 at the forward speed of 120 *km/h*. This load shift is below the limit recommended in the European standard [15]. The study concluded minimal effects of liquid slosh on the lateral load shift and wheel-rail forces, which is likely due to relatively higher fill volume of 85% considered.

Hazrati *et al.* [96] suggested that neglecting the liquid cargo movements may lead to underestimation of the tank car roll motion and dynamic load ratios during curving. Both the roll motion and load transfer were found to be significant for low fill level ratios. The liquid cargo movement could eliminate the performance gain of the low *c.g.* height due to the lower fill height. It was further suggested that effects of liquid slosh subject to yaw oscillations of the tank have not yet been investigated thoroughly for the railway cars, with the exception of the model proposed by Di Gialleonardo *et al.* [94] considering multiple uncoupled pendulums along the length of the tank. This approach may be valid only when the liquid cargo can be consider by multiple uncoupled bulks separated by rigid partitions.

Although simple quasi-static or mechanical-equivalent models could provide efficient simulations of the coupled liquid-tank car system, their applications are limited to two dimensional and circular cross-section tanks. The limited studies of liquid slosh in railway tankers have used the equivalent mechanism approach which required prior identification of parameters and is not applicable for three-dimensional inputs [87]. While the computational fluid dynamic models can provide accurate estimations of dynamic slosh forces, their excessive computational demand inhibit the implementations in the multibody dynamic vehicle models [84, 97]. Alternate methods based on multi-modal and boundary element approaches will be meritorious for analysis involving different tank cross-sections in a computationally efficient manner [64].

Based on reviewed literature, the linear slosh theory can be used to develop an analytical model of liquid slosh in moving tanks of different cross-sections. The linear slosh formulations have been reported in many studies and the systematic method has been outlined in detail by Kolaei *et al.* [64, 98]. The equations of motion for the liquid in a rigid container can be simplified assuming an ideal liquid with negligible viscosity effect as well as incompressible and irrotational flows. Under these conditions, the Navier-Stokes equations reduce to Euler equations [88]. Based on the potential flow

theory for irrotational flows, fluid velocity can be derived from a velocity potential so that the gradient of the potential function yields the flow velocity. The linearized boundary-value problem of liquid sloshing for two-dimensional containers can be expressed in the form of the Laplace equation of the velocity potential function. The method offers considerable computational efficiency and can be easily implemented for co-simulations with the multi-body dynamic codes [6, 99]. The major motivation for the proposed method is to generate an accurate prediction for transient liquid slosh that could be extended to three-dimensional models for real-time simulations.

1.3 Scope and objective of the dissertation research

From the review of studies on railway freight cars, dynamics of fluid slosh, fluid-structure interactions, as well as its potential influences on the dynamic performance and safety of partly filled railway tanker, clearly provide a scope for the research and contributions in the field. The thesis research is thus aimed at formulations of a vehicle model incorporating comprehensive representation of the friction wedges in the secondary suspension together with an effective liquid slosh model, which can be integrated for efficient analyses of the coupled liquid cargo-vehicle system dynamics. The resulting coupled model is used to study the effects of cargo slosh within a partially filled railway tank car on response measures relevant to curving, hunting and switch-passing, which constitute the primary objective of the dissertation research. The specific goals are summarized below:

a) Develop a multi-body dynamic (*MBD*) model of a freight wagon, capturing the non-smoothness of contact and friction that exists between different components of a freight truck;
b) Examine validity of the *MBD* model for lateral stability and curving responses using the available data;
c) Formulate an analytical model of the liquid cargo within the partly-filled cylindrical container subject to lateral acceleration, roll motion and yaw oscillations of the tank to obtain dynamic slosh force and roll moment, and liquid cargo shift;
d) Examine validity of the slosh model using the reported slosh mode frequencies and hydrodynamic coefficients;
e) Develop a co-simulation scheme for analyses of the coupled liquid cargo-wagon models under lateral, roll and yaw motions of the tank car; and
f) Investigate the effects of cargo slosh on hunting, roll stability and derailment potential of the partly-filled railway tank car considering different fill volumes and forward speeds.

1.4 Organization of the dissertation

This dissertation is prepared according to the manuscript-based format described in "Thesis Preparation, Examination Procedures and Regulations" guidelines of the School of Graduate Studies, Concordia University. The thesis is organized in six chapters, which addresses the research goals stated in section 1.3. The first chapter presents the review of relevant studies, and the scope and objectives of the thesis research. The final chapter (Chapter 6) presents the major contributions and conclusions of the research work together with suggestions for further work. Chapters 2 to 5 are based on the manuscripts that have been either published or submitted for publications in peer-reviewed journals, which are summarized below.

Chapter 2 presents the multi-body dynamic model of a freight wagon incorporating a set of three-piece freight bogie with frictional wedges and wheel-rail contact model. This chapter is based on the following article published in the Journal of Rail and Rapid Transit:

Hazrati Ashtiani I, Rakheja S and Ahmed AKW, "*Influence of friction wedge characteristics on lateral response and hunting of freight wagons with three-piece bogies*". Proceedings of the Institution of Mechanical Engineers, Part F: Journal of Rail and Rapid Transit, 2016: Page 877-891.

The *MBS* modelling approach of friction wedges based on point-plane contact is presented in this chapter. The nonlinear damping characteristics of the suspension system of three-piece bogie are investigated considering nonsmooth unilateral contact, multi-axial motions and geometry of the wedges and slip-stick friction forces. The parameters of contact pairs were identified to achieve an efficient numerical demand with adequate accuracy. The resulting 114-degrees-of-freedom wagon model incorporated constraints due to side bearings, axle boxes, and the centre plates, while the wheel-rail contact forces were obtained using the algorithm. The simulation results were obtained to study hunting properties of the wagon in terms of critical speed and the predominant oscillation frequency, and the effects of wedge friction and geometry on stability characteristics of the freight car. The contributions of this chapter address the objective a and b of the dissertation addressed above.

Chapter 3 presents liquid cargo model based on linear slosh theory together with mode summation and its validation and integration to the vehicle model presented in Chapter 2 to study the effects of liquid slosh on hunting phenomena of the railway tank car. The contributions of this

chapter address the objectives *c* and *d*, and partly *e* and *f*. The chapter presents following article that has been submitted for review for publication in the *Journal of Multibody System Dynamics.*

Hazrati Ashtiani I, Rakheja S and Ahmed AKW, "*Hunting analysis of a railway tank car subject to partially filled state of the tanker*", (2018) Submitted to Multibody System Dynamics.

The chapter presents an analytical liquid slosh model to capture the response of the liquid cargo up to five natural modes in the roll plane. The validity of the proposed slosh model is illustrated through comparisons of the model responses with the reported data in terms of modal frequencies and hydrodynamic coefficients. A co-simulation scheme is presented to integrate the liquid cargo model with the nonlinear multi-body dynamic (*MBD*) model of the railway tank car with a set of three-piece bogies, as described in Chapter 2. The coupled model simulations are performed to evaluate lateral dynamic responses and critical hunting speeds under different filled conditions. The results obtained with the proposed linear slosh model for different fill ratios are compared with those obtained with equivalent rigid cargo to highlight the effects of liquid cargo slosh. The results are also compared with those obtained from a simple pendulum slosh model.

Chapter 4 presents the following article submitted for review to the *Journal of Vehicle System Dynamics*:

Hazrati Ashtiani I, Rakheja S and Ahmed AKW, "*Effects of coupled liquid cargo sloshing on roll response of partly filled railway tank cars*" (2018) Submitted to Vehicle System Dynamics.

The paper summarizes the co-simulation scheme integrating the liquid cargo and vehicle models, developed in Chapter 3, to study the effects of slosh force and moment on the vehicle responses during curving. The contributions of this chapter partly address the objective *f*. The additional slosh force and moment arising from the free surface motion for the partially filled state of the tank are obtained to study their effects on the wheel-rail contact forces and dynamic response of the rail vehicle during curving. The liquid slosh effects during curving maneuvers are discussed through analyses of the roll motion of the tank car, and unloading and derailment ratios. The results are further compared with those obtained for the equivalent rigid cargo to assess the contributions of liquid cargo sloshing. The results clearly demonstrated that partial fill state of tank car and resulting slosh could lead to significantly higher magnitudes of dynamic responses of the car, and may result in separation of the wheel from the rail at a relatively lower lateral accelerations and forward speeds, when compared to the rigid cargo car.

Chapter 5 presents the effects of dynamic liquid slosh on the tank car responses during a switch-passing maneuver. The coupled model integrates a more comprehensive liquid slosh model considering the effects of roll and yaw motions of the tank car, in addition to the lateral acceleration, as stated in objective *c*. This chapter presents the following article submitted for review in the Journal of Rail and Rapid Transit:

Hazrati Ashtiani I, Rakheja S and Ahmed AKW, "*Investigation of coupled railway tank car and liquid cargo response subject to switch passing maneuver*", Proceedings of the Institution of Mechanical Engineers, Part F: Journal of Rail and Rapid Transit.

The influences of the liquid cargo motion on different performance measures of the railway tank car are investigated during transient of a railway switch negotiations. Owing to the considerable yaw motion of the car during such maneuvers, the liquid slosh mode presented in Chapter 3 is further enhanced to incorporate the roll and yaw motion excitations. The co-simulations of the refined slosh model and the vehicle model are performed under transient lateral, roll and yaw excitations encountered during switch passing maneuvers. The forces and moment due to sloshing within the partly-filled tank are evaluated through summation of the first four antisymmetric natural modes. The validity of the slosh model is illustrated through comparisons with the responses obtained from computational fluid dynamic model. The effects of liquid slosh dynamics on responses of the coupled system are presented in terms of roll angle, and unloading and different derailment ratios. The results suggested more significant effects of the liquid cargo slosh on the response measures when compared to those observed during steady curving. It is shown that liquid slosh can lead to significantly larger dynamic response magnitudes of the wagon, when compared to those obtained for the equivalent rigid cargo. The results also revealed greater potential for separation of the wheel from the rail for the partly-filled tank car at relatively lower forward speeds.

CHAPTER 2

Influence of friction wedge characteristics on lateral response and hunting of freight wagon with three-piece bogies

2.1 Introduction

The lateral instability and derailment potentials of railway vehicles have been widely investigated using diverse methods. These have helped identify safe operating limits, standardized guidelines [14, 15], and roles of different components designs and operating conditions. Owing to increasing demands for high load capacity and high-speed freight cars, such efforts are continuing for realizing designs with enhanced lateral stability limits [100]. The lateral stability of a railway vehicle is directly related to sustained self-excited lateral and yaw motions of the wheelsets and bogies, commonly referred to as hunting, which is known to be inherent mechanics of the wheel-rail geometry. The hunting is initiated as a limit cycle motion with increasing forward speed and it could lead to comprehensive levels of lateral wheel-rail forces and thus the derailment or track panel shift.

Early studies on railway vehicle lateral stability based on linearized wheel/rail contact and suspension models typically showed zero lateral mode damping when a critical speed was reached [9, 10]. Owing to the inherently nonlinear kinematic and constitutive relations for the wheel-rail contact as well as truck and suspension components, quasi-linear functions describing essential components' characteristics have been employed in the hunting studies. For instance, UIC 519 [16] represents a methodology for deriving quasi-linear function for describing a given wheel-rail profile, referred to as equivalent conicity. The quasi-linear analyses, however, generally showed poor correlations with the measured critical speeds [17]. Huilgol [18] demonstrated the presence of *Hopf* bifurcation in the dynamic responses of a wheelset model incorporating nonlinear wheel-rail contact force. A number of studies have investigated bifurcations in the responses of rail vehicles considering nonlinear wheel and rail profiles and creep forces relationships [*e.g.*, 21, 100, 101]. The results have raised concerns about adequacy of the critical speed derived from the linear theory since subcritical *Hopf* bifurcation is common in railway vehicles responses [102, 103]. Yang and Chen [21] also investigated dynamic responses of a rail truck model with suspension nonlinearity, and concluded that hysteresis suspension nonlinearity contributes to supercritical bifurcation. Ahmadian and Yang [101] investigated hunting and *Hopf* bifurcation in the responses

of a single wheelset with non-linear yaw damper together with the flange contact, considering a simplified conical wheel profile and creep forces obtained from the Kalker's linear contact model [104]. The study showed higher critical speed with increasing yaw damping of a single wheelset. Increasing yaw damping beyond a certain value, however, resulted in lower critical speed due to stronger coupling between the wheelset and the bogie frame, which could not be observed in the linear analyses. Through analyses of both the linear and non-linear wheel/rail creep models, Polach [12, 20] concluded that the linearized analysis could lead to lower critical speeds compared to those predicted from the non-linear models. For this study, Polach recommended a very conservative parameter of the wheel/rail contact and emphasized the application of non-linear stability evaluations of the vehicle with friction dampers [12].

The reported studies have also employed somewhat different response measures for obtaining the nonlinear critical speed corresponding to an instability. These include magnitudes of lateral and yaw displacements of the wheelset to a given input [20, 105], axle force transmitted to the track [12, 13] and lateral accelerations of the bogie frame or the wheelset [14, 15]. Such responses are evaluated under a short duration pulse excitation coupled with the track irregularity. A few analytical and experimental roller rig studies have identified critical speeds by monitoring oscillatory response of the wheelset and the truck under an initial condition disturbance. Molatefi *et al.* [106, 107] simulated this method to determine hunting velocities of different unloaded freight wagons considering suspension and wheel-rail contact nonlinearities. The results suggested strong dependence of limit cycle motions of the bogie on both the forward velocity and the initial disturbance magnitude, in addition to a non-linear relation between the frequency of oscillations and speed.

While the linear analyses have provided valuable guidance on influences of various subsystems' parameters, geometries and profiles, in-depth nonlinear component modeling and analysis are essential for accurate predictions of critical speeds and dynamic responses. From the review of reported nonlinear models, it is evident that even the most complex and detailed nonlinear models encompass simplified representations of the friction damping present in the secondary suspension [23, 33]. The friction wedges in the secondary suspension of a three-piece bogie exhibit strongly nonlinear damping properties attributed to complex variations in the contact forces, contacting surfaces geometry and the friction coefficient. Moreover, these yield substantial magnitudes of multi-directional variable damping, which could help realize enhanced performance

limits over a wide range of loading conditions. The reported studies generally consider friction wedge as a simplified constraint and an equivalent linear or vertical/lateral friction damper. Harder [29] developed a specific element in the ADAMS platform for simulation of a specific type of wedge design, which provided a constant friction damping regardless of loading. Ballew [108] studied the effects of geometry and inertial properties of friction wedges on dynamic responses of a four-degrees-of-freedom (DoF) half-truck model considering motions in the vertical, lateral, pitch and yaw directions. The study showed that magnitudes of friction forces obtained from the model were considerably lower than those from the NUCARS simulations. Steets [33] developed a three-dimensional (3-D) multi-body dynamic (*MBD*) model for characterizing friction wedge interactions with the bolster and the side frame, and discussed the key differences in responses, when compared with the NUCARS simulation results.

The effects of wedge friction nonlinearity on hunting critical speeds have been addressed in some studies. Xia [31] used a two-dimensional (2-D) dry friction model including stick and slip motions to study the effects wedge friction nonlinearity on hunting characteristics of a freight truck. Such a model would lead to a stiff system of equations requiring significantly smaller integration step for simulations and could cause high-frequency oscillations in responses due to the stick phenomenon. Xia [109] subsequently implemented switching conditions to model the wedge friction forces and showed strongly coupled motions of the wedge and the bolster under low amplitude excitations and that the friction plays an important role in limiting vertical resonance of the bolster. It was also observed that lateral excitation of the bolster will cause both lateral and vertical vibration in the wedges. The study concluded that the critical speed evaluated from the nonlinear analysis is substantially lower than that from the linear analysis. Kaiser *et al.* [32] investigated dynamic responses of friction wedges assuming stick-slip Coulomb friction using a single-DoF model. The response to low amplitude and low-frequency vertical excitations was dominated by the sticking phase of the contact. The response to larger amplitude or higher frequency excitations was weakly nonlinear due to dominant slippage phase of the contact. The experiments conducted on a scaled model of a wedge confirmed two types of slip-stick conditions, and revealed occurrence of slip phenomenon at frequencies above 30 *Hz*. Klauser [30] proposed a detailed finite-element model of friction wedges to determine contact pressure distribution on wedge surfaces that provided accurate warp stiffness modeling.

From the reported studies, it is evident that complex geometry coupled with interactions of the wedges with side-frames and the bolster cause considerable variations in effective damping properties of the secondary suspension along all the translation and rotational axes. Such variations would also affect the lateral dynamics and hunting characteristics of the truck, which has not been yet been reported.

In this study, a detailed model of the friction wedges is formulated to characterize their multi-axis stiffness and damping properties considering the geometric nonlinearities and loading conditions. The secondary suspension system of a three-piece bogie is modelled in details with multi-directional effects of spring nests as well as the friction wedge design along with the creep and suspension forces in the *Universal Mechanism* (*UM*) software [110]. The multi-axis model of the suspension system is integrated into a nonlinear model of a freight wagon to study the effects of wedges' interactions with the lateral dynamics and hunting responses. The effects of geometry and tribology characteristics of wedges on lateral response of the system, along with loading conditions of coil springs, are further investigated in terms of the nonlinear critical speed.

2.2. Multi-body model of a freight-car with three-piece bogies

A multi-body dynamic model of a freight wagon is developed incorporating a car body and a set of three-piece bogies or trucks. Figure 2.1 illustrates the side and top views of a typical bogie together with the fixed inertial axis system. The frictional forces at the contact surfaces of the wedges, center plate and the side bearings provide the essential suspension damping. Among these, the wedge contacts yield complex multi-dimensional friction forces, which are function of loading on the bolster and the wedge geometry, while the mass of a wedge is very small compared to those of the other components. Furthermore, multi-axis relative motions of the wedges contribute to multi-dimensional secondary suspension forces. The component models are formulated in a systematic manner so as to characterize friction and spring forces along the lateral and vertical directions, and moments along the yaw, roll and warp axes, which are known to strongly influence the lateral dynamics and hunting behaviour of the bogie [23]. Each bogie is modeled considering nine rigid bodies, including friction wedges, side frames, wheelsets and bolster, which are coupled through contact surfaces and suspension springs, and connected to the car body through the center plate and side bearings. A 114-DoF model of the freight-car is thus formulated in the *UM* software considering 6-DoF motions of each rigid body subject to constraints imposed by unidirectional contact forces, multi-axis motions of the springs and wheel/rail contact.

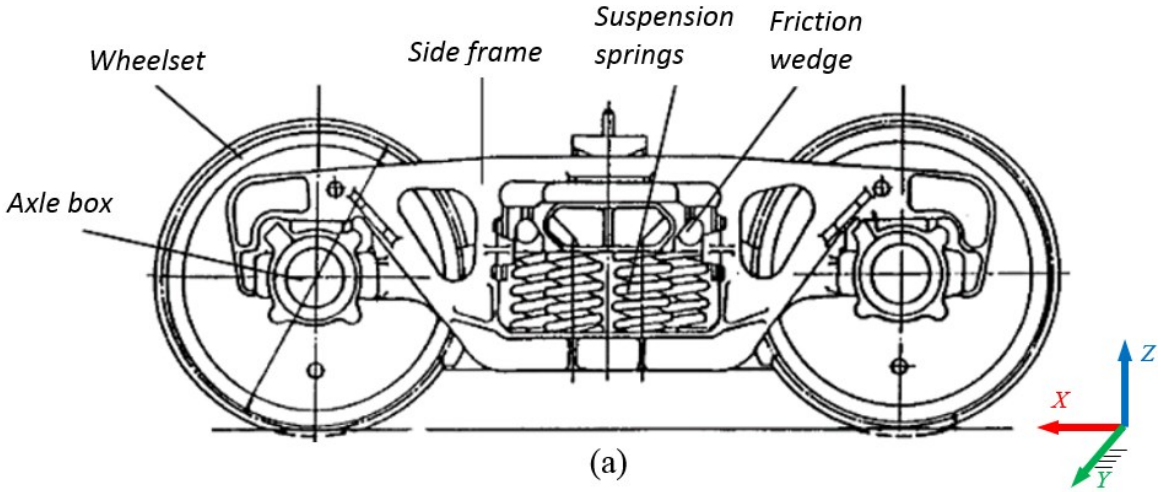

(a)

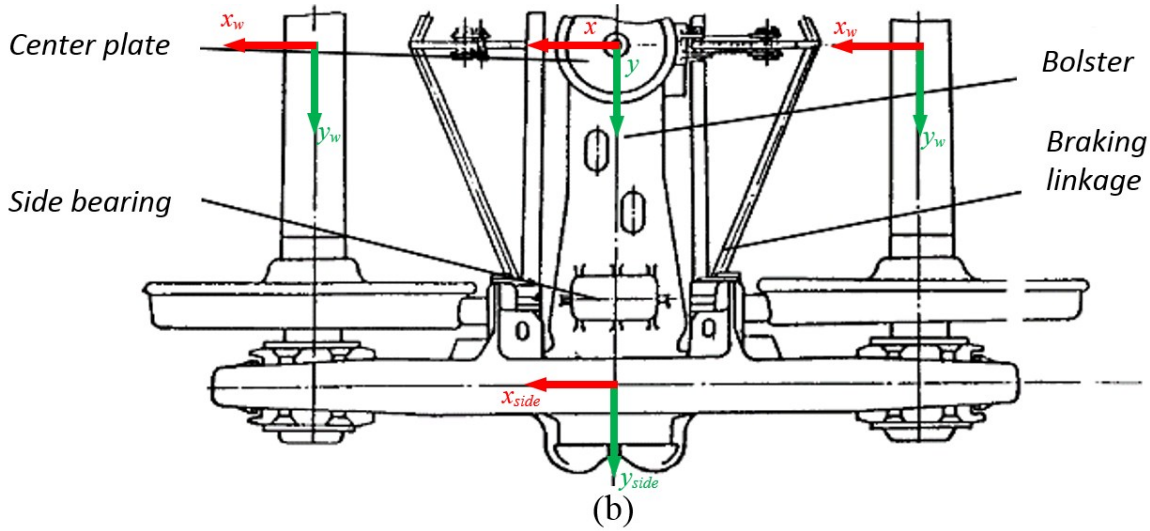

Figure 2.1: (a) Side-view; and (b) top-view of a typical three piece bogie [38].

Table 2.1 presents the inertial and some of the geometric parameters including the coordinates of the mass centers (*c.g.*) of the baseline bogie components [109-112]. I_x, I_y and I_z in the table are mass moments of inertia of components about *x*-, *y*- and *z*-axis of the body-fixed coordinate system with origin located at the *c.g.* of the respective component, while the fixed inertial axis system (*X*,*Y*,*Z*) is shown in Figure 2.1.

Table 2.1: Inertial and geometric properties of the components [109-111].

Component	Mass (kg)	I_x ($kg \cdot m^2$)	I_y ($kg \cdot m^2$)	I_z ($kg \cdot m^2$)	*c.g.* height* (m)	Additional Geometric parameters
Wheelset	1,500	925	200	925	0.475	Track width = 1.5 m Wheel base = 1.85 m
Bolster	596	323	7.25	326.3	0.701	
Side-frame	526.3	13.6	175	161.8	0.480	$y^{**} = \pm 0.978$ m
Wedge	21.6	0.08	0.103	0.102	0.567	$x^{***} = 0.335$; $y^{**} = \pm 0.978$ m
Car body	12,400	21,840	74,785	87,666	1.910	Center plates longitudinal distance = 8.650 m

* *c.g.* heights with respect to the top of the rail;

** lateral position with respect to the middle of the track;

*** longitudinal position with respect to the center plate.

2.2.1 Suspension springs modelling

In the secondary suspension of the bogie, each wedge is seated on a set of helical springs, while the bolster is supported by a set of five bolster springs on the left- and right-sides, as shown in Figure 2.2. Each spring set is a parallel and concentric arrangement of inner and outer springs. The suspension springs are generally considered as linear springs in the axial direction alone [23, 109]. The couplings between different motions and the reaction moments, however, cause transverse and bending deformations of the springs leading to substantial forces and moments along the non-axial directions [113].

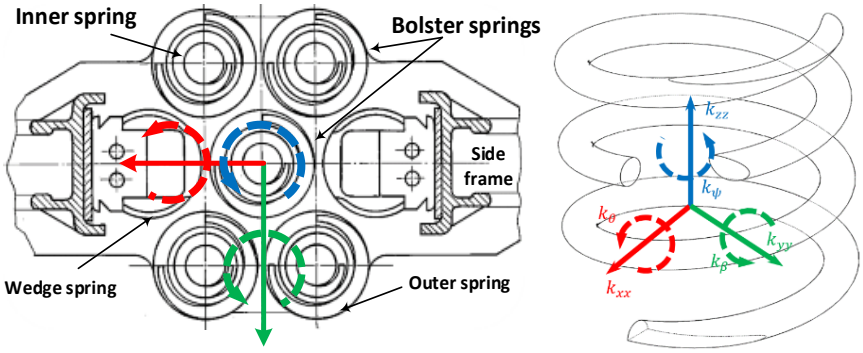

Figure 2.2: Multi-directional deflection and effective stiffness of suspension springs.

The effective stiffness of the suspension springs are thus defined considering the coupling among translational and rotational motions, and non-axial reaction forces, such that [113]:

$$\begin{bmatrix} F_x \\ F_y \\ F_z \\ M_x \\ M_y \\ M_z \end{bmatrix} = \begin{bmatrix} k_{xx} & 0 & 0 & 0 & k_{xx}H/2 & 0 \\ 0 & k_{yy} & 0 & -k_{yy}H/2 & 0 & 0 \\ 0 & 0 & k_{zz} & 0 & 0 & 0 \\ 0 & -k_{xx}H/2 & 0 & k_{\theta} & 0 & 0 \\ k_{yy}H/2 & 0 & 0 & 0 & k_{\beta} & 0 \\ 0 & 0 & 0 & 0 & 0 & k_{\psi} \end{bmatrix} \begin{bmatrix} x \\ y \\ z \\ \theta \\ \beta \\ \psi \end{bmatrix} \tag{2.1}$$

In the above matrix, k_{xx}, k_{yy} and k_{zz} are the effective stiffness of the wedges and bolster springs along the longitudinal (x), lateral (y) and vertical (z) axis, respectively. k_{θ} and k_{β} are the bending stiffness of the springs corresponding to angular deformations about x- and y- axis (θ and β), respectively. k_{ψ} is torsional stiffness attributed to yaw deformation ψ about the z-axis. F_x, F_y and F_z are the forces developed by each spring along the x, y, z axis, respectively, and M_x, M_y and M_z are the respective moments. In the above equation, H denotes the spring height. The effective

stiffness of the spring along each axis is related to the spring geometry, material properties, spring height and number of active coils, and given by [110, 113]:

$$k_{zz} = \frac{Gd^4}{64nR^3}; \quad k_{\psi} = \frac{Ed^4}{128nR}; \quad k_{xx} = k_{yy} = \frac{1}{\frac{1}{2(1+\nu)k_{zz}} + \frac{H^2(2+\nu)}{24k_{\psi}}}$$

$$k_{\theta} = k_{\beta} = \frac{2k_{\psi}}{(2+\nu) - \frac{H^2(2+\nu)}{8k_{\psi}\left(\frac{1}{2(1+\nu)k_{zz}} + \frac{H^2(2+\nu)}{6k_{\psi}}\right)}} \tag{2.2}$$

Where E and G are Young's and shear moduli of the spring material, ν is Poisson's ratio, d is the wire diameter, R is mean coil radius and n is number of active coils. Table 2.2 summarizes the equivalent stiffness values of the wedge and bolster springs, along the x, y, z, θ, β and ψ axes, which were computed for the typical spring designs (d=20 *mm*, R=56 *mm*, n=6.45 for inner spring; d= 30 *mm*, R=85 *mm*, n=4 for the outer spring) and their installation position. The height of each spring was taken as 256 *mm*, while the effects of variations in the height on the non-axial effective stiffness were neglected together with the damping due to the springs.

Table 2.2: Total effective stiffness coefficients of the secondary suspension springs supporting the wedge and the bolster.

Component	k_z (*kN/m*)	$k_x = k_y$ (*kN/m*)	$k_\theta = k_\beta$ (*kN·m/rad*)	k_ψ (*kN·m/rad*)
Wedge spring	585	479	12	5
Bolster spring nest	2,930	2,397	73/97*	25

*The bending stiffness of the bolster spring due to longitudinal/lateral deformations of the spring.

2.2.2 Frictional wedges modelling

The friction damping in the bogie is modeled considering the wedge geometry and its coupling with the bolster and the side frame. Using the modeling approach presented by Pogrelov *et al.* [114], *Universal Mechanisum* [110] and Wu *et al.* [23], each wedge in the truck suspension is modeled as a 6-DoF dynamic system considering its inertial properties. As shown in Figure 2.3, the wedge surface contacting the bolster is inclined at an angle of 45° (wedge angle, α), while the vertical face of the wedge contacts the side frame. The domain of the wedge contact surface with the side frame is described by the coordinates of four corner points in the lateral plane of the wedge and the side frame, $A_1..A_4$, and the corresponding normal plane of the side frame, denoted as $N_{side\ frame}$ in Figure 2.3(a). The contact domain of the wedge and the bolster is defined in a similar manner through coordinates of wedge edges contacting the bolster, $B_1..B_4$, and the normal plane of the bolster, $N_{bolster}$. There exists a lateral clearance (in the order of 1 *mm*) between the wedge and the bolster, which is incorporated by defining the contact points of the two side walls of the wedge, $C_1..C_4$, as shown in Figure 2.3(b).

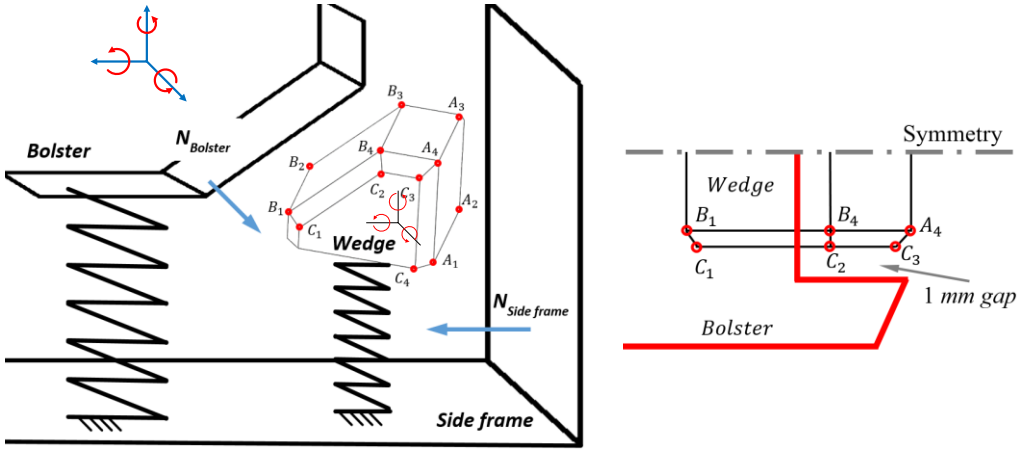

(a) (b)

Figure 2.3: Schematic of the contact points-planes between the wedge and the bolster, and wedge and the side frame; (a) Isometric view; and (b) top view of the bolster showing, 1 *mm* lateral gap between the wedge and the bolster.

The point-plane contact model available in *UM* platform is used to estimate the normal and friction forces at each contact point and surface. The normal forces in the point-plane contact are modelled assuming an elastic-dissipative function of penetration in the contact point as:

$$F_N = \begin{cases} K_c\Delta + C_c\dfrac{d\Delta}{dt} & \text{if } \Delta > 0 \\ 0 & \text{if } \Delta < 0 \end{cases} \tag{2.3}$$

where K_c and C_c are the contact stiffness and damping constants, respectively, and Δ is the penetration. The condition of the penetration simulates a unilateral normal contact model with zero adhesion. The simulations in the *Universal Mechanism* platform address the non-smooth characteristics associated with the stick-slip transition. The friction force, $\overrightarrow{F_s}$ in sticking phase is obtained considering the friction as a viscoelastic element. The resulting force $\overrightarrow{F_s}$ and dynamic deformation in the direction of the friction force is stored for addition in the successive integration steps to ensure the continuity of the friction force. The slip mode is assumed when the friction force magnitude exceeds $\mu_0 F_N$, where μ_0 is static friction coefficient. The sliding friction force is evaluated considering Coulomb's friction, such that $\overrightarrow{F_s} = -\mu_s F_N \vec{v}_s/|\vec{v}_s|$, where μ_s is dynamic friction coefficient, and $\vec{v}_s$ is the sliding velocity vector and F_N is normal contact force obtained from Equation (2.3). The dynamic friction coefficient μ_s is defined as a function of the sliding velocity considering the Stribeck velocity v_{str}, such that [110]:

$$\mu_s(v_s) = \mu_\infty + (\mu_0 - \mu_\infty)e^{-\left(v_s/v_{str}\right)^\delta} \tag{2.4}$$

Where μ_∞ is friction coefficient at a high sliding velocity, and δ is an empirical exponent used to smoothen the friction coefficients during sliding velocity transition.

2.2.3 Identification of contact parameters

The wedge contacts in the freight car suspension system constitute very high contact stiffness, which yield a stiff system of differential equations resulting in not only greater computational demand but also noise in the system responses [23]. The contact stiffness and damping properties, K_c and C_c, are identified considering the computational demand as well as the convergence of the system responses. The contact stiffness is estimated assuming that the oscillations in the contact forces acting on the wedges occur at substantially higher frequencies than the frequency range of the dominant dynamic responses that occur only up to 20 *Hz* [23, 110, 115]. An initial estimate of the contact stiffness is obtained assuming this frequency as 100 *Hz*, considering single-DoF dynamics of the wedge [23]. The contact stiffness is gradually increased up to 20 times the initially assumed value, and the resulting force-displacement responses are evaluated for both the convergence and computing time requirement in terms of the integration step-size. The contact stiffness was selected so as to achieve minimal high frequency oscillations in the contact force with a reasonable integration time step. For this purpose, a virtual test rig of the bogie was created in the *UM* platform considering vertical harmonic motion of the bolster. The test rig comprised the bolster and wedges, while the two side frames were fixed. A vertical harmonic displacement excitation was applied to the bolster at the vertical mode resonant frequency of the bolster, which is estimated from [116]: $f_z = \sqrt{(2K_z^b + 4K_z^w)/(m_b + 0.5 \times m_c)}/2\pi$, where K_z^b and K_z^w are effective stiffness of the bolster and wedge springs; m_b and m_c are masses due to bolster and car body, respectively.

The simulations were performed under 5 *mm* vertical displacement excitation considering static and sliding friction coefficients, μ_0 and μ_∞, respectively, as 0.30 and 0.25 for the wedge-side frame contact, and 0.12 and 0.10 for the wedge-bolster contact surfaces [23, 115]. The contact stiffness was varied from the initially assumed value of 8.29 to 165.8 *MN/m*, and the responses were obtained considering two different damping ratios (ζ= 0.01 and 0.1) due to contact damping constant, C_c. The equations of motion for the virtual test rig were solved using the Park method [110, 117] with time step varying from 1×10^{-12} to a maximum of 0.001 *sec*, and error tolerance of 1×10^{-8}.

Figure 2.4 illustrates variations in the vertical component of the bolster contact force with vertical motion and velocity for three different values of contact stiffness and two damping ratios.

The results were obtained for the unloaded bogie. The directions of loading and unloading during the motion cycle are also shown in the Figure 2.4. The simulation results indicate sharp changes in the contact force in the vicinity of low contact velocities due to stick-slip transition. Notable oscillations in the contact force are evident for the baseline contact stiffness value (8.29 *MN/m*), which tend to subside with increase in the contact stiffness. Increasing contact damping ratio, ζ, from 0.01 to 0.1 also diminishes oscillations in the contact force. Furthermore, only minimal variations in the contact force are observed with variations in the contact stiffness exceeding 7 times the baseline value (58 *MN/m*). This trend is attributed to the fact that a higher contact stiffness causes relatively smaller penetration of the contacting surfaces. The results thus suggest a convergence of the solutions with contact stiffness in excess of 58 *MN/m*, irrespective of the contact damping values considered in the simulations. The integration time step was generally around 0.1 ms for simulations corresponding to baseline contact stiffness, which gradually decreased to 0.025 ms, when the contact stiffness was increased 20 times (169 *MN/m*), suggesting substantially higher computational demand with higher contact stiffness.

The contact stiffness equal to 7 times the base value of 8.29 *MN/m* together with 0.1 contact damping ratio was subsequently chosen as a compromise to achieve relatively low oscillations and convergent solutions. Table 2.3 summarizes the selected wedge-bolster and wedge-side frame contact parameters for subsequent analyses.

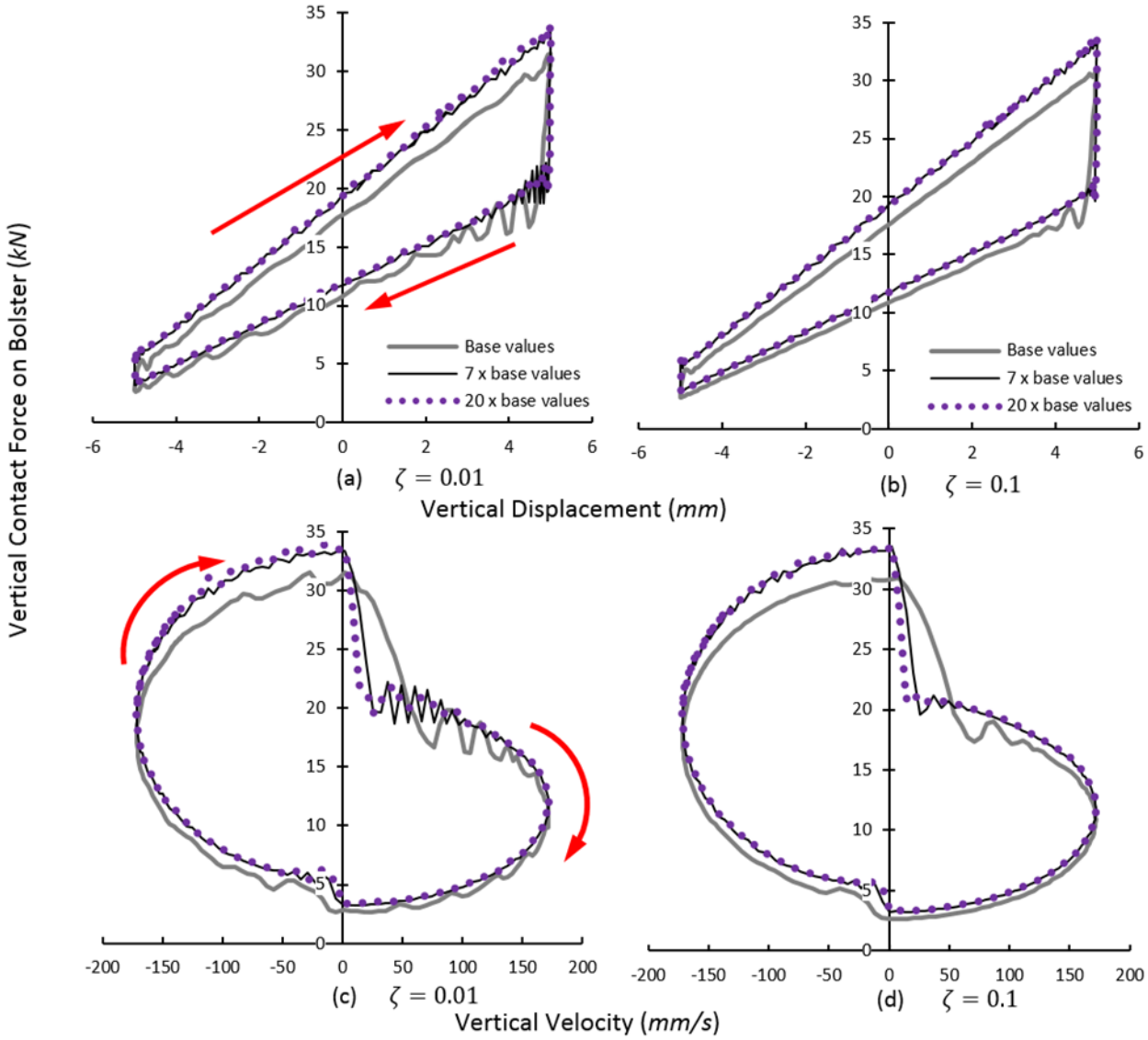

Figure 2.4: Effects of variations in contact stiffness and damping on (a,b) vertical contact force-displacement and; (c,d) vertical contact force-velocity response characteristics.

Table 2.3: Contact parameters of different components of the wagon.

Contact	K_c *MN/m*	C_c *kN·m/s*	μ_0	μ_∞	δ	v_{str} *mm/s*
Wedge-bolster	58	6.98	0.12	0.1	1	1
Wedge-side frame	58	6.98	0.3	0.25	1	1
Center plate-center bowl	135	340	0.20	0.17	1	0
Car body-side bearings	300	900	0.30	0.25	1	0
Axle box-Side frame	100	30	0.36	0.30	1	0

The contact force characteristics were further obtained for the loaded wagon by increasing the static springs' deflection to 30 *mm* to represent the loading condition, while the contact parameters are defined based on Table 2.3. The vertical excitation frequency of the bolster was decreased from 5.47 to 2.41 *Hz*, assuming 58 000 *kg* cargo load and axle load of 20 tons. Figure 2.5 illustrates variations in the resulting vertical contact force with the bolster displacement (limited to 5 *mm* amplitude) and velocity along the vertical direction for both the loaded and unloaded conditions. The results show significantly higher change in the forces of the loaded car near zero velocity, as it would be expected. The dissipated energy in the loaded condition is also significantly higher compared to that for the unloaded car. Moreover, the changes in the excitation frequency do not seem to affect convergence of the solutions. The identified contact parameters are thus considered adequate, irrespective of the variations in the frequency of bolster motion and loading condition.

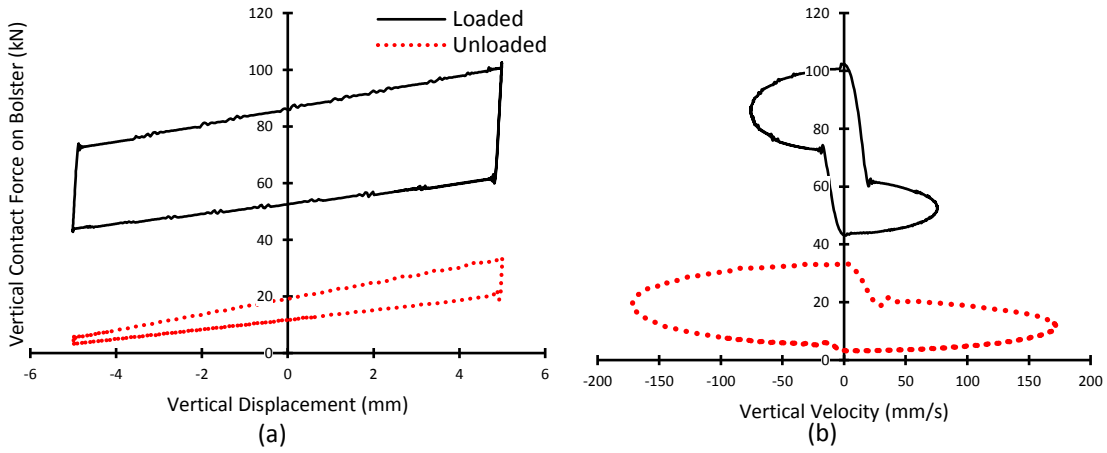

Figure 2.5: Effect of loading condition on response of contact forces in vertical direction; (a) force-displacement and (b) force-velocity responses.

The lateral components of the contact forces were also evaluated considering a harmonic excitation of the bolster along the lateral direction. The simulations were performed using the same test rig and identified contact parameters for both loaded as well as unloaded car. Figure 2.6 illustrates variations in lateral component of the contact force with displacement and velocity, obtained under 5 *mm* bolster displacement at 1 *Hz*. The results are presented for both loaded as well as unloaded car. The results show relatively small high frequency oscillations and significantly higher dissipated energy for the loaded condition compared to the unloaded car.

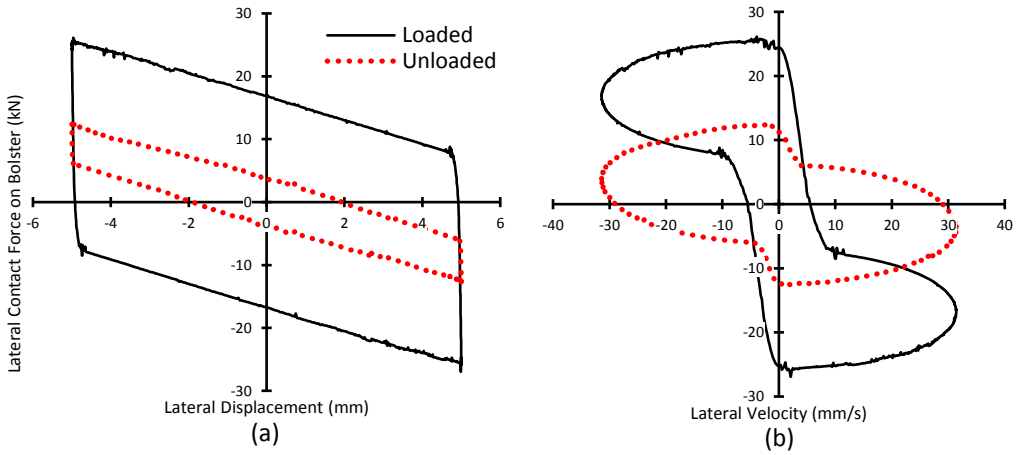

Figure 2.6: Lateral response of system subject to the lateral direction for loaded unloaded condition; (a) lateral displacement; and (b) lateral velocity.

Apart from the wedges contact, the model also considers the contact and friction forces/moments developed at the center plate and the side bearings, and between the axle box and the side frame. The hunting oscillations of the rail vehicle are known to contribute to substantial contact forces/moments and thus the damping, particularly in the yaw direction. The contact forces/moment developed at the center plate and the side bearings in addition to the connection between the axle box and the side frame are evaluated in the similar manner, and the identified contact parameters are summarized in Table 2.3, where the clearance between the car body and the side bearings is taken as 4 *mm*.

2.3 Stability analysis of wagon

The multi-body dynamic model of the three-piece bogie with the car body is used to evaluate lateral stability (hunting) limits in terms of the critical forward speed. The analyses are performed for the unloaded wagon. A multi-directional wheel/rail contact model incorporating the lateral, vertical and roll motions of the wheelset is used. The model also includes the flange contact, which is vital for an in-depth investigation of the hunting behavior. The Kalker's *FastSim* [104] algorithm is used to calculate the creep forces and moment in the contact patch. In this study, the contact region is discretized by 10 × 20 cells, and the normal and tangential forces are evaluated considering the UIC 60 rail profile and S1002 wheel profile with identical material properties. Each wheelset is modeled as a six-DoF dynamic system so as to permit the wheel to climb over the rail within the profiles constraints or hunting between the wheel and rail gap. The friction coefficient of the wheel and rail contact surfaces is taken as 0.25 for both the tread and flange regions.

One of the important parameters that affect the stability margin of the bogie is the rail inclination, the orientation of the rail profile about the longitudinal axis of the track, which is taken as 1/40 radian [3, 20, 107]. The given profiles and rail inclination lead to a single point contact condition, when the roll angle and lateral displacement of the wheelset are less than 1 degree and 6.7 *mm*, respectively. The two-point contact condition will then change to single point at flange for higher lateral movements. The methodology for treating the single and multiple wheel/rail contact conditions are described in the *Universal Mechanism* user's manual [110].

2.3.1 Sensitivity analysis of the lateral response of the system

The lateral dynamic responses of the leading wheelset were obtained under a harmonic lateral disturbance on a straight track at different speeds. The track disturbance is defined as a half-sinusoid lateral deviation Δy of the track with wavelength of 9 *m*. The chosen wavelength is comparable to the distance between the two center plates, which ensures yaw and lateral disturbances of the car body and the bogies.

The lateral dynamic responses of the leading wheelset, invariably, exhibit periodic motions, which may either decay with time (stationary) or assume sustained limit cycle depending upon the forward speed and the disturbance amplitude. As an example, Figure 2.7 illustrates the velocity-displacement phase plane orbits of the leading wheelset (critical wheelset) at two different speeds (17 and 23 *m/s*) under a 5 *mm* lateral disturbance. The results show that the wheelset motion decays with time at the lower forward speed of 17 *m/s*, where the disturbance energy is not sufficient to generate sustained periodic oscillations. Increasing the speed to 23 *m/s*, however, yields sustained oscillations of the wheelset limited by the wheel-rail guiding mechanism, as indicated in Figure 2.7(b). The steady-state peak velocity of the wheelset ($\dot{y}_w$) approaches near 150 *mm/s*. The amplitude of the lateral disturbance of the wheelset (y_w) approaches 7 *mm*, as constrained by the wheel-rail profile, leading to wheelset hunting. Slight oscillations observed in the phase-plane plot near ± 6 *mm* displacements are attributed to the downward sliding of the wheel after climbing over the rail.

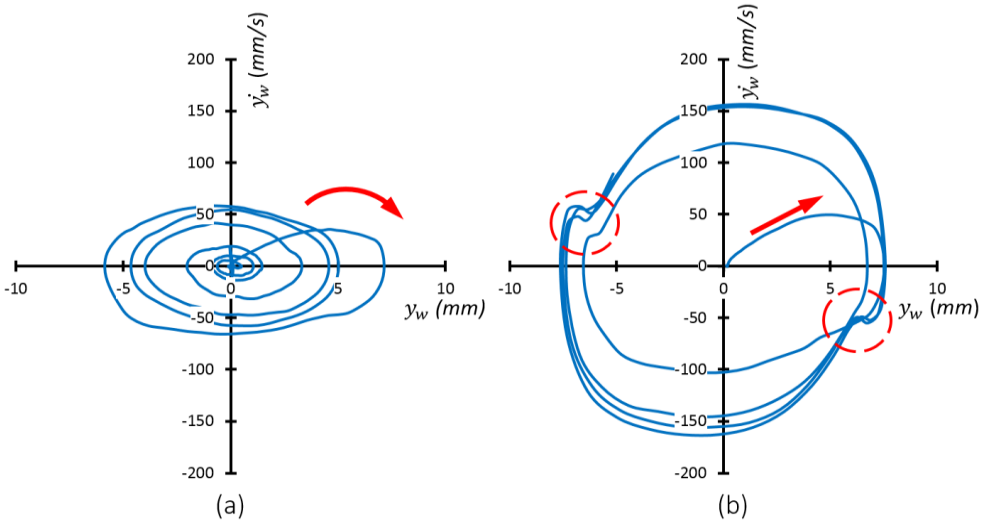

Figure 2.7: Phase plane orbits of the leading wheelset subjected to 5 *mm* lateral disturbance at two different speeds: (a) 17 *m/s* and (b) 23 *m/s*.

The lateral dynamic responses of the wagon are strongly dependent upon the forward speed and the rail disturbance amplitude. The hunting behaviour of the nonlinear model is thus investigated considering different disturbance amplitudes, ranging from 1 to 6 *mm*, at different speeds. The steady-state lateral displacement responses were analyzed to identify presence of wheelset hunting. Owing to the system nonlinearities, the lateral displacement oscillations were observed to be slightly asymmetric about the equilibrium position. The mean of maximum and absolute minimum values was thus considered as the amplitude of the wheelset lateral displacement. The simulations were performed for a period of 15 *s*, while last 5 *s* data were used for evaluating the steady state lateral displacement amplitude.

Figure 2.8 presents the lateral displacement amplitude response of the leading wheelset at different speeds, ranging from 19 to 24 *m/s*, as a function of the lateral disturbance. The results show that the lateral displacement amplitude increases with increasing disturbance amplitude and approaches steady-state values, irrespective of the forward speed considered. The displacement responses at different speeds, however, increase sharply and approach steady-state values under particular disturbance magnitudes suggesting the presence of hunting oscillations of the wheelset. The rapid increase in the response relates to transition of the stable damped response (stationary) to limit cycle periodic motion (hunting). At higher forward speeds, the hunting occurs under relatively small disturbance magnitudes. For instance, at 24 *m/s* the hunting is initiated under only 1.5 *mm* disturbance. At lower speed of 19 *m/s*, the hunting is observed when the disturbance exceeds 3.5 *mm*.

The results also show relatively lower amplitude peaks in responses corresponding to lower disturbance amplitudes (1.5 to 2.5 *mm*) at speeds up to 22 *m/s*. These peaks attributed to effects of car body hunting on amplitude of the wheelset motion. The car body hunting depends on the configuration of suspension system, and is reported to occur at relatively lower frequencies and speeds [9, 109, 118]. With increasing speed, the car body hunting tends to occur under relatively smaller displacement amplitudes. For a given speed, further increase in the disturbance amplitude tends to diminish the wheelset response amplitude, which is followed by rapid increase leading to wheelset hunting.

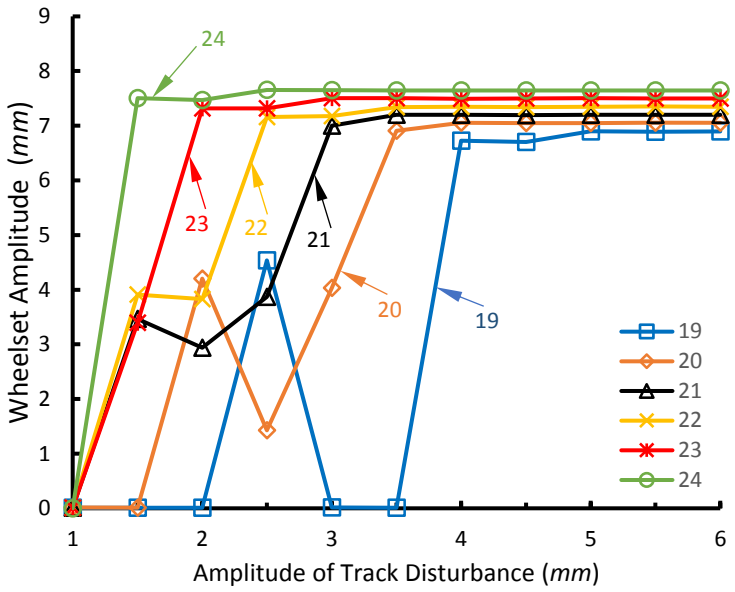

Figure 2.8: Lateral displacement responses of the first wheelset under varying magnitudes of lateral track disturbance at different speeds.

The frequency of lateral oscillations of a wheelset, according to the Klingel theory, is directly related to the forward speed [9, 107]. The effect of track disturbance and forward speed on the frequency of the limit cycle oscillations were further investigated using *Fast Fourier Transform* (*FFT*) technique. Figure 2.9 illustrates variations in the dominant frequency of steady state lateral wheelset oscillations as a function of the track disturbance amplitude and the speed. The responses of the railway vehicle systems in the presence of hysteric forces have been reported to be chaotic, especially at speeds higher than the critical speed [109, 116, 119]. The dominant frequency of the steady state response is thus considered for the analysis. The results presented in Figure 2.9 clearly indicate that the frequency of lateral oscillation in the critical wheelset is a function of both the forward velocity and the magnitude of the disturbance in a highly nonlinear manner. The frequency of hunting oscillations initiated at the speed of 18 *m/s* under track disturbances larger than 5 *mm* is about 2.5 *Hz*. This frequency is comparable with those reported by Xia and True [109] and Zhai and Wang [112]. At higher forward speeds, the lateral oscillations of the leading wheelset occur at a relatively higher frequency. The oscillation frequency of 3.2 *Hz* was obtained for the speed of 23 *m/s*. Frequencies within two narrow ranges were observed for the 20 to 22 *m/s* speed range under different track disturbance magnitudes. The lower frequency near 2 *Hz* is correlated to the low sway movements of the car body and its coupling with lateral oscillations of the wheelset.

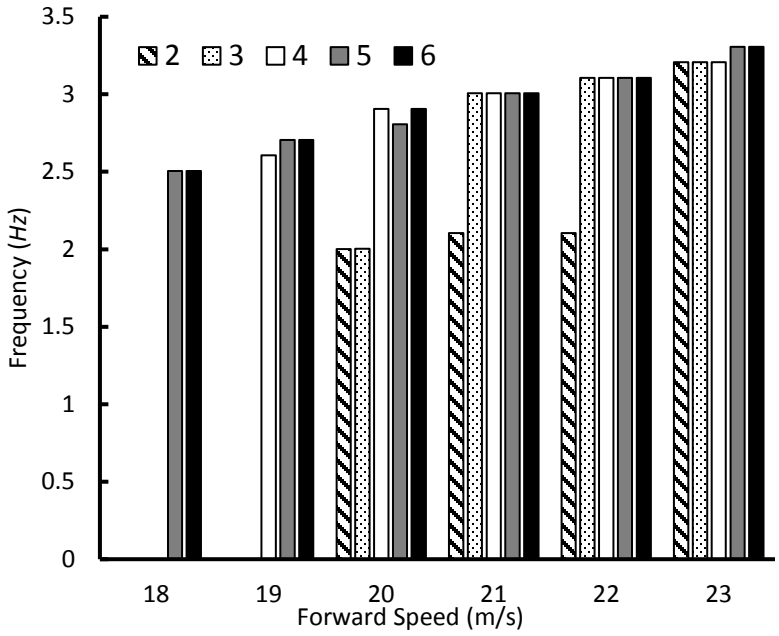

Figure 2.9: Variations in the dominant frequency of lateral movements of the first wheelset of the wagon as a function of the forward speed and lateral disturbance magnitude.

2.3.2 Bifurcation analysis

The hunting stability limit is frequently expressed in terms of critical speed, defined as the lowest speed leading to limit cycle motion of the wheelset within the flange clearance [9, 120]. The critical speed of the model is identified by constructing a bifurcation diagram, using the methodology presented by True [121] (also denoted as 'True strategy'), and Stichel [119]. Figure 2.10 summarizes the method used to construct the bifurcation diagram, a plot of wheelset lateral response magnitude vs the forward speed. The analysis method may also be used for identifying the super-critical bifurcation through response analyses under increasing speeds when the wheelset lateral amplitude is less than the available clearance between the wheel and the rail.

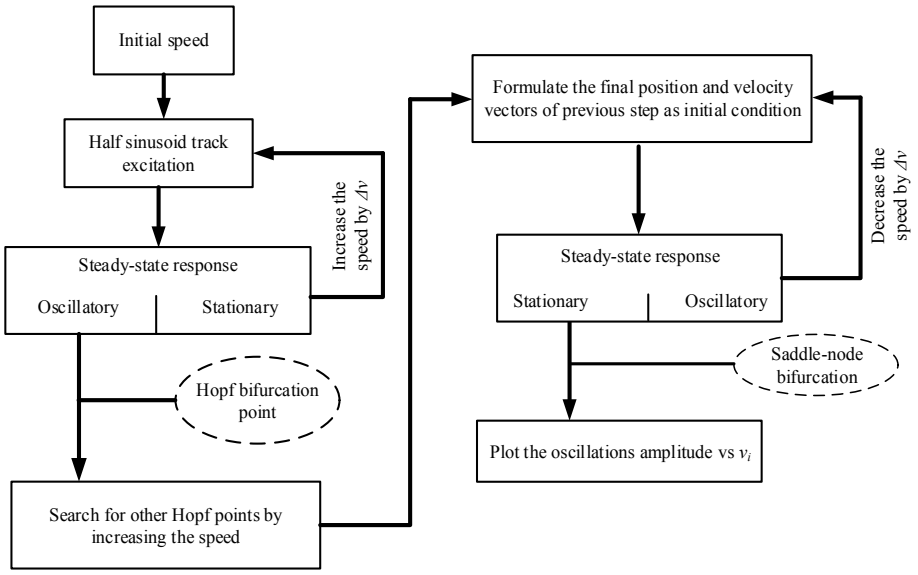

Figure 2.10: Simulation procedure for identifying bifurcation points and limit cycle response.

Repeated simulations were performed under increasing forward speeds (from 10 *m/s*) and track disturbance amplitude of 1 *mm*. The first bifurcation point is identified at a forward speed when the stationary solution loses its stability and a periodic hunting motion becomes evident. This transition from the stationary response of the leading wheelset to the periodic motion was observed at the forward speed of 32 *m/s*, as shown in Figure 2.11, which is the *Hopf* bifurcation point. The steady response of the system, however, is strongly dependent upon magnitude of the track disturbance (Figure 2.8) apart from the dominant frequency of track excitation (wavelength). The presence of the other bifurcation points should also be evaluated for higher speeds. The simulations were thus continued up to 40 *m/s* speed to identify the additional bifurcation points, if present. This

also permitted the analyses under relatively higher velocity excitations to reduce the sensitivity of the limit cycle response to the track excitation.

The forward speed was then gradually reduced (Δv=1 *m/s*), while the steady state position and velocity responses corresponding to excitation at the previous speed served as initial conditions. The steady-state lateral response amplitude of the wheelset decreased with decreasing speed, as shown by the bold line in Figure 2.11. The simulations were continued until a stationary solution was obtained at the speed of 15 *m/s* (Figure 2.11), which is considered as the saddle point, also termed as the critical hunting speed of the vehicle [109, 121, 122].

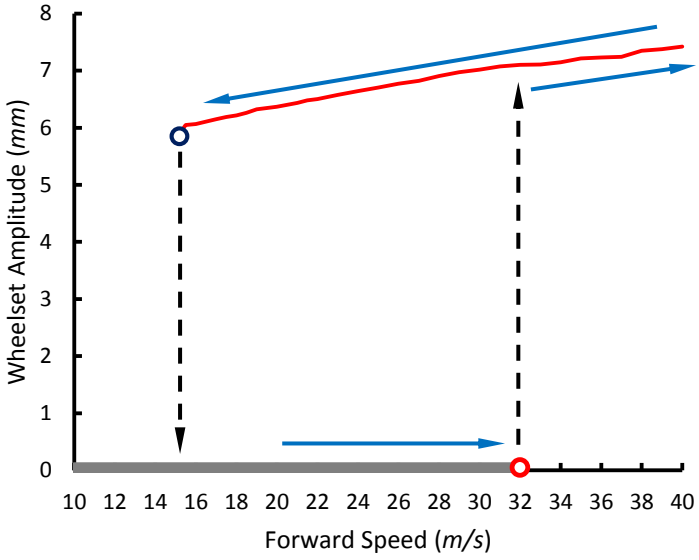

Figure 2.11: Bifurcation diagram of the response of the unloaded wagon with three-piece bogies.

The results in Figure 2.11 show the presence of a subcritical *Hopf* bifurcation, which has been reported in many studies on lateral dynamic responses of railway wagons with three-piece bogies in the presence of the hysteretic forces [101, 109]. The critical speed obtained from this analysis (15 *m/s*) is lower than that observed in Figure 2.9 (18 *m/s*), which is due to differences in the excitation conditions and the simulation method. The 'True strategy' method [121] imposes relatively higher disturbance energy associated with the initial conditions arising from hunting situation at a even higher speed. Such discrepancies in the critical speeds obtained using different approaches have also been reported in a some studies [120, 121]. The identified critical speed is also lower than 21.5 *m/s* reported by Zhai and Wang [112] through measurements and 20.5 *m/s*

reported by Xia [109] from simulations. These differences are likely due to differences in the test wagon configurations and modeling considerations, respectively. Zhai and Wang [112] reported the critical speed of a test wagon employing different bogies (Z8A), while Xia [109] considered relatively higher friction coefficients for wedge and center plates surfaces, which likely contributed to a higher critical speed.

2.3.3 Effects of wedge parameters on lateral stability of wagon

The critical speed and hunting stability of the wagon are strongly related to the effective damping of the secondary suspension. The geometry and friction coefficients of contacting planes of the wedges along with the clearances, determine the effective damping of the system. The proposed model of the wagon and the wedges is used to evaluate the effects of wedge parameters on the stability limits of the railway car. For this purpose, six different configurations of the wedges are considered involving two different wedge angles (45° and 60°) and variations in the friction coefficient, as summarized in Table 2.4. Type I and II configurations represent the wedge angle (α) of 45 and 60 degrees, respectively, while the those denoted as *Modified* are realized considering 20% higher friction coefficient. The *Symmetric* configurations in Table 2.4 consider identical friction between the wedge-bolster and wedge-side frame surfaces.

Table 2.4: Geometry and friction parameters of the selected wedge configurations.

Configuration		Wedge angle, α (degrees)	Friction Coefficient			
			Wedge-Bolster		Wedge-Side frame	
			μ_0	μ_∞	μ_0	μ_∞
Type I	Baseline	45	0.12	0.10	0.30	0.25
	Modified	45	0.14	0.12	0.36	0.30
	Symmetric	45	0.30	0.25	0.30	0.25
Type II	Baseline	60	0.12	0.10	0.30	0.25
	Modified	60	0.14	0.12	0.36	0.30
	Symmetric	60	0.30	0.25	0.30	0.25

Figure 2.12 illustrates bifurcation diagrams of the responses of the model employing the selected wedge configurations, which were constructed using the method described in Figure 2.10. While a subcritical *Hopf* bifurcation is observed in all cases, the effect of variations in wedge parameters on the bifurcation and saddle points are evident. Increasing the wedge angle from 45 to 60 degrees leads to relatively higher critical speed of the wheelset, irrespective of the friction coefficients. Increasing the wedge angle to 60° (Type II) from 45° (Type I) together with the baseline friction coefficients resulted in increase in the hunting speed from 15 and 19 *m/s*. This is due to greater inclination of the wedge surface and thereby friction force between the wedge and the bolster. Increasing the friction coefficients of the contact surfaces of the wedges by 20% however, revealed only smaller increase in the higher hunting speed for both the wedge types. The critical speed increases by nearly 1 *m/s* for both types of wedges, when the friction coefficient is increased by

20%, as seen in Figure 2.12. The results thus suggest that the wedge inclination contributes to higher effective damping compared to the friction coefficient. A combination of higher wedge angle and friction coefficients, however, could lead to a sustainably higher critical speed of 23 *m/s*. This is evident from the responses of the wagon with symmetric wedge configurations, where the friction coefficient of the wedge-bolster surfaces is increased significantly, as seen in Figure 2.12 (f). Orlova and Romen [26] also suggested that increasing the friction coefficient and the wedge angle could provide higher damping over the service life of the wedges.

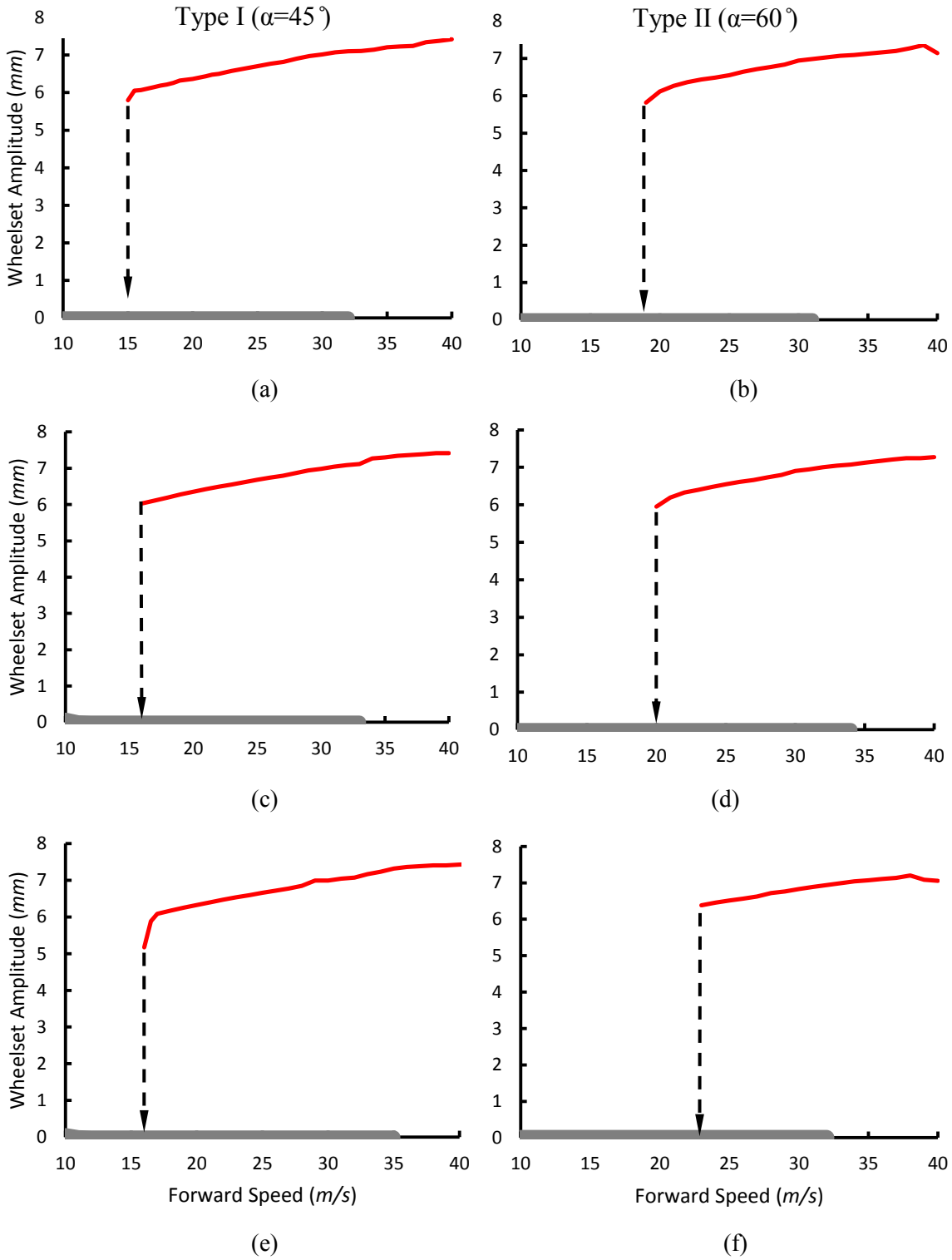

Figure 2.12: Influences of variations in wedge angle and friction coefficients on the bifurcation diagram: (a) Type I-Baseline (b) Type II-Baseline; (c) Type I-Modified; (d) Type II-Modified; (e) Type I-Symmetric; (f) Type II-Symmetric.

The amplitudes of response oscillations of the system may vary in a chaotic manner at relatively higher speeds in the presence of the friction forces [109, 119]. Simulations are performed to study the effect of friction coefficient on the amplitudes of lateral dynamic responses. As an example, Figure 2.13 illustrates the phase-plane orbital responses of the bolster motion of the wagon employing baseline wedges and their symmetric configuration with higher friction coefficients (Table 2.4) at a forward speed of 39 *m/s*. The bolster response with the baseline wedges is nearly symmetric about its equilibrium and it exhibits only minimal variations. Increasing the friction between the wedges and the bolster, however, yields considerable variations in response amplitudes. This is likely caused by the higher slip-stick tendency due to higher friction coefficient. The results thus suggest that higher friction could yield chaotic oscillations. Furthermore, higher friction causes nearly 5 *mm* offset in the bolster lateral displacement response with respect to the track centerline, as seen in Figure 2.13.

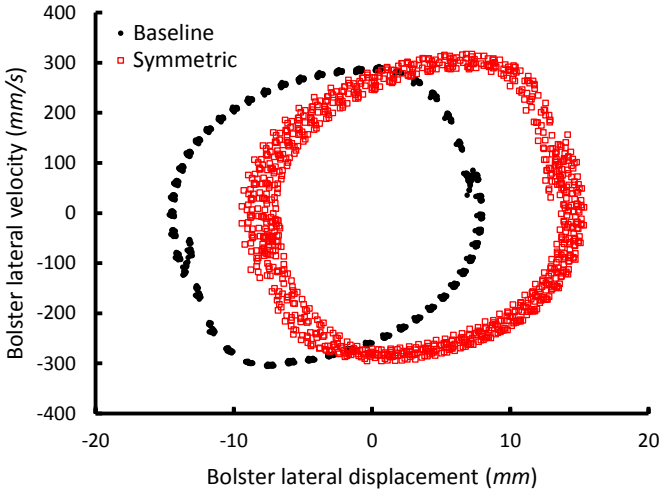

Figure 2.13: Influence of wedge-bolster friction coefficient on the lateral velocity-lateral displacement responses of the first bolster at a forward speed of 39 *m/s* (α=45°).

The friction forces developed at the wedge-bolster interfaces are also dependent upon the preload imposed by the suspension springs supporting the wedges. The effect of the springs' preload on the hunting critical speed is further investigated. The change in preload of spring is realized by increasing the free length of the wedge spring by 10 *mm* with respect to the baseline parameters employed in the previous simulations. The higher preload in the wedge springs, however, resulted in increase in the static *c.g.* height of the car body by 2 *mm*, while its effect on the kinematic

envelope of the wagon is considered negligible. The simulations were subsequently performed to identify critical speeds of the wagon employing six different configurations of the wedges (Table 2.4). Figure 2.14 illustrates the percent increase in critical speed for all configuration caused by increasing the springs preload. Increasing the spring preload resulted in notably higher critical speed, irrespective of the wedges configuration. The results suggest that increase in the preload due to wedge springs can enhance the hunting critical speed by as much as 30%, especially when coupled with high wedge angle (α=60̊) and higher wedge-bolster friction. The critical speed approaches 28 *m/s* with increased preload of *Type II* wedges coupled with symmetric friction coefficients. This is attributed to the fact that increasing the spring preload imposes higher normal force and thereby the friction force at the wedge interfaces with bolster and side frame.

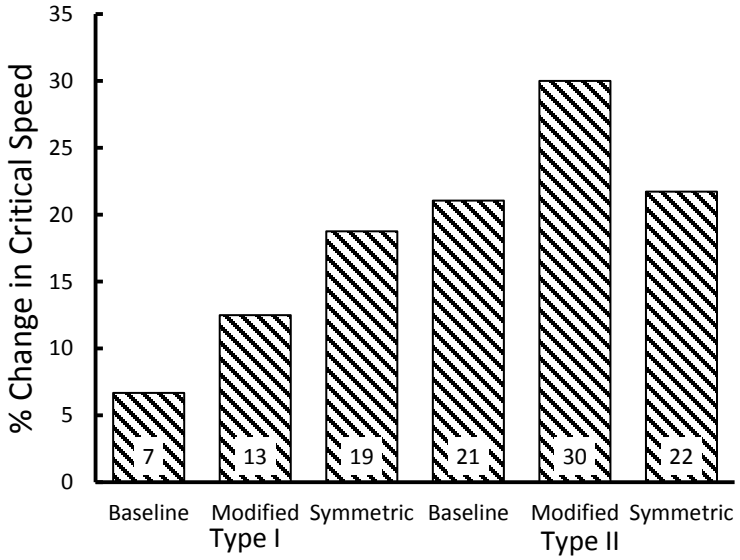

Figure 2.14: Percentage change in the identified critical speed by 10 *mm* preload of wedge springs.

2.4 Conclusions

A comprehensive model of friction wedges of the secondary suspension is formulated and integrated to the model of a freight wagon with three-piece bogies to study its lateral stability and critical speed limits with particular focus on nonlinear characterization of the friction wedges. Comparing to the reported methods for characterizing the damping properties of wedges, the proposed model based on points-plane contact method could describe the highly nonlinear responses of frictional wedges in a computationally efficient manner so as to facilitate parametric study. The results revealed relatively lower damping levels in both the lateral and vertical directions for the unloaded wagon compared to the loaded wagon. A subcritical *Hopf* bifurcation in the responses of the wagon was identified, which suggested a critical speed of 15 *m/s*. The sensitivity analysis of the nonlinear system revealed strong dependency of the response of the system on both the forward speed and the track disturbance amplitude. The simulation results further revealed hunting frequency of 2.5 *Hz* near the critical speed, which increased to about 3.2 *Hz* at higher speeds, where partial wheel climb was initiated. It was further shown that increasing the wedge angle could yield substantial gain in the critical speed, while increasing the friction coefficient of the contact surfaces resulted in only marginal increase in the critical speed. Increasing the surface friction, however, can cause greater chaotic oscillations in lateral dynamic responses of the system at higher speeds. Increasing the springs preload on the wedge could further help limit wheelset lateral oscillations leading to higher critical speeds. The proposed model of wedges contact could also be applied to evaluate the effects of worn wedges and increased clearances, and for identifying optimal wedge design.

CHAPTER 3

Hunting analysis of a railway tank car subject to the partially filled state of the tanker

3.1 Introduction

With increasing demand for high load capacity and high-speeds for railway freight cars, the safe operation of the railway rolling stock has been widely emphasized. The stability limits of railway vehicles have been extensively investigated to establish their safe operating limits and to seek improved designs [9, 10]. The phenomenon of lateral hunting oscillations of the rail vehicle near its critical speeds is known to cause substantial variations in the lateral wheel-rail forces that may lead to greater derailment or track panel shift potential.

Apart from wheel/rail and component forces, the dynamic responses of a partly filled railway tank wagon may be affected by the forces and moments caused by the fluid motions, known as sloshing. While the potentially destabilizing effects of slosh forces and moments have been widely reported for road tankers, only a few studies have investigated such impacts in rail vehicles, especially for the hunting analysis [25, 123]. The dynamic response of partially-filled tank vehicles has been studied with different approaches to derive forces and moments due to cargo slosh within a partly-filled tank, which range from simple quasi-static [7], mechanical-equivalent [87] to nonlinear fluid slosh models [84].

The quasi-static analysis of slosh is a simplified approach to analyze the steady-state directional performance and roll stability of vehicles. It has been shown that transient slosh dynamic forces and moments are substantially higher than the magnitudes of steady-state forces predicted from the quasi-static approach [84]. On the other hand, the nonlinear *Computational Fluid Dynamic* (*CFD*) methods permit the analysis of transient slosh forces and moments but their applications to vehicle dynamics analyses have been limited due to excessive computational demands [63-65]. Alternatively, the linear slosh theory or mechanical equivalent models based on linear theory have been applied to evaluate cargo movements and slosh forces. It has been suggested that the linear theory can efficiently predict slosh responses under low magnitude excitations, but may lead to considerable errors in the vicinity of the slosh resonance frequencies [64, 75, 90]. The mechanical equivalent models of liquid can be conveniently integrated into the multibody models of a vehicle system for response analysis of the coupled vehicle-cargo system in a time-efficient manner. The

parameters of such models are commonly identified from linear slosh theory or through laboratory measurements [86, 87].

The studies reporting the fluid slosh effects in railways have mostly employed simple pendulum models or equivalent models [3, 94, 95]. Khandelwal and Nigam [91] employed a pendulum model to study liquid slosh in a rectangular tanker coupled with bounce and bounce/pitch models of a wagon subject to track irregularities and longitudinal acceleration. The study showed that fluid slosh could serve as a damper when excitation frequencies are distant from the fundamental slosh frequency. Bogomaz *et al.* [92] developed the roll, pitch and yaw plane models of a partly-filled tank car using equivalent pendulum models of fluid slosh, and identified the model parameters from solutions of the boundary value problem over the liquid domain coupled with a modal solution of the free surface. The simulation model in the pitch plane alone was validated through tests conducted on a tank car subject to longitudinal impacts at different speeds. The simulation results obtained with simplified models of a tank car incorporating linear suspension and wheel/rail contact revealed notable contributions of fluid slosh to lateral and vertical accelerations under excitations caused by rail irregularities and curving.

Di Gialleonardo *et al.* [94] investigated the wheel unloading and thus derailment potential of a partly-filled railway tank car subject to 'S'-curve maneuvers at different speeds. The simulation results obtained with a 35 degree-of-freedom (DoF) model of a 4-axle tank car revealed relatively higher wheel unloading in the presence of fluid slosh. Relatively higher wheel unloading was reported for the third wheelset during the trailing section of the s-curve, while liquid sloshing only marginally affected the flange climb derailment. The study also showed greater load shift when the 'S'-curve frequency was close to the natural frequency of the mechanical-equivalent model.

The lateral slosh force and roll moment, in particular, could alter the dynamic forces developed at wheel-rail contact and thereby affect the hunting stability of partly-filled tank wagon. The effect of liquid cargo movement within a partly-filled rail car on its hunting speed, however, has been attempted in a few recent studies [25, 123]. Hazrati *et al.* [25] reported that the liquid cargo movements within the tank car could serve as a damper for suppressing lateral hunting oscillations. The equivalent pendulum model proposed by Salem *et al.* [87] was used for simulation of lateral liquid slosh. This trend was likely due to the relatively higher frequency of hunting oscillation compared to the fundamental slosh frequency as suggested by Khandelwal and Nigam [91]. Wang *et al.* [123] proposed the integration of a low order continuum based slosh model with a multibody

model of a railway tank car incorporating viscosity and inertia distribution. The approximate runtime was reported as 1440 seconds for each second of simulation on a single-core Intel Core i5-2400 processor platform. The significant contribution of the liquid slosh on resulting variations in wheel-rail contact condition was observed. Shi *et al.* [5] examined the effect of liquid slosh on curve negotiation and braking scenarios of a railway tank car. The absolute nodal coordinate formulation (*ANCF*) was used to capture the response of the liquid cargo. The study showed that the liquid cargo slosh in curve negotiations at speeds higher than the balanced speed could generate excessive unloading effect.

In this study, the hunting response of a partly-filled tank wagon is investigated using a linear slosh model proposed by Kolaei *et al.* [64, 99] and compared with those obtained from a simple pendulum slosh model. The dynamic fluid slosh models are integrated to a comprehensive model of the wagon incorporating non-smooth and nonlinear damping and stiffness properties of friction wedges, as described in [34]. The effect of slosh force and moment on the hunting critical speed is demonstrated by comparing the responses of the car with equivalent rigid cargo. The hunting performance in terms of critical speed is obtained as a function of the liquid cargo fill ratio considering constant cargo load.

3.2 Model formulation

3.2.1 Multi-body model of the tank car

The multi-body dynamic (*MBD*) model of a railway tank car is developed in *Universal Mechanism* (*UM*) software [110, 124], incorporated a car body and a pair of three-piece bogies. Each bogie is modeled considering nine rigid bodies, including friction wedges, side frames, wheelsets and bolster, which are coupled through contact surfaces and suspension springs. The couplings of the car body with the bogies are incorporated through the center plate and side bearings of each bogie. A 114-DoF model of the railway tank car is thus formulated in the *UM* software considering 6-DoF motions of each rigid body subject to constraints imposed by unilateral contact forces generated in the wedges, center plate and side bearings in addition to multi-axis forces due to suspension springs and wheel/rail contact. The simulation parameters for the dynamic model of the wagon along with the methodology to identify contact pairs parameters have been presented in details in [34].

The friction forces in different components of the bogie are modeled considering their geometry and clearances. The point-plane contact approach is used for simulation of the friction forces [34, 124]. The normal forces in the point-plane contact are modeled assuming an elastic-dissipative function of penetration of the contact point. The Coulomb friction model is used to simulate the friction force in the contact plane, considering the sliding and sticking conditions. The Stribeck formulation is used to simulate the transition from static friction to the dynamic condition [34, 110]. The clearances between different components of the vehicle system are also incorporated in this contact simulation approach. As indicated in Figure 3.1, the gap between wedge and bolster, t_b^w, provides a lower lateral stiffness for lateral movements smaller than 10 mm. The clearances between the wedges and the side frame is defined so as to limit the lateral movements of the bolster and wedges with respect to the side frame. The stiffness and damping constants of the contact elements are defined as 58 MN/m and 6.98 k$N.m/s$, respectively, based on methodology presented in [34]. Moreover, the clearances between the wheelset and the axle box, presented in Figure 3.1(b), are defined as 3 mm in the lateral and longitudinal directions.

The roll angle of the car body is constrained via interaction of the car body with the bolster in center plate and side bearings. A group of unilateral contact points simulates the interaction of components in the center plate, as shown in Figure 3.1(c). The static and dynamic friction

coefficients of 0.2 and 0.17, respectively, are assumed, as suggested in [28, 125]. Moreover, a 4 *mm* gap between the side bearing and the underfloor of the car body is assumed to simulate the unworn condition of the conventional side bearing. Higher values of friction dynamic and static coefficients (0.25 and 0.3, respectively) are assumed for the contact points within the bearing contact [28, 35].

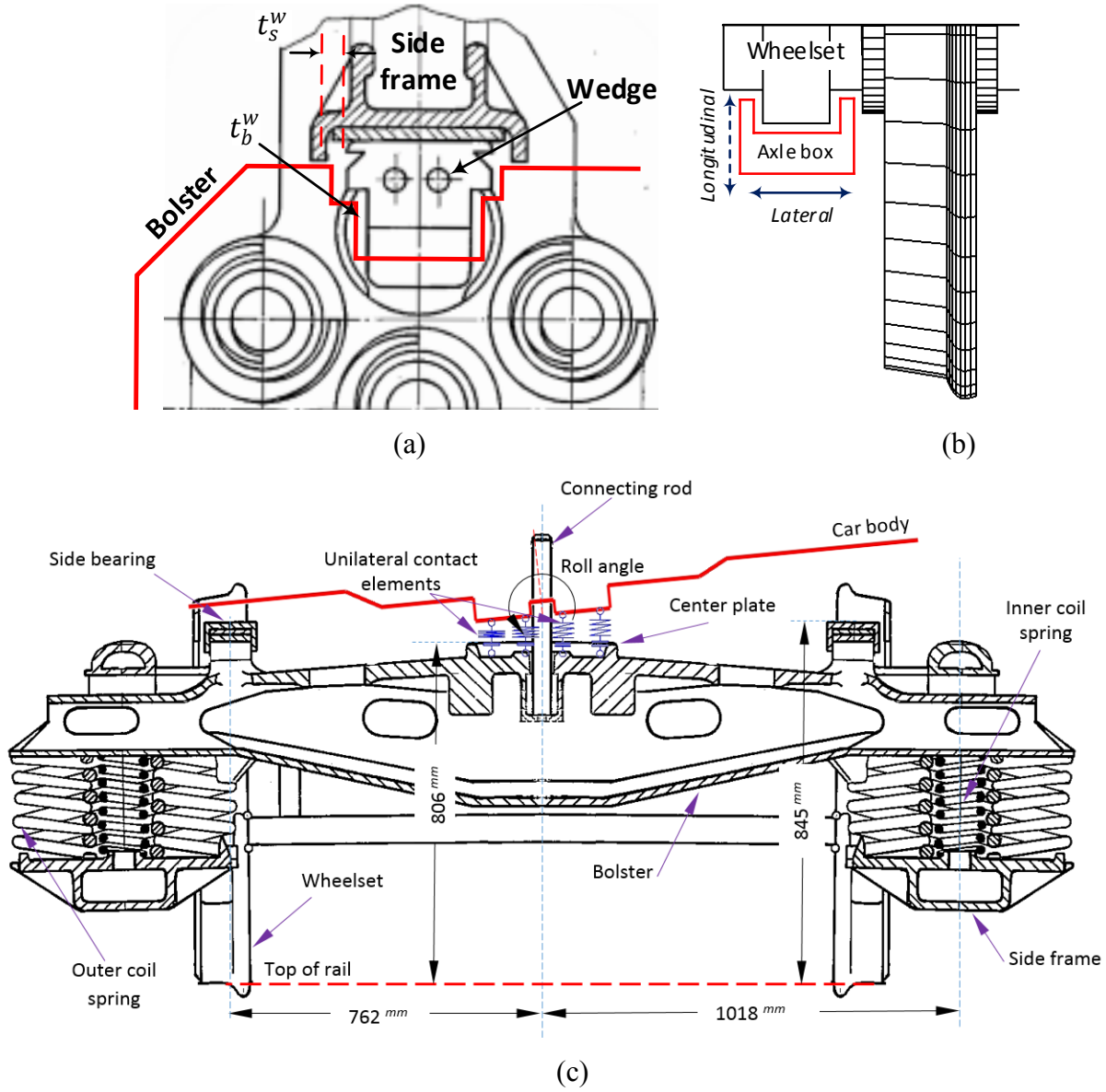

Figure 3.1: Schematic view of the clearances between (a) the wedge and the bolster/side frame; (b) the wheelset and the axle box; and (c) the car body and the bolster via the center plate.

A multi-directional wheel/rail contact model is formulated incorporating the lateral, vertical and roll motions of the wheelset, including the flange contact, which is vital for an in-depth

investigation of the hunting behavior. The Kalker's *FastSim* model [104] is applied to determine the creep forces and moment at the wheel/rail interface considering an elliptical contact patch. For this purpose, each contact patch is discretized into 10 equal width strips along the rolling direction of the wheel, while each of these strips is further divided into 10 cells of equal length. The slip or stick condition of each cell and resultant tangential contact forces is determined based on Kalker's *FastSim* algorithm [104].

3.2.2 Liquid cargo slosh analysis

The additional dynamic loads due to partly-filled liquid cargo within the tank car are analyzed using two approaches: a simplified pendulum model and linear slosh theory considering summation of lower free surface oscillation modes, as shown in Figures 3.2(b) and (c), respectively. The liquid cargo is also represented by an equivalent rigid cargo, as shown in Figure 3.2(a). In case of the simple pendulum model, the cargo mass is free to rotate around the geometric center of tank (point *O*) at the fundamental oscillation frequency, which is expressed as a function of the liquid cargo fill ratio, as $\sqrt{g/z_{c.g.}}/2\pi$ *Hz*. $z_{c.g.}$ is the vertical coordinate of the liquid cargo mass center for a given fill ratio, defined as the ratio of fill height to the tank diameter, with respect to the geometric center of the tank. The single-degree-of-freedom pendulum model of the liquid cargo is integrated to the vehicle model to study the response characteritics of the coupled liquid cargo and tank car model.

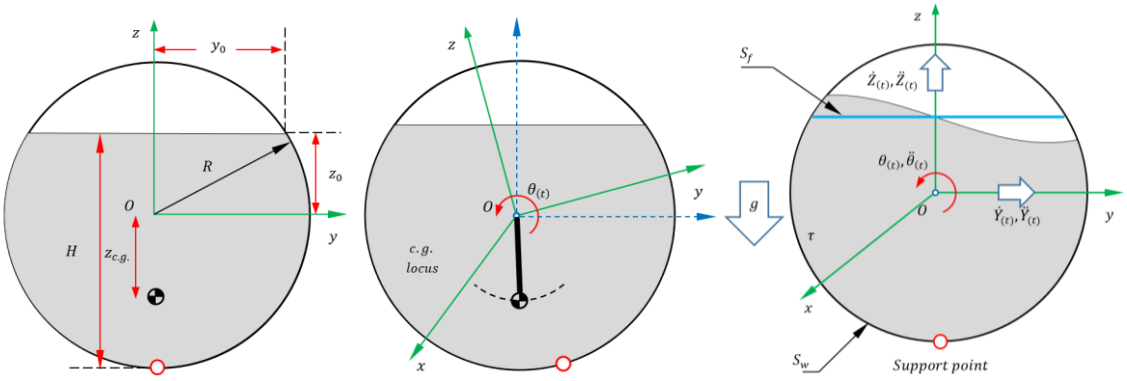

(a) (b) (c)

Figure 3.2: Different cargo models and partially filled terms, (a) frozen, (b) pendulum and (c) liquid slosh models.

The tank car may experience notable roll and yaw motions during curving or while hunting, apart from the lateral motion. The simple pendulum model cannot account for free surface motion caused by roll and yaw motions of the vehicle. Moreover, the pendulum model is limited only to the fundamental slosh modes, while it has been shown that the free surface motion in road tankers is more appropriately described by summation of the lower four modes. Considering that the hunting mode frequency is substantially higher than the fundamental mode slosh frequency (near 0.5 *Hz*), the simple pendulum model may not accurately describe the slosh force and moment. Alternatively, linear slosh models, proposed by Kolaei *et al.* [64, 99], and Faltinsen and Timokha [126], may be applied to incorporate the contributions of higher oscillation modes, in addition to the roll as well

yaw motions of the car, in a computationally efficient manner. In this study, the linear slosh model based on modes summation, proposed by Kolaei *et al.* [64, 99], is used considering the lower four antisymmetric modes. For the partly-filled cylindrical tank of radius *R* and liquid fill height *H*, shown in Figure 3.2(a), the equations of fluid motion in the roll plane are derived in the tank-fixed coordinate system *Oyz*, while the tank is subjected to simultaneous lateral, vertical and roll motions. The coordinates of the free-surface at the intersection of the tank wall are denoted by y_0 and z_0, as shown in Figure 3.2(a). In Figure 3.2(c), τ, S_f and S_w represent the fluid domain, liquid free-surface and wetted surface of the tank wall, respectively. Assuming incompressible and irrotational flow in the flow domain τ, the equation of motion of the liquid is formulated in the form of the Laplace equation of velocity potential function Φ, as:

$$\boldsymbol{\nabla}^2\Phi = \boldsymbol{\nabla}^2(\Phi_{\mathrm{R}} + \Phi_{\mathrm{S}}) = 0 \qquad \text{in} \qquad \tau \tag{3.1}$$

where Φ_{R} and Φ_{S} represent the velocity potential attributed to the rigid body motion of the liquid bulk and relative motion to the liquid cargo with respect to the tank in the liquid domain, τ. For a cylindrical tank subject to lateral, vertical and roll excitations, the rigid body potential, Φ_{R}, can be expressed as:

$$\Phi_{\mathrm{R}} = \dot{Y}(t)y + \dot{Z}(t)(z - z_0) + \dot{\theta}(t)\Phi_{st} \tag{3.2}$$

where $\dot{Y}(t)$ and $\dot{Z}(t)$ are the lateral and vertical velocities of the container, respectively. The Φ_{st} is the potential associated with rolling motion of container, $\theta(t)$, which is known as the Stokes-Joukowski potential [78, 126]. It has been reporting that the effect of viscosity of commonly transported products is negligibly small compared to the inertia effect [126, 127]. The rigid body potential, Φ_{R}, thus does not depend on the roll rate of the container. Using the multimodal approach [28], the potential Φ_{S} can be expressed as a function of the lateral, vertical and roll motions of the liquid free surface through superposition of natural modes, φ_i:

$$\Phi_{\mathrm{S}}(y, z, t) = \sum_{i=1}^{\infty} \gamma_i(\mathrm{t})\varphi_i(y, z) \tag{3.3}$$

Where γ_i represent the generalized coordinates. The modal superposition together with the free-surface boundary condition are applied to express the free surface motion by a set of ordinary differential equations in the generalized coordinates, γ_i:

$$\ddot{\gamma}_i + 2\xi_i\sigma_i\dot{\gamma}_i + \sigma_i^2\gamma_i = -\ddot{Y}\frac{\kappa_i\lambda_i}{y_0} \qquad \text{on } S_f \tag{3.4}$$

where $\ddot{Y}$ is the effective lateral acceleration encountered at the geometric center of the container, which accounts for contribution of roll motion of the container. σ_i is circular frequency of the free surface oscillations, which is related to $\kappa_i = {\sigma_i}^2/g$, where g is acceleration due to gravity. In the above equation, λ_i and ξ_i are the time-invariable hydrodynamic coefficients and modal damping ratios attributed to liquid viscosity , respectively, given by [78, 99]:

$$\xi_i = \frac{v_s^{0.5}}{2\sqrt{2g^{0.5}R^{1.5}}}\left[{\kappa_i}^{-0.25}\left\{\frac{\bar{\psi}_i}{\kappa_i y_0} + \frac{R}{L}\right\}\right] \tag{3.5}$$

$$\lambda_i = \int_{S_f} y\varphi_i dS \tag{3.6}$$

where ν_s is the fluid kinematic viscosity and L is length of the tank, and $\bar{\psi}_i$ is the normalized damping ratio that depends on the tangential velocity at the wetted boundary, and obtained from:

$$\bar{\psi}_i = \int_{S_f}\left(\frac{\partial\varphi_i}{\partial s}\right)^2 dS \tag{3.7}$$

It should be noted that the λ_i for symmetric modes are zero and only the antisymmetric modes are excited by the lateral acceleration and roll angle responses of the container. Since the coefficients in differential equations (3.4) are time-independent, these are not required to be evaluted at each time step and under different exteranl inputs. This ensures computational efficiency of the modal method and facilitates co-simulations of the liquid slosh model with the vehicle dynamic model. The natural slosh modes and frequencies are obtained using the Ritz variational method [16], while

solutions of the differential equations (3.4) yield hydrodynamic pressure distribution, $P(y,z,t)$ using the linearized Bernoulli's equation [126]. The total lateral force, $F_y(t)$, acting on the container wall, per unit length of the container, is then obtained from integration of $P(y,z,t)$ over the tank wetted area, S_w, such that:

$$F_y(t) = \int_{S_w} P(y,z,t)dz = F_{y,R}(t) + F_{y,S}(t) \tag{3.8}$$

The lateral slosh force can also be expressed in two components, $F_{y,R}$ and $F_{y,S}$, attributed to rigid body and free surface motion of the liquid, respectively, expressed as:

$$F_{y,R}(t) = -\rho\ddot{Y}\int_{S_w} ydz = -m(\ddot{Y} + \theta g) \tag{3.9}$$

$$F_{y,S}(t) = -\frac{\rho}{g}\sum_{i=1}^{\infty}\lambda_i\sigma_i^2\dot{\gamma}_i(\mathrm{t}) \tag{3.10}$$

where m is fluid mass per unit length of the tank and ρ is fluid density (Figure 3.2). The vertical force acting on the container, $F_z(t)$, can also be obtained from:

$$F_z(t) = F_{z,R}(t) = \int_{S_w} P(y,z,t)dy = -m(g + \ddot{Z}) \tag{3.11}$$

It should be noted that the vertical component of the slosh force is zero, $F_{z,S}(t) = 0$, due to geometric symmetry of the circular tank. The moment due to liquid cargo motion about the support point of tank can be determined by integrating the hydrodynamic pressure over the wetted surface of the tank:

$$\begin{aligned} M_{Support}(t) &= -\int_{S_w} P(y,z,t)\,[ydy + (R+z)dz] \\ &= M_R(t) + M_V(t) + M_S(t) \end{aligned} \tag{3.12}$$

The above equation yields total overturning moment of liquid cargo for the unit length of the tank, which may be expressed as summation of three different components, namely, the rigid body moment (M_R), moment due to vertical load transfer (M_V) and moment due to lateral slosh force (M_S). These components are obtained from:

$$M_R(t) = \rho(\ddot{Y} + \theta g) \int_{S_w} y(R+z)dz = m\left(R + z_{c.g.}\right)(\ddot{Y} + \theta g) \tag{3.13}$$

$$M_V(t) = \rho(\ddot{Y} + \theta g) \int_{S_w} y^2 dy = \frac{2}{3}\rho y_0^3(\ddot{Y} + \theta g) \tag{3.14}$$

$$M_S(t) = \frac{\rho}{g}\, R \sum_{i=1}^{\infty} \lambda_i \sigma_i^2 \dot{\gamma}_i(\mathrm{t}) = R \times F_{y,S}(t) \tag{3.15}$$

The component $M_V(t)$ can be regarded as the moment due to lateral shift of the liquid cargo subject to lateral acceleration and roll motion of the tank.

The yaw oscillations of car body constitute the essential oscillation mode in hunting of a railway wagon, while its effect on resulting slosh force and moment has been invariably neglected. The multimodal method is further refined to estimate the contribution of the yaw excitation. For this purpose, the liquid in the entire tank length is divided into n equal length flow domains. The effective lateral acceleration excitation, $\ddot{Y}^1 \ldots \ddot{Y}^n$, is evaluated for each flow domain of length dl considering the yaw response and the geometry. The potential functions and the resulting slosh force and roll moment for each flow domain are subsequently evaluated through solutions of equations (3.4) via co-simulations of the vehicle and slosh models, as shown in Figure 3.3.

3.3 Method of analysis

The *MBD* model of the railway tank car coupled with liquid slosh model is evaluated to identify the critical speeds corresponding to a lateral instability (hunting). In complex dynamic models with non-smooth contact forces, it is utterly difficult to find the critical hunting speed of the vehicle using specific methods such as path following [35, 105]. On the other hand, linearized hunting in the presence of non-smooth friction forces in the suspension system of the wagon could lead to considerable errors [35, 121]. In this study, the hunting critical speed is initially identified under a single track disturbance with lateral amplitude of 5 *mm* and wavelength of the 11 *m*, as suggested in [28, 35]. The response of the vehicle subject to this excitation is evaluated for different forward speeds to identify different *Hopf* points of the system, where the steady-state response of the system changes from stationary to undamped oscillatory response. Subsequently, forward speed of the vehicle is gradually decreased from the that corresponding to the unstable condition with a relatively small longitudinal deceleration to identify the saddle-node in the bifurcation diagram, where the undamped oscillatory response of the system changes to damped stationary response. The multi-directional friction forces generated in different components of the suspension, as well as wedges, center plate and side bearings, in addition to creep forces in the wheel-rail interface, contribute to gradual attenuation of the oscillatory response.

The simulations are performed for the ORE-S1002 and UIC 60 wheel/rail profiles considering negligible rail inclination. The wheel-rail friction coefficient is assumed as 0.5 in the flange and tread contact regions, considering the standard gauge (1.435 *m*). The length of the 2.8 diameter tank is taken as 12 *m*, while the contributions due to of curved end caps are assumed negligible. The simulations are perfumed for different fill ratios, while the total cargo load is held constant (596 *kN*). Three different fill ratios are considered by varying the liquid cargo density, as illustrated in Table 3.1. A higher density of cargo such as sulphuric acid would lead to a lower *c.g.* position and fill ratio, while it would lead to greater liquid cargo movement, and thus higher slosh force and moment. The stiff system of differential equations is solved using the Park method [110], where the time step is permitted to vary from minimum of $1\times10^{-12}s$ to maximum of 1 *ms* with an error tolerance of 1×10^{-8}.

Table 3.1: Fill conditions under of tank car subject to different liquid cargos.

Liquid cargo	Fill ratio	Density (kg/m^3)	Dynamic viscosity (m^2/s)	*c.g.* height* (m)	Fundamental natural frequency of cargo (Hz)	
					Pendulum	Liquid
Fuel	97%	800	5×10^{-6}	0.012	4.57	1.01
Water	74%	1000	1×10^{-6}	0.252	0.99	0.57
Sulfuric acid	45%	1817	14.5×10^{-6}	0.670	0.60	0.47

*) with respect to geometry center of the tank car.

The simulations are performed for the coupled liquid-slosh and the vehicle model in a co-simulation manner using three different liquid slosh models. These include the simple pendulum model, uniform multi-modal linear slosh model along the tank length neglecting contribution due to yaw excitation, and linear slosh model under excitations incorporating the yaw excitation. The liquid slosh model is solved in Matlab/Simulink based on time invariable coefficients for a given fill ratio. The co-simulation is initiated at time $t = 0$ assuming negligible force and moment attributed to cargo slosh ($F_{y,S}(t) = 0; M_V(t) = 0$). The lateral, roll and yaw responses of the tank car are used to obtain the liquid slosh force and moment responses in a subsequent instant. The dynamic responses of the tank car with liquid cargo at the same instant are evaluated by integrating the lateral slosh force $F_{y,S}(t)$ and roll moment $M_V(t)$ into the vehicle model via the co-simulation scheme. The validity of the slosh models is initially examined on the basis of reported modal frequencies and hydrodynamic coefficients. The model is then used to identify the critical hunting speed of the tank car under different fill conditions.

The hunting critical speeds are also obtained for the equivalent rigid cargo model, which would permit the assessments of the liquid slosh effects. The equivalent rigid cargo model also represents the contributions due to vertical and lateral inertial forces, $F_z(t)$ and $F_{y,R}(t)$, and the corresponding roll moment, $M_R(t)$ attributed to the rigid body motion of the cargo.

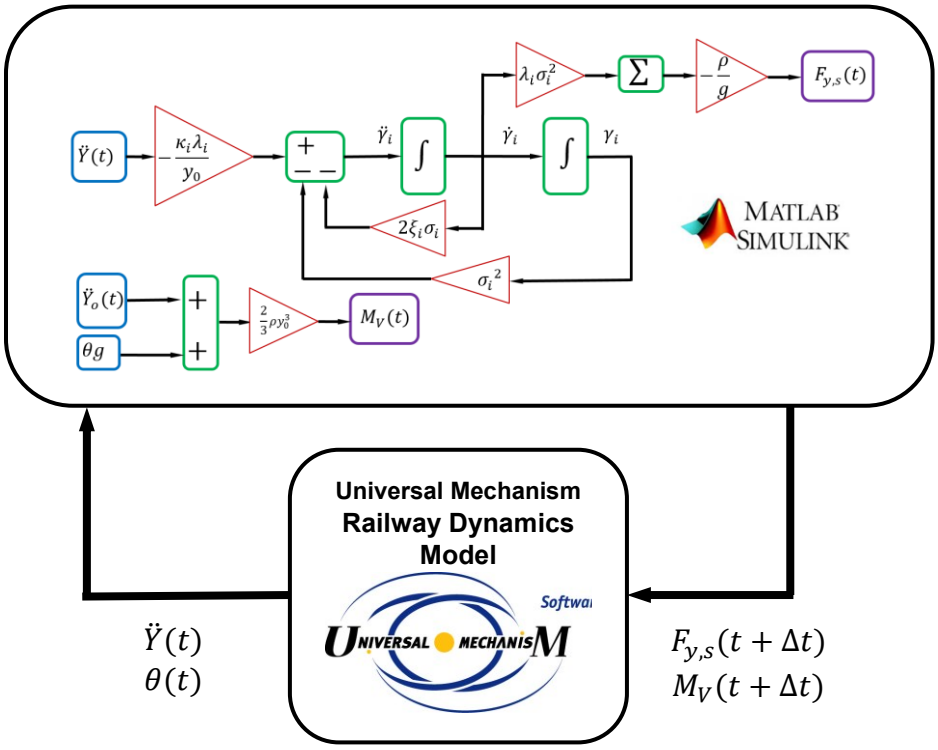

Figure 3.3: The vehicle and slosh models co-simulation scheme.

3.4 Results and discussions

3.4.1. Liquid slosh natural frequency and hydrodynamic coefficients

The natural slosh modes and frequencies for different fill ratios (*H/2R*) are obtained using the Ritz variational method, as described in [64, 78]. A set of normalized frequencies and hydrodynamic coefficients are defined as:

$$\bar{\sigma}_i = \sqrt{R}\sigma_i \text{ and } \bar{\lambda}_i = \lambda_i / R^2 \tag{3.16}$$

These normalized coefficients, which are required to solve the differential equation (3.4), are presented in Table 3.2 for three different *H/2R* values and number of modes [78]. The presented normalized natural frequencies have a good correlation with reported values with Faltinsen and Timokha [78]. It should be further noted that only antisymmetric modes of slosh (odds number of i) contributes to the liquid slosh response.

Table 3.2: Normalized slosh normalized natural frequencies and hydrodynamic coefficients for nine modes for different fill ratios.

Fill ratio	97%			74%			45%		
Normalized parameter	$\bar{\sigma}_i$	$\bar{\lambda}_i$	$\bar{\psi}_i$	$\bar{\sigma}_i$	$\bar{\lambda}_i$	$\bar{\psi}_i$	$\bar{\sigma}_i$	$\bar{\lambda}_i$	$\bar{\psi}_i$
$i = 1$	7.5320	0.0923	2.2286	4.2785	0.6193	1.1756	3.5668	0.8048	1.6070
$i = 2$	10.0680	0	3.0718	6.0553	0	2.0886	5.4018	0	3.8710
$i = 3$	12.2436	0.0181	5.6898	7.3841	0.0868	3.2328	6.7259	0.0696	5.5150
$i = 4$	13.9759	0	6.4924	8.4962	0	4.1900	7.8057	0	7.2950
$i = 5$	15.5883	0.0082	9.1720	9.4805	0.0361	5.3312	8.7483	0.0246	9.0540
$i = 6$	16.9935	0	9.9950	10.3677	0	6.3806	9.5961	0	10.8600
$i = 7$	18.3327	0.0049	12.7040	11.1866	0.0202	7.4376	10.3741	0.0125	12.6400
$i = 8$	19.5497	0	13.5140	11.9474	0	8.6990	11.0970	0	14.4500
$i = 9$	20.7169	0.0033	16.2660	12.6638	0.0131	9.5480	11.7753	0.0076	16.2400

Specific consideration is emphasized in order to incorporate the effect of mass moment of inertia in roll direction for the liquid model. The distributions of the Stokes-Joukowski potential function ϕ_{st}, on the free surface is used to obtained effective mass moment of inertia of the fluid for a cylindrical tank. The mass moment of inertia of the fluid about the point *O* could be defined as [6, 126]:

$$J_o^{Liquid} = \rho \int_{S_f+S_w} \phi_{st} \frac{\partial \phi_{st}}{\partial n} ds \quad \xrightarrow{\frac{\partial \phi_{st}}{\partial n}=0 \; on \; the \; wall} \quad J_o^{Liquid} = \rho \int_{S_f} y\phi_{st} \, ds \tag{3.17}$$

On the other hand, the mass moment of inertia of a frozen liquid is simply calculated as:

$$J_o^{Frozen} = \rho \int_{\tau} (y^2 + z^2) d\tau \tag{3.18}$$

Kolaei *et al.* [6] evaluated the integral by quadratic interpolating function. The normalized mass moment of inertia parameter about tank center could be defined as $\overline{J_O} = J_O/mR^2$ as presented in Figure 3.4 as a function of fill ratio. The graphs also compare the effective mass moment of inertia of the fluid with those of the frozen liquid and the simple pendulum cargo. The mass moment of inertia of fluid about the center of circular tank is less than that of the frozen liquid irrespective of the fill ratio. The trend suggests that only a portion of the fluid is rotating with roll motion of container. For very low fill ratios, the deviation of the fluid mass moment of inertia compared to that of the frozen fluid is very small. The deviation, however, substantially increases with increase in the fill ratio. It can also be seen from the values that the normalized mass moment of inertia of the Liquid model decreases monotonically with the fill ratio, suggesting lower contribution of the fluid in the roll motion of the container. The mass moment of inertia of the frozen fluid, however, initially decreases with increase in the fill ratio for $H/2R \leq 0.75$, and then increases and approach 0.5, which is the normalized mass moment of inertia of a circular disk. The effective mass moment of inertia with simple pendulum model is lower than both of the frozen and liquid models. The analogy between boiled and not boiled egg could help to understand the difference in moment of inertial for frozen liquid and liquid in a completely filled tank [126].

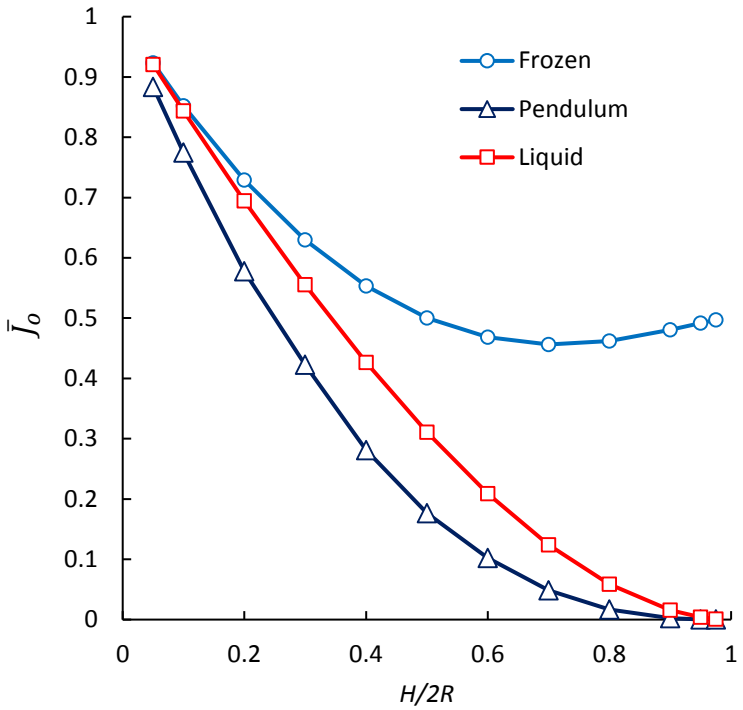

Figure 3.4: The comparison of the normalized roll mass moment of inertia of fluid as a function of fill conditions for frozen, pendulum, and liquid models.

The liquid moment of inertia is incorporated in the *MBD* mode by applying the additional M_{roll} moment as:

$$M_{roll} = \left(J_o^{Frozen} - J_o^{Liquid}\right)\ddot{\theta} \tag{3.19}$$

The validity of implemented slosh model subject to yaw excitation is examined by comparing the response with alternative computational fluid dynamic (*CFD*) models developed in Ansys-CFX platform. The analytical and numerical models evaluated for 74% filled tank with water (ρ=998.2 kg/m^3 and kinematic viscosity $\nu_s = 1.0048 \times 10^{-6}$ m^2/s) subject to a typical yaw excitation of tank car, shown in Figure 3.5(a). The *CFD* model, as a two-phase flow of water and air, is simulated using a transient pressure-based solver in volume of fluid (*VOF*) domain assuming the laminar flow [72]. The model is meshed to 130245 Hex8 element types as 8-node trilinear hexahedral element, which yields approximately 9 hours run-time on a single core of Xenon® CPU E3-1271 v3. The lateral acceleration of front and rear end of the tank, when subjected to a pure yaw excitation, are 180 degrees out phase and thus could generate an additional yaw moment. To

incorporate the resultant liquid slosh moments due to yaw excitations of the tank, the length of the tank is divided into 12 subsections of dl=1 m length and the tank-fixed lateral acceleration of the center points of each section is used to evaluate the resultant liquid sloshing response. The summation of five anti-symmetric modes is considered in this investigation for representing the liquid slosh response.

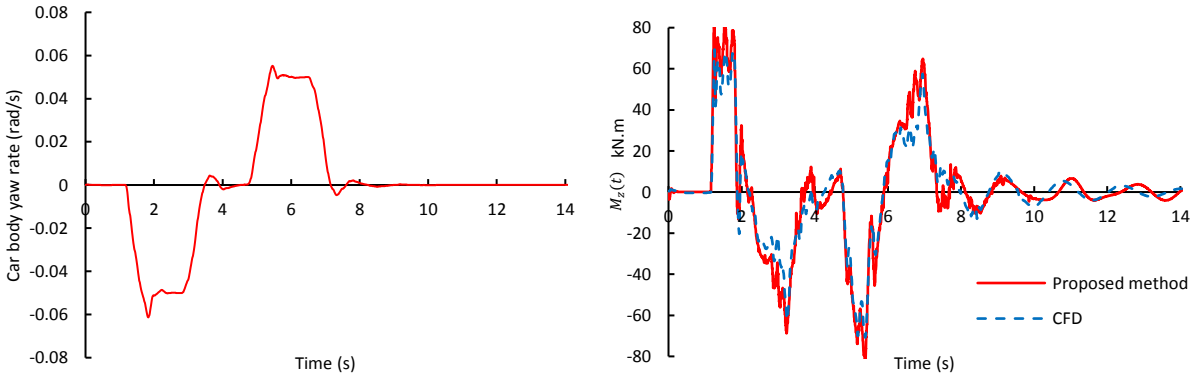

(a) (b)

Figure 3.5: (a) Car body yaw rate input; and (b) comparison of the proposed yaw slosh simulation response with *CFD* simulation for 74% fill with water.

As shown in Figure 3.5(b) the developed analytical method could represent the trend of response in an efficient manner. As the graphs present, the analytical model yields slightly overestimation of the yaw slosh moment compared to *CFD*. On the other hand, the runtime of the analytical slosh model is almost real-time. In view of these results, the summation of the five asymmetric modes of liquid slosh for 12 sections along the tank are considered sufficient to efficiently simulate the effects of sloshing on the dynamic response of partially filled tank cars.

3.4.2 Hunting analysis of empty tank car

The bifurcation diagram of the empty railway tank car is presented in Figure 3.6. The *Hopf* points of the bifurcation diagram is identified by evaluation the response of the system subject to the defined track irregularity in different forward speeds. The lateral oscillations of the leading wheelset of wagon, *w1*, is observed to change from a stationary zero to undamped oscillatory response at forward speed of the 16 *m/s*, indicated as 'o' in Figure 3.6. The undamped oscillatory responses of both bogies of the empty tank car are observed at forward speed of 18 *m/s* shown as '×'. At speed higher than 18 *m/s*, it is further observed that there is 180-degree phase difference in the oscillations of the two bogies which indicate initiation of hunting mode oscillations of the car body. The phase difference in the lateral movements of the bogies is observed to reduce to zero at forward speeds higher than 29 *m/s*, shown as '□'. The response of the system is then evaluated for higher speeds, up to 40 *m/s*, to confirm that no other unstable mode for the system exists. The forward speed of the vehicle is then gradually reduced with 0.2 m/s^2 deceleration from the unstable state of the system at 40 *m/s* forward speed. The defined longitudinal deceleration of wagon is small enough to eliminate the effects of longitudinal movements of the liquid cargo and could be similar to the stepwise reduction of the forward speed [35, 119, 120] as an alternative method for evaluation of hunting behavior.

The variations in amplitude of lateral movements of the leading wheelsets of the bogies (*w1* and *w3*) and yaw rate of the car body are shown in Figure 3.6 as the longitudinal speed is reduced. As presented, the amplitude of undamped lateral movement of the wheelsets reduces as the forward speed is reduced. In-phase lateral movements of the *w1* and *w3* at forward speeds higher than 30 *m/s* lead to small amplitude of the car body yaw rate. The yaw oscillations of the car body are then excited at 27.5 *m/s*, which is also indicated as variation in response of the first wheelsets of the bogies. The lateral amplitude of the wheelsets along with yaw rate of the car body are reduced by reducing the forward speed and return to their stationary response at forward speed of 15.45 and 16.54 *m/s* for *w1* and *w2* respectively. This forward speed is correlated to the saddle-node of the bifurcation diagram and critical speed of the empty wagon. The trend of the responses in Figure 3.6 presents a subcritical *Hopf* bifurcation for an unloaded freight car. This trend has been observed in the presence of the hysteretic forces in several studies [35, 105, 119]. The same approach is further applied to evaluate the lateral response of the railway tank car in different fill conditions of the liquid cargo.

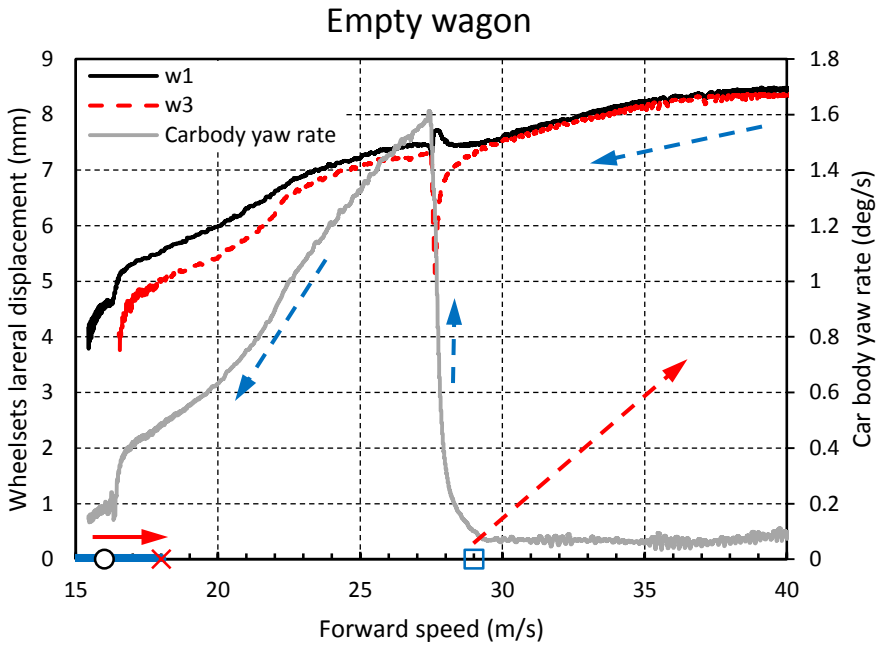

Figure 3.6: Bifurcation diagram of the empty wagon.

3.4.3 Hunting analysis of partly filled tank car

The nonlinear dynamic responses of the tank car for three different fill conditions are investigated through evaluation of the bifurcation diagram of the system and identification of critical hunting speeds. The responses of the system with different models of liquid cargo represented as '*Frozen'*, and '*Pendulum'* are compared with response of the system with developed liquid model. The liquid model is also considered with and without effects of the liquid movements subject to yaw excitations of car body, referred to as '*Liquid'* and '*Liquid without yaw slosh*', respectively. The steady-state lateral movements of the leading wheelset of the railway tank car subject to the one cycle track excitation, as mentioned before, are used to examine the lateral stability of system. The lateral oscillations of the leading wheelsets of the bogies for the 97%-filled tank car using different modeling approaches are presented in Figure 3.7 at forward speed of 40 *m/s*. At this speed, the steady state lateral oscillations amplitude of the leading wheelset, *w1*, is approximately 6 *mm* for the *Frozen* cargo model. Furthermore, as indicated in Figure 3.7(a), the phase difference in the lateral oscillation of the leading wheelsets of bogies is zero, which corresponds to the excitation of the hunting mode of bogie. On the other hand, the amplitude of wheelsets oscillations in *Pendulum* and other two *Liquid* models are damped to zero following similar response to the identical disturbance. The difference could be correlated to the considerable difference in $\bar{J}_O$ parameters at

high fill conditions indicated in Figure 3.4. The additional contributions of the yaw slosh effect could be observed comparing Figures 3.7(c) and (d). As observed, the additional yaw slosh effects lead to higher number of oscillations of the system and additional two seconds before reaching the damped response.

The magnitude of the lateral oscillation of wheelsets in all of the modeling approaches are increased to 6~7 *mm* for the higher forward speed of 48 *m/s*, as shown in Figure 3.8. The higher forward speed leads to in-phase oscillations of the wheelsets for each of the modeling approaches. The response indicates that regardless of cargo movement contributions, the bogies will experience limit cycle hunting oscillations at this speed.

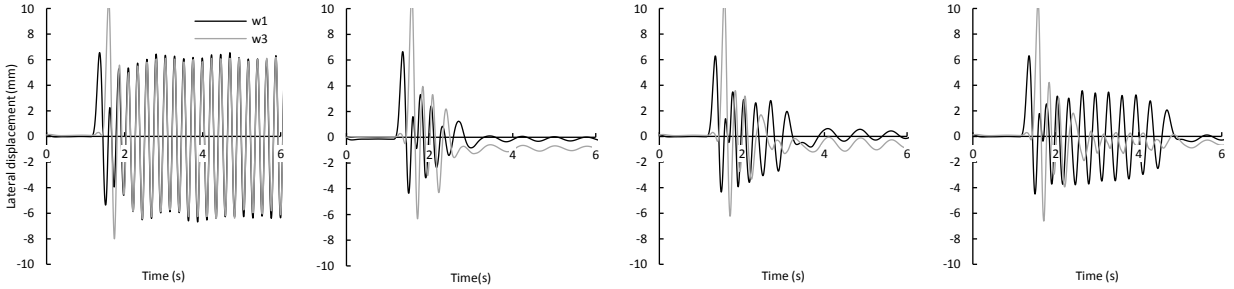

(a) (b) (c) (d)

Figure 3.7: Lateral movements of the first and third wheelsets for 97% filled in different modeling approaches (a) *Frozen* (b) *Pendulum*, (c) *Liquid* cargos without slosh yaw effect and (d) *Liquid* at 40 *m/s* forward speed.

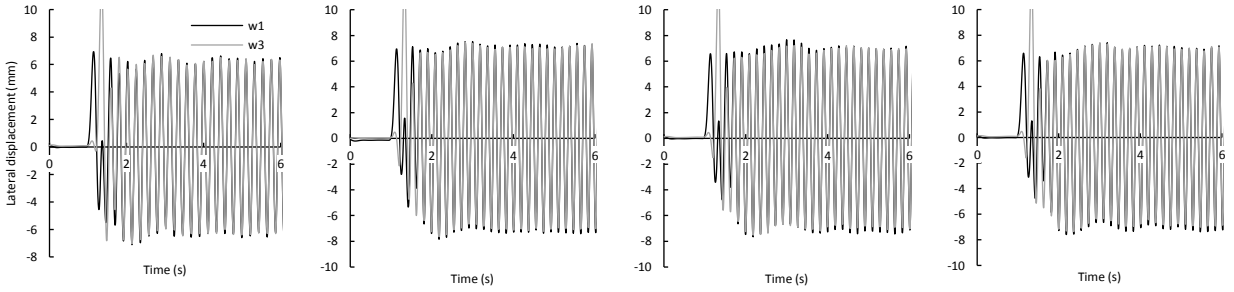

(a) (b) (c) (d)

Figure 3.8: Lateral movements of the first and third wheelsets for 97% fill level in different modeling approaches (a) *Frozen* (b) *Pendulum*, (c) *Liquid* cargos without slosh yaw effect and (d) *Liquid* at 48 *m/s* forward speed.

The responses of the system, with different liquid modeling approaches, are evaluated subject to the track excitation in range of speed form 30 to 50 *m/s* for different liquid densities. The *Hopf* bifurcation points of the system could be correlated to the points where amplitude of the oscillation

is changed from damped to a undamped oscillatory response for a given speed. The lowest speed that leads to initiation of oscillatory response subject to the defined excitation of the track are given in Table 3.3 for different fill conditions and modeling approaches.

Table 3.3: Forward speeds of the vehicle for different fill conditions and modeling approaches that lead to the initiation of oscillatory hunting response.

	Fill ratio		
	45%	74%	97%
Modeling approach	*Hopf* bifurcation point (*m/s*)		
Frozen	49.0	41.0	39.5
Pendulum	46.0	48.0	46.0
Liquid without yaw slosh	42.0	47.5	47.5
Liquid	37.5	45.5	47.0

The *Hopf* bifurcation point of partly filled tank car in *Frozen* model is observed at higher speeds while fill ratio and corresponding *c.g.* position of the system are lower. On the other hand, initiation of undamped oscillatory response of the wheelsets in *Pendulum* model are observed at higher speeds compared to *Frozen* modeling approach when fill levels are higher. For 97% fill level, there is a considerable difference in the *Hopf* point speeds in *Frozen* modeling approach compare to the other alternative methods. This trend can be directly correlated to the effect of roll moment of inertia as discussed before. For the lower fill condition, higher contributions of liquid slosh can be correlated to the larger free length of the partly filled state of liquid cargo. In this case, the higher slosh force and moment lead to the initiation of undamped response of system at lower speeds. The undamped response of the system in 45% fill condition is observed at 37.5 *m/s*, which is 30% lower than the one observed with *Frozen* modeling approach. The liquid slosh contribution subject to yaw excitation also reduces the forward speeds further at which the hunting oscillations is initiated. Moreover, the contribution of yaw slosh effect alone for 45 % fill ratio is found to be as high as 13%.

The saddle-node of the bifurcation diagram for different fill condition of the liquid cargo is then identified by reducing the forward speed of the railway tank car from the undamped hunting condition, as performed for empty wagon. Figure 3.9 presents the lateral response of the leading wheelset of the system in three different fill conditions and the four different modeling approaches considered. The amplitude of the lateral movements of the first wheelset of the bogie (critical wheelset), is determined by using a 0.5 *s* moving window. The moving amplitude method indicates

the chaotic response of the system at which amplitude of the oscillation is found to change stochastically.

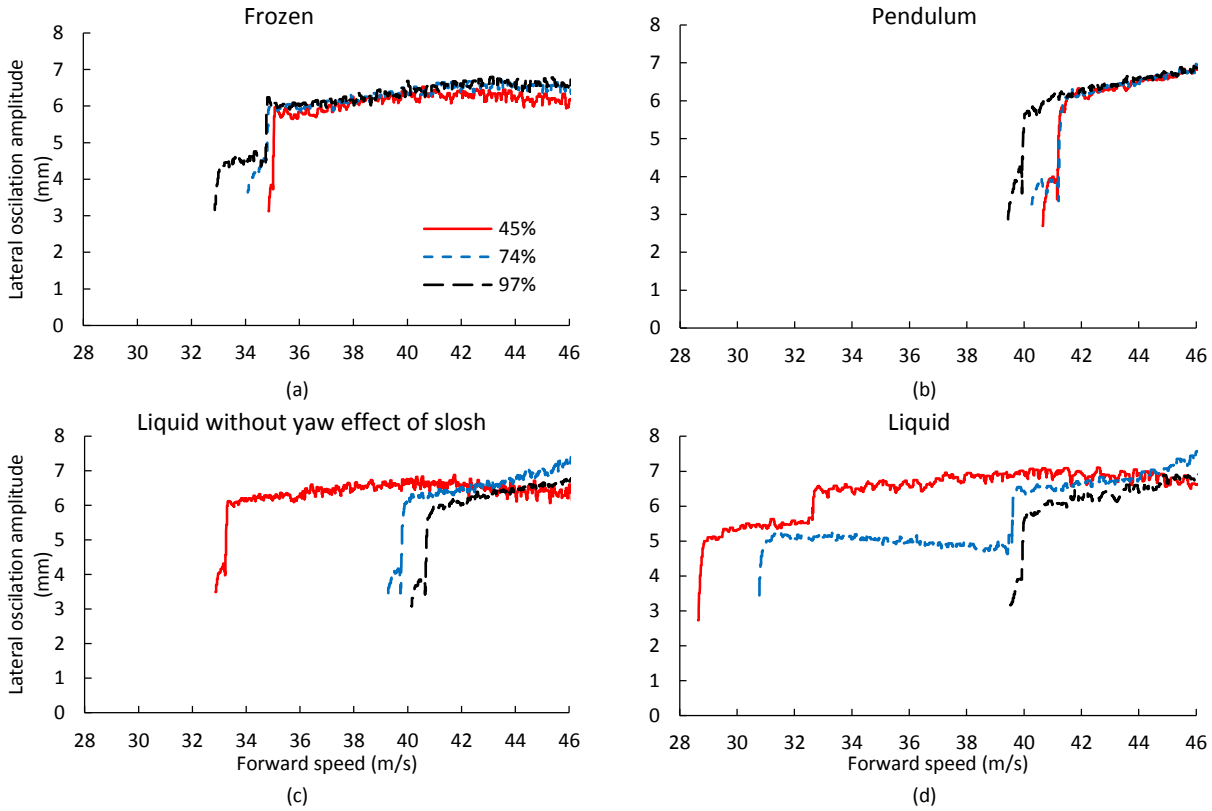

Figure 3.9: Bifurcation diagram of the partially filled railway tank car for (a) *Frozen*, (b) *Pendulum*, (c) *Liquid without yaw effect of slosh* and (d) *Liquid* modeling approaches of cargo.

The saddle-node of bifurcation diagram is used to identify the critical hunting speed of the wagon, which is observed to be sensitive to both modeling approach and fill ratio. Since this speed is lower than the lowest *Hopf* bifurcation points, the state could be classified as subcritical *Hopf* bifurcation [121]. In general, the identified critical speed of the wagon in loaded condition is observed to be higher than the reported critical speed of an empty wagon [*e.g.*, 34, 116].

The lower fill condition in *Frozen* modeling approach leads to lower *c.g.* height of the system and saddle-node of the bifurcation diagram at relatively higher speeds, as shown in Figure 3.9(a). Moreover, in the 97% filled condition, the saddle-node of the bifurcation diagram for *Pendulum* and two different *Liquid* modeling approaches are almost identical which is correlated with minimal effects of the liquid slosh forces for high fill conditions. The critical speed for the 97%-filled tank using *Pendulum* and *Liquid* models with and without yaw slosh effects are observed as

39.75 *m/s*, which is higher than the 34.5 *m/s* observed for the *Frozen* model. The lower effective roll moment of inertia of the cargo compared to *Frozen* model acts as a damper for lateral oscillations of the wheelset and increases the critical hunting speed in high fill condition by 15%. The abrupt change in the amplitude of lateral oscillations of the leading wheelset between 34 to 36 *m/s* is observed for all fill ratio when *Frozen* modeling approach is used. In these simulations, such a trend is further observed to be attributed to dissipation of the lateral movements of the wheelset in the second bogie of the vehicle. As expected, lateral movements of the *Pendulum* cargo essentially act as a damper for lateral wheelset oscillations and shifts the step-shape change of the bifurcation diagram to a higher speed, as shown in Figures 3.9(a) and (b).

On the other hand, simulation of the liquid cargo response using up to five natural modes leads to a different trend as shown in Figures 3.9(d) and (c). The effects of the car body hunting mode are evaluated by comparison of bifurcation diagram of *Liquid* models with and without yaw slosh effects. The saddle nodes and trend of bifurcation diagrams for two *Liquid* slosh models are similar for 97% fill conditions, as seen in Figures 3.9(c) and (d). The contribution of yaw moment of the liquid slosh is more dominate in partly filled state of the tank where critical hunting speed is lower when yaw contributions of liquid slosh are considered. The significant contribution of lateral liquid slosh force and roll moment are observed when Figures 3.9(c) and (d) are compared with *Pendulum* model shown in Figure 3.9(b). Comparing the moderate fill condition of 74%, the lateral oscillations of second bogie in *Liquid* cargo models are damped at lower forward speed, as presented in the step-shape of the graph in Figure 3.9(c). The identified critical speeds of the railway tank car for a fixed axle load with different fill ratios and modeling approaches are summarized in Table 3.4.

Table 3.4: Critical hunting speeds of the railway tank car for different fill ratios.

	Fill ratio		
	45%	74%	97%
Modeling approach	Critical speed (*m/s*)		
Frozen	34.81	34.00	32.80
Pendulum	40.66	40.25	39.45
Liquid without yaw slosh	32.87	39.25	40.00
Liquid	28.67	30.75	39.55

The results show that the critical speed of the simulated tank car in high fill condition is significantly influenced by the roll moment of inertia of the system. Considering the cargo as frozen bulk leads to underestimation of the critical speed since the liquid in this fill condition could act as

a damper for lateral oscillations of the wheelsets. The results further show that very similar critical speed is predicted regardless of the modeling approach considered to represent liquid motions at high fill levels. For partial fill conditions on the other hand, fluid motions lead to lower critical speeds where the contribution of the yaw slosh moment could be very significant on identified critical speed. The *Pendulum* model, can simulate the free roll oscillations of cargo with respect to tank and is effective just for high fill levels, but will overestimate the critical speed significantly in comparison to proposed liquid models as the fill level is reduced. For low fill levels where liquid slosh will influence the dynamics, the proposed liquid model predicts a critical speed of 28.67 *m/s* which is 41% less than that predicted by simple pendulum model. Neglecting the liquid slosh response subject to yaw excitations of tank car yields a critical speed of 32.87 *m/s* or 15% overestimation of critical speed.

3.5 Conclusions

A nonlinear dynamic model of a railway tank car with three-piece bogie is simulated to investigate its lateral response. The primary focus of this investigation is to examine the influence of liquid cargo sloshing on the lateral stability performances of tank cars. In order to systematically examine the effect of fluid motions, four different models are developed, namely rigid cargo represented as frozen liquid, equivalent pendulum to represent liquid slosh forces, and linear slosh model with and without yaw slosh moments. For the linear slosh model, the lateral movements of fluid in various fill ratio of a circular tank cross section is represented by five natural modes of liquid movements. The proposed slosh model is integrated with a 114 DoF model of the tank car and used to study the stability of the system in a computationally efficient manner. The critical hunting speed of the wagon characterized by the limit cycle motion of the leading wheelset is established for three different fill levels with identical total weight. A partially filled tanker with various densities of cargo leading to different fill ratio, yields a different critical hunting speeds. The higher fill condition of the cargo leads to the higher resultant *c.g.* position and lower critical hunting speeds while the cargo is assumed as frozen. Simulation of the free rotation of the cargo bulk with respect to tank leads to higher critical hunting speed in high fill conditions as cargo relative motion introduces damping to the system. The pendulum representation of the cargo leads to higher hunting speeds compare to frozen modeling approach it also acts as a damper for lateral oscillations of the tank car. However, the critical hunting speed is not sensitive to the variation of liquid density

and *c.g.* height, while the cargo is treated as simple pendulum and thus clearly inadequate to represent fluid slosh in a partially filled tank car. On the other hand, when the tank is nearly full, all slosh models considered lead to same critical hunting speed which is higher than the speed predicted for frozen cargo. Such response is expected due to the small free length of liquid cargo and negligible effects of slosh. For partial fill condition, the proposed liquid model with and without consideration of yaw slosh moment lead to lower critical speed compare to the results obtained from frozen and pendulum approaches. The liquid slosh response in partly filled condition has a tendency to eliminate the dissipative effects of the cargo observed in simple pendulum approach. Furthermore, initiation of the yaw oscillations of car body leads to additional slosh moment which cause a further destabilizing effect and even lower critical speed. This trend is more prominent for lowest fill level considered in comparison to the medium fill level. Sloshing of liquid in a partially filled railway tank car can thus significantly deteriorate the critical hunting speed performance.

CHAPTER 4

Effects of coupled liquid cargo sloshing on roll response of partly filled railway tank cars

4.1 Introduction

General-purpose tank cars during operation may encounter partial fill conditions due to differences in weight density of the products and limits on the track loads. The movement of the liquid free surface within the partly-filled container during braking or curving maneuvers, known as liquid sloshing, can impose additional forces and moments on the tank car and the train. These may greatly alter the wheel-rail contact forces leading to adverse effects on dynamic responses of the railway tank car [96]. The adverse effects of the sloshing liquid cargo have been extensively investigated for road [*e.g.*, 99], aerospace [*e.g.*, 65], and marine [*e.g.*, 126] transport systems. The effects of liquid slosh on responses of the tank cars during curving and braking, however, have been reported in relatively fewer studies [3, 5]. The dynamics of partly-filled tank trucks have been most widely reported, which have established that the slosh forces and moments considerably deteriorate the roll stability limits and braking performance of partly-filled tank trucks [*e.g.*, 84, 128]. These have evolved into widely different methods for analyzing the slosh forces and moments, which include the simple quasi-static motion of the liquid bulk [7], mechanical analogs of the moving cargo [87], and linear and nonlinear fluid slosh methods [64, 84].

A quasi-static model permits analyses of load shifts along the longitudinal and lateral axis in the steady-state during braking and cornering, and rollover threshold limits of partially-filled vehicles. This model, however, cannot evaluate the effects of transient fluid slosh, which is known to impose substantially greater magnitudes of slosh forces and moments [84, 96]. Mechanical-equivalent models of the sloshing cargo such as pendulum and mass-spring-damper models have been proposed to study the steady-state as well as transient effects of cargo slosh in road, rail and marine transport systems [87, 95, 126]. The mechanical-equivalent models are generally formulated to mimic the fundamental slosh frequencies in the lateral and longitudinal directions on the basis of those reported by Budiansky [90] and McCarty *et al.* [75], respectively. Younesian *et al.* [3] integrated a longitudinal axis mechanical equivalent model of liquid slosh to a three-dimensional model of a partly-filled tank car to study load shifts during braking in a curve at different speeds considering the super-elevation, and track irregularities, for different fill levels and speeds. The study demonstrated considerable load shift in the longitudinal axis, while the potential

unloading due to sloshing in the roll plane could not be predicted since the slosh model was limited only to the pitch plane. The study suggested that neglecting fluid slosh in a partly-filled tank car could lead to underestimation of the derailment potential and wheel unloading by 18 and 25 percent. Transportation of high-density liquid cargo in a high capacity railway tank was also reported to be more critical as it has been reported for road tankers [7]. Vera *et al.* [95] implemented a similar longitudinal axis mass-spring model distributed along the length of a 87%-filled compartmented tank together with an uncoupled simple pendulum model in the roll plane to study fluid slosh in the lateral and longitudinal axes. The study showed negligible effect of fluid slosh on the running safety of the train, likely due to consideration of the compartmented tank and relatively high fill level. Di Gialleonardo *et al.* [94] characterized the lateral liquid slosh by introducing nine uncoupled lateral mass-spring systems distributed uniformly along the length of the tank car. The higher unloading and derailment ratio was observed under the influence of liquid movement.

The mechanical models are considered meritorious since these can be conveniently integrated to multi-body dynamic (*MBD*) models for simulations of the coupled cargo and vehicle/tank car system in a computationally efficient manner. The developments of such models, however, pose considerable challenges in identifications of model parameter, which are dependent upon the tank geometry and the fill volume in a highly complex manner. Nonlinear computational fluid dynamic (*CFD*) methods based on the Navier-Stokes formulations have been widely used to determine the transient slosh within partly-filled tanks of different cross-sections with and without baffles, while their implementations in vehicle models have been limited due to excessive computational demands [63-65]. Alternatively, Shi *et al.* [5] proposed a continuum based fluid constitutive model, which was integrated to *MBD* model of a rail vehicle through the development of a fluid-tank contact algorithm to study dynamic responses during curve negotiation and ECP braking. The study showed relatively higher coupler force and greater variations in the wheel loads due to fluid slosh under braking, when compared to that observed with the rigid cargo. Wang *et al.* [123] developed a low order continuum model of a rectangular cross-section tank and iterated it to an *MBD* railway vehicle model to study slosh effect during curving. The study concluded greater potential for wheel-rail separation and thus the derailment in the presence of fluid slosh, especially at higher operating speeds.

The methods employed in the aforementioned studies are also computationally demanding similar to the *CFD* methods. Alternatively, linear slosh theory has been used to simulate fluid slosh

in a computationally efficient manner assuming inviscid and irrotational flows [99, 126]. The validity of linear slosh theory in predicting mode shapes and natural frequencies of liquid slosh, and hydrodynamic forces has been presented in several studies [64, 126]. It has been shown that the linear theory can effectively predict the slosh forces and moments under excitations likely to be encountered during typical vehicle maneuvers, although it underestimates the resonant slosh when separation of the free surface occurs [64]. The linear slosh theory has been widely used for predicting slosh modes, and forces and moments in partly-filled arbitrary cross-section tanks with and without baffles of varying geometry [6, 98]. The linear slosh theory permits analyses of three-dimensional slosh under simultaneous braking and curving in a highly efficient manner [129], which is not possible with mechanical-equivalent slosh models, and is computationally demanding with the continuum-based or *CFD* models. Moreover, the linear slosh models can be conveniently integrated to *MBD* vehicle models to analyze coupled liquid-vehicle system responses, although it has not yet been attempted for railway vehicles.

In this study, the liquid slosh within a partly-filled tank is analyzed using a linear slosh model. A comprehensive multi-body dynamic model of a tank car incorporating non-smooth and nonlinear damping as well as stiffness properties of friction wedges employed in the secondary suspensions, developed in *Universal Mechanism* (*UM*) platform, is considered to study the effect of fluid slosh on responses during curving. For this purpose, the slosh model, developed in Matlab/Simulink is integrated to the vehicle model via co-simulation technique in order to establish a coupling between the liquid slosh and vehicle dynamic responses. The responses of the coupled liquid-vehicle model under selected maneuvers are evaluated considering different fill heights of the liquid cargo and forward speeds. The simulations are performed to identify speed corresponding to wheel-rail separation during curving, denoted as the critical curving speed. The response characteristics of the partly-filled tank car are compared with those of the car with an equivalent rigid cargo in order to illustrate adverse effects of liquid cargo slosh on the directional performance of the railway vehicle.

4.2 Model formulations

4.2.1 Multi-body dynamic model of the tank car

A multi-body dynamic (*MBD*) model of a railway tank car, comprising the underframe, a circular cross-section tank and a set of three-piece bogies, is developed in *Universal Mechanism* (*UM*) software [110, 124], as shown in Figure 4.1. Each bogie is modeled considering nine rigid bodies,

including friction wedges, side frames, wheelsets and bolster, which are coupled through contact surfaces, suspension springs, and connected to the car body through the center plate and side bearings. A 114-degrees-of-freedom (*DoF*) model of the freight-car is thus formulated in the *UM* software considering 6-DoF motions of each rigid body subject to constraints imposed by unilateral contact forces due to suspension wedges, multi-axis motions of the springs and wheel/rail contact. The model has been described in details in [28] together with the model parameters and a methodology to identify parameters related to wedges contact with the bolster and the side-frame.

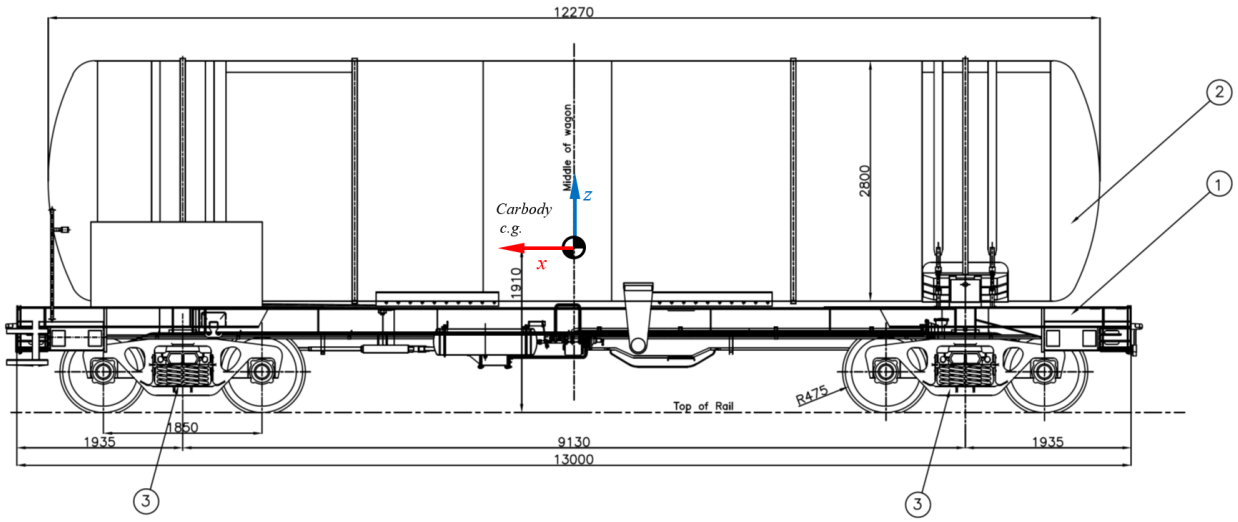

Figure 4.1: Schematic of the railway tank car model with three-piece bogies: 1) underframe, 2) tanker, 3) three-piece bogie (dimensions are in *mm*).

The dynamic responses of each wedge in the secondary suspension, considered as a rigid body with six-DoF, are derived considering its interactions with the side frame and the bolster. The geometric constraints of each frictional wedge are represented by groups of point-plane contacts with both the side-frame and the bolster. The stiffness and damping parameters of each contact pair were identified through a convergence analysis so as to achieve an acceptable compromise between accuracy of the response and the computational time [35]. The effective multi-axis stiffness constants of the secondary suspension springs are also identified considering the physical properties of the coil springs, as described in [28, 34]. The car body, comprising the tank and the underframe, is considered as a rigid body, which is supported on center plates of each bogie, as shown in Figure 4.2. The center plates supporting the car body undergo relative rotations with respect to the bolster in the yaw, roll and pitch directions. Under a roll motion, encountered during

curving, the car body may interact with the side bearings on the outside track, when the relative motion between the car body and the side bearing exceeds the represented gap, which is taken as 4 *mm* (Figure. 4.2). The interactions between the side bearings and the underframe are modeled using the point-plane contact approach, as described in [35].

The relative rotation of the car body with respect to the bolster may also yield partial separation of the center plate from the bolster, as presented in Figure 4.2. This contact separation may be more pronounced under lateral load transfer caused by liquid slosh in the partly-filled tank. The interactions between the center plate and the bolster is also modeled using the same approach, where the contact points are defined in accordance with the geometric constraints. The planar movements of the center plate in the center bowl are simulated considering four-point plane contact elements. Each point contact is defined by an equivalent contact stiffness and damping constant, taken as 135 *MN/m* and 900 *KNs/m*, respectively, which provided convergence of the response with negligible penetration of the contacting elements and a reasonable computational demand [28]. The friction between the lubricated contact between the center plate and the bolster is modeled considering dynamic and static friction coefficients as 0.17 and 0.2, respectively, while the transition between the dynamic and static friction coefficient is simulated using the Stribeck formulation [28, 35]

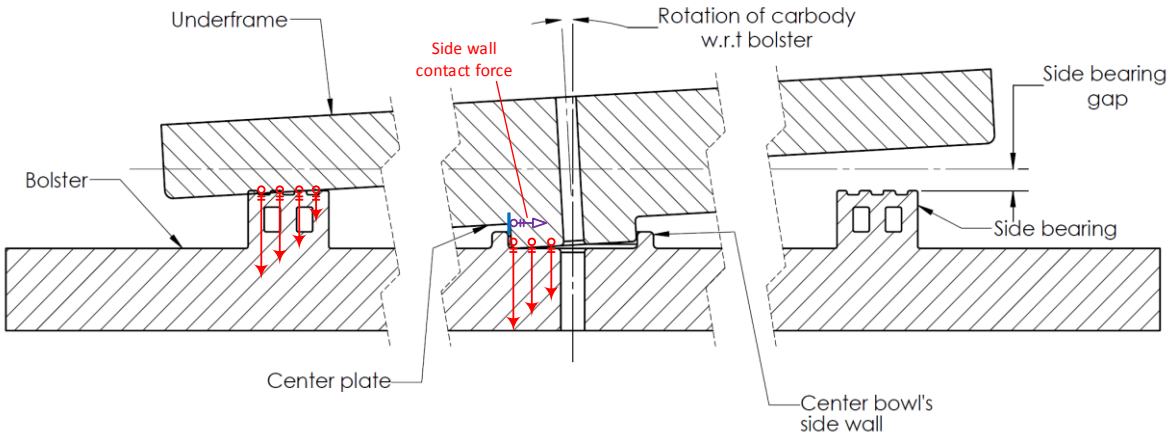

Figure 4.2: Interactions of the car body with the bolster and the center plate, represented by planar visco-elastic contact elements.

The point-plane contact approach could effectively estimate the friction moments developed at the center plates and side bearings in an efficient manner under relative rotations of the contacting

bodies encountered during curving maneuver. The variations in interactions between the car body and the center plate (bogie) under varying loads can also be described accurately using this modeling approach. The model is thus considered vital in case of fluid slosh, where the normal loads may vary considerably.

A multi-directional wheel/rail contact model is further used in the vehicle model to determine the contact forces and moments as functions of the translational and rotational motions of the wheelset, including the flange contact. For this purpose, The Kalker's *FastSim* algorithm [104] is applied to determine the creep forces and moment at the wheel/rail interface considering an elliptical contact patch.

4.2.2 Liquid slosh model

Consider a partly-filled cylindrical tank of radius *R* and liquid fill height *H*, as shown in Figure 4.3. The equations of fluid motion in the roll plane are derived in the tank-fixed coordinate system *Oyz*, located at the geometric center of the tank, while the tank is subjected to simultaneous lateral, vertical and roll excitations arising from the vehicle response during a given maneuver. The coordinates of the free-surface at the intersection of the tank wall are denoted by y_0 and z_0, as shown in Figure 4.3. In this figure, τ, S_f and S_w represent the fluid domain, liquid free-surface and wetted surface area of the tank wall, respectively. The general equation of motion for an ideal fluid, assuming incompressible and irrotational flows, can be expressed in the form of the Laplace equation of the velocity potential function Φ, such that:

$$\boldsymbol{\nabla}^2\Phi = \boldsymbol{\nabla}^2(\Phi_R + \Phi_S) = 0 \qquad \text{in } \tau \tag{4.1}$$

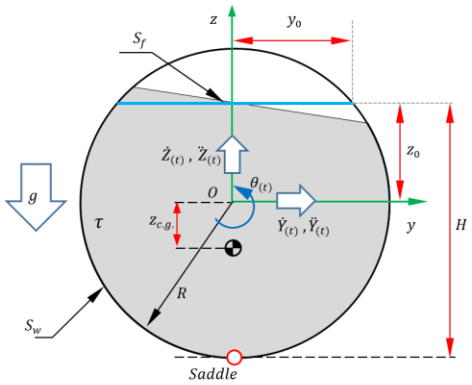

Figure 4.3: Two-dimensional fluid motion in a circular cross-section tank.

where Φ_R and Φ_S are two components of the velocity potential corresponding to the rigid body motion of the fluid and liquid motion relative to the container, respectively. It can be shown that for a cylindrical tank under lateral, vertical and roll excitations about the center of the tank, the rigid body potential, Φ_R, can be expressed as [98, 126]:

$$\Phi_R = \dot{Y}(t)y + \dot{Z}(t)(z - z_0) \tag{4.2}$$

where $\dot{Y}(t)$ and $\dot{Z}(t)$ are the lateral and vertical velocities of the container, respectively. It should be noted that the rigid body potential, Φ_R, in the above equation does not depend on the roll rate of the container sine the roll motion of a cylindrical tank about its center cannot influence the rigid body potential in case of inviscid flows. This is considered valid since the viscosity effect of most liquids is nearly negligible compared to the inertia effect [126].

Based on the multimodal method [126], the potential Φ_S attributed to liquid slosh can be expressed as a function of the lateral and vertical motions of the fluid (*y,z*) through superposition of natural modes, φ_i, expressed in the generalized coordinates, γ_i:

$$\Phi_S(y, z, t) = \sum_{i=1}^{\infty} \gamma_i(t)\varphi_i(y, z) \tag{4.3}$$

Substituting the above equation into the free-surface boundary condition results in the following set of ordinary differential equations [64]:

$$\ddot{\gamma}_i + 2\xi_i\sigma_i\dot{\gamma}_i + \sigma_i^2\gamma_i = -\ddot{Y}\lambda_i \qquad \text{on } S_f \tag{4.4}$$

where $\ddot{Y}$ is the time derivative of the effective lateral acceleration acting at the geometric center of the container and σ_i is circular frequency of the liquid oscillations. In the above equation, ξ_i and λ_i are the damping coefficients due to the liquid viscosity and hydrodynamic coefficients, respectively, given by [78, 99]:

$$\xi_i = \frac{g}{2\sqrt{2}R} v_s^{1/2} \sigma_i^{-5/2} \int_{S_w} \left(\frac{\partial \varphi_i}{\partial s}\right)^2 dS \tag{4.5}$$

$$\lambda_i = \frac{\int_{S_f} y\varphi_i dS}{\int_{S_f} (\varphi_i)^2 dS} \tag{4.6}$$

where v_s is the fluid kinematic viscosity and g is acceleration due to gravity. Here the natural slosh modes and frequencies are obtained using the Ritz variational method as described in [64]. The solutions of the differential equation (4.4) yield hydrodynamic pressure, $P(y, z, t)$, which directly relates to the slosh force and moment. The hydrodynamic pressure distribution on the container wall can be obtained from the linearized Bernoulli's equation [126], such that:

$$\begin{aligned} P(y,z,t) &= -\rho g(z - z_0 + \theta y) - \rho \frac{\partial(\Phi_R + \Phi_S)}{\partial t} = \\ &-\rho g(z - z_0 + \theta y) - \rho \left\{ \ddot{Y} y + \ddot{Z}(z - z_0) + \sum_{i=1}^{\infty} \dot{\gamma}_i(t) \varphi_i(y,z) \right\} \end{aligned} \tag{4.7}$$

where ρ is fluid density and θ is roll angle of the tank about its origin O (Figure 4.3). The total lateral force, $F_y(t)$, acting on the container wall, per unit length of the container, is obtained from integration of hydrodynamic pressure over the tank wetted area, S_w, such that:

$$F_y(t) = \int_{S_w} P dz = F_{y,R}(t) + F_{y,S}(t) \tag{4.8}$$

where $F_{y,R}$ and $F_{y,S}$ are components of the lateral force attributed to rigid body and slosh motions of the liquid, respectively, expressed as:

$$F_{y,R}(t) = -\rho(\ddot{Y} + \theta g) \int_{S_w} y dz = -m(\ddot{Y} + \theta g) \tag{4.9}$$

$$F_{y,S}(t) = -\frac{\rho}{g}\sum_{i=1}^{\infty}\lambda_i\sigma_i^2\dot{\gamma}_i(\mathrm{t}) \tag{4.10}$$

where m is the fluid mass per unit length of the tank. The vertical force due to liquid cargo acting on the container, $F_z(t)$, can also be obtained from:

$$F_z(t) = F_{z,R}(t) = \int_{S_w} P(y,z,t)\,dy = -m(g+\ddot{Z}) \tag{4.11}$$

It should be noted that the sloshing part of the vertical force is zero, $F_{z,S}(t) = 0$, due to geometric symmetry of the circular tank. The moment of liquid cargo about the saddle point of tank can be determined by integrating the hydrodynamic pressure, Equation (4.7) over the wet surface of the tank:

$$M_{Saddle}(t) = -\int_{S_w} P(y,z,t)\,[ydy + (R+z)dz] \tag{4.12}$$

Integration of the above moment yields the total overturning moment of liquid cargo for unit length that can be defined as the summation of three different components of rigid body moment (M_R), moment due to the vertical load transfer (M_V) and the moment of lateral slosh force (M_S) as:

$$M_{Saddle}(t) = M_R(t) + M_V(t) + M_S(t) \tag{4.13}$$

The components of the overturning moments of the liquid cargo can be express as:

$$M_R(t) = \rho(\ddot{Y}+\theta g)\int_{S_w} y(R+z)dz = m\big(R+z_{c.g.}\big)(\ddot{Y}+\theta g) \tag{4.14}$$

$$M_V(t) = \rho(\ddot{Y}+\theta g)\int_{S_w} y^2 dy = \frac{2}{3}\rho y_0^3(\ddot{Y}+\theta g) \tag{4.15}$$

$$M_S(t) = \frac{\rho}{g} R \sum_{i=1}^{\infty} \lambda_i \sigma_i^2 \dot{\gamma}_i(\mathrm{t}) = R \times F_{y,S}(t) \tag{4.16}$$

where $z_{c.g.}$ in Equation (4.14) is the position of center of gravity for liquid cargo with respect to tank geometry center, point *O*. The y_0 in Equation (4.15) is the half of the free length of free surface as shown in Figure 4.4. The $M_V(t)$ can be regarded as the moment due to lateral shift of liquid cargo subject to lateral acceleration.

4.3 Method of analysis

The dynamic responses of the tank car with liquid cargo are evaluated by integrating the lateral slosh force $F_{y,S}(t)$ and roll moment $M_V(t)$, obtained from Equations 4.10 and 4.15, respectively, into the vehicle model via the co-simulation scheme, shown in Figure 4.4. The liquid cargo in the vehicle model is considered as an equivalent rigid cargo, which permits to account for the contributions due to vertical and lateral inertial forces, $F_z(t)$ and $F_{y,R}(t)$, attributed to rigid body motion of the cargo, and the corresponding roll moment. The yaw and pitch moments due to rigid body motion are also incorporated. The co-simulation is initiated at time $t = 0$ assuming negligible force and moment attributed to cargo slosh ($F_{y,S}(t) = 0;\ M_V(t) = 0$). The resulting lateral acceleration and roll angle responses of the car body at the geometric center of the tank (point *O* in Figure 4.3) in the tank-fixed coordinate are applied as inputs to the fluid slosh model in Matlab/Simulink. The solutions of the slosh equation (4.4) yield lateral force and roll moment attributed to liquid cargo slosh at the subsequent instant, which are manipulated to compute the total force and moment over the entire tank length. The tank is modeled as a 12 *m* long and 2.8 *m* diameter horizontal cylinder with flat ends, assuming negligible contribution due to curved endcaps. The lateral force and roll moment are subsequently taken as external inputs to the geometric center of tank in the *UM* vehicle model.

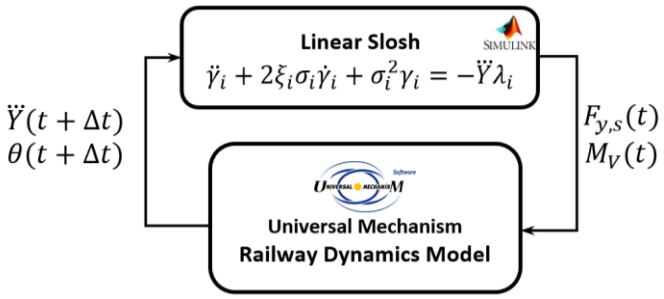

Figure 4.4: The vehicle and slosh models co-simulation scheme.

Different load scenarios are considered to evaluate the dynamic response of the railway tank car under different fill ratios, defined as the ratio of free surface height *H* to the tank diameter (*H*/2*R*). The simulations are performed for different curving maneuvers, considering new ORE-S1002 and UIC60 wheel/rail profiles with zero rail inclination. The geometry of the curved track is defined to include a 20 *m* straight line segment, followed by a transient section connecting the tangential line

to a constant radius curve, R_c=600 m. The curvature of the 200 m long curved segment is linearly increased from 0 to 1/R_c over a length of 50 m to realize gradual curving. The curved segment is subsequently followed by a 50 m long tangent segment. The lateral acceleration developed in a super-elevated curved track is balanced by the gravity component of the car body at a speed v_{bal}. Assuming negligible contributions of dynamics of the suspension and the cargo, v_{bal} for the steady curved track can be estimated from [38]:

$$v_{bal} = \sqrt{\frac{g \times R_c \times \Delta}{track\ gauge}} \tag{4.17}$$

where Δ is super-elevation of the outer rail with respect to the inner one. In the presence of liquid slosh, the slosh force may affect the balance speed v_{bal}. The tank car tends to tilt inward of the curved segment, when $v < v_{bal}$, and outward when $v > v_{bal}$. The simulations are performed for the track with and without a super-elevation in order to investigate the influence of slosh force and moment on v_{bal}. For this purpose, a super-elevation of the constant radius segment (0.0736 m) is introduced, which increases/decreases linearly over the transient segments of the curved track.

The simulations of *MBD* model of the car are performed using the Park method [117] with variable time step ranging from a minimum of 1×10^{-12} to maximum of 0.001 s with an error tolerance of 1×10^{-8}. The selected solver parameters were observed to be adequate for handling contact problems associated with wheel-rail and suspension components of the bogie in a computationally efficient manner. The friction coefficient between the wheel and rail profile was considered as 0.25, as recommended in [52].

4.4 Result and discussions

The validity of the liquid slosh model is initially examined by comparing the responses in terms of slosh frequencies, hydrodynamic coefficients and the lateral slosh force with those reported in different studies. The coupled liquid slosh and tank car model is subsequently analyzed to evaluate the effects of slosh force/moment on the car body responses during passing a curve. The responses are also compared with those obtained for the car body with an equivalent rigid cargo to illustrate the adverse effects of cargo slosh, if any.

4.4.1 Validation of the liquid slosh model

Figure 4.5(a) illustrates the normalized frequencies, $\Omega_i = \sigma_i^2 \, R/g$, corresponding to the first four anti-symmetric modes for different fill ratios, ranging from 30 to 90%. Faltinsen and Timokha [78] and McIver [130] reported nearly identical normalized frequencies of slosh within a partly-filled circular cross-section tank, as seen in the figure. Figure 4.5(b) further compares the corresponding normalized hydrodynamic coefficients, $Q_i = \lambda_i/R$, with those reported in [35]. The comparisons suggest very good agreements in the model responses with the reported studies, irrespective of the fill ratio. The slosh frequencies and hydrodynamic coefficients for the lower 4 antisymmetric modes are evaluated since the fluid slosh in ground transport systems dominates only in the low frequency range, especially the fundamental mode. The results show nearly monotonic increase in slosh frequencies with increasing fill volume. Substantially higher rate of increase in the slosh frequencies is evident under fill ratios exceeding 70%, which is attributed to decrease in liquid free surface length. The hydrodynamic coefficients, on the other hand, tend to peak in the vicinity of 50 to 60% fill ratio, which suggests higher slosh force in this fill range. These also suggest substantially lower slosh under higher fill ratios.

The validity of the linear slosh model is further examined by comparing the resultant slosh force with that obtained from a computational fluid dynamic (*CFD*) model in the Fluent platform of the tank, as reported in [84]. Both the linear and nonlinear analyses are performed for the tank filled with water (ρ=998.2 kg/m^3 and kinematic viscosity $\nu_s = 1.0048 \times 10^{-6}$ m^2/s) with fill ratio, *H/2R*=0.5. The nonlinear simulations are performed for lateral acceleration excitations of three different constant magnitudes (1, 2 and 3 m/s^2). Figure 4.5(c) compares the resulting slosh force responses, normalized with respect to the inertial force of an equivalent rigid cargo $F_y/(m\ddot{Y})$, with that obtained from the linear slosh model. The linear slosh response is obtained from summation

of lower four anti-symmetric modes, since fluid slosh in partly-filled road and railways tanks predominates at very low frequencies near the fundamental mode frequency. It has thus been suggested that consideration of only 4 to 5 antisymmetric modes can yield accurate predictions of slosh force in a highly efficient manner [84, 129]. The results obtained from both, the linear and nonlinear analyses, show that the mean force is identical to the $F_{y,R}$ due to rigid body motion of the cargo, while the peak force corresponding to fluid slosh is 40-50% greater than the mean force. A few studies employing nonlinear computational fluid dynamic (*CFD*) simulations have also reported that the transient slosh contributes to about 40% increase in the peak force under 50% fill condition [6, 64, 84]. These studies employed cylindrical tanks of relatively smaller diameter road tanks compared to the railway tank considered in this study, which would lead to lower peak force due to the smaller free surface length. The results also show that the linear model overestimates the peak force under higher lateral acceleration excitation, which is due to the flow separation under higher excitation. The linear model, however, can provide reasonably good estimations of the slosh force under excitations that are likely to be encountered in railways in a highly efficient manner.

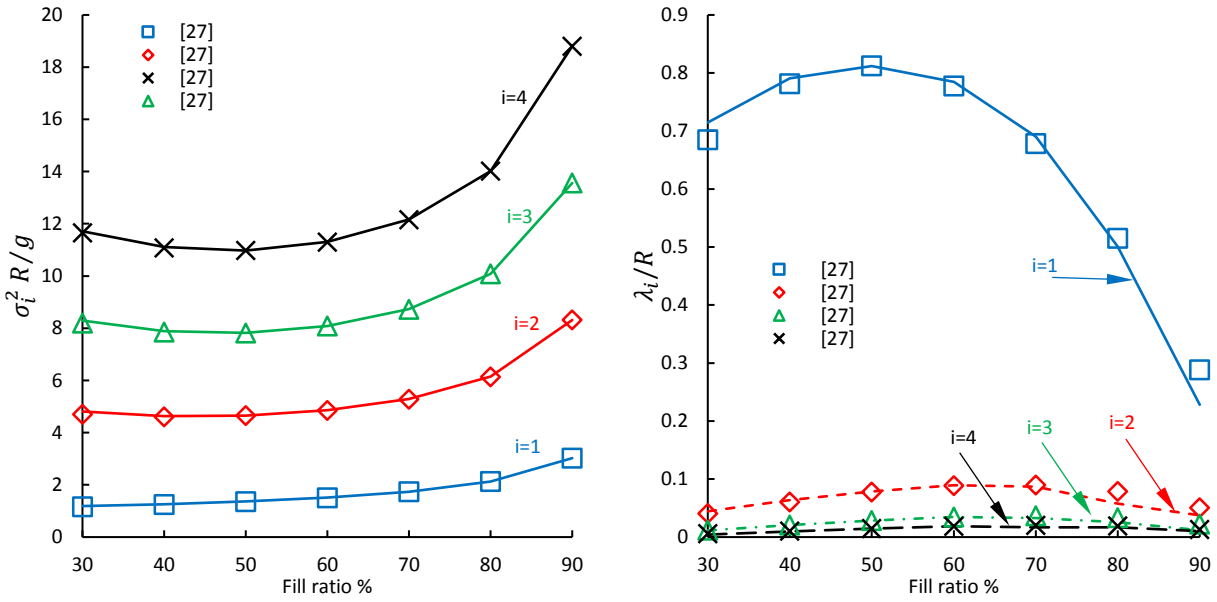

(a) (b)

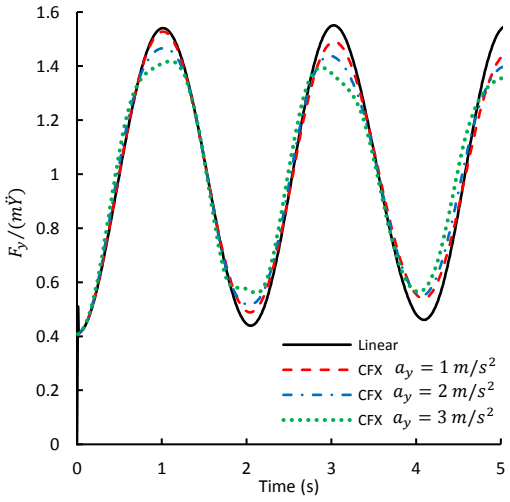

(c)

Figure 4.5: (a,b) Comparisons of normalized frequencies and hydrodynamic coefficients corresponding to four lower antisymmetric modes obtained from the model with those in the reported studies; and (c) variations in resultant normalized lateral slosh force for the 50%-filled tank subject to a constant lateral acceleration.

4.4.2 Effects of liquid cargo Sloshing during curving

The response characteristics of the car with a partly-filled tank during curving are evaluated considering different fill height ratios, $H/2R$, ranging from 0.6 to 0.9, while total cargo load is held constant (569 *kN*) irrespective of the fill height. The variations in the fill ratio is obtained by varying the density of the liquid cargo. The lateral slosh force is evaluated considering the summation of four anti-symmetric modes. The simulations are also performed considering equivalent rigid cargo in order to illustrate the effect of liquid cargo sloshing. Figure 4.6: compares the roll angle responses of the car body during the right-handed curve with liquid and equivalent rigid cargos and different fill ratios. The results are presented for the constant forward speed of 17 *m/s*. The results show substantially higher car body roll for the liquid cargo compared to the equivalent rigid cargo. During steady curving, the roll angle response of the car body with 60 and 70% filled liquid tank are respectively 83% and 67% higher than those with the equivalent rigid cargo. The magnitude of cargo slosh, however, decreases with increasing fill ratio. The steady-curving roll angle response of the 90% filled liquid car is only 9% higher than that of the car with equivalent rigid cargo. This is due to reduced free surface length under higher fill volume. For the equivalent rigid cargo, the magnitude of the car body roll is lower for the lower fill ratio due to lower *c.g.* height compared to the higher fill ratio. This trend is, however, not evident for the liquid cargo. Relatively higher

magnitudes of the roll angle are observed for lower fill ratios, in the 60%-80% range, which is attributed to considerably higher movement of the free surface and thus the lateral load shift and roll moment under lower fill ratios. The roll angle responses of the liquid cargo vehicle also exhibit notable oscillations, which predominantly occur at frequencies ranging from 0.5 *Hz* to about 0.66 *Hz* depending on the fill ratio. These frequencies also correlate very well with the fundamental slosh frequencies obtained for the 60% and 90% fill ratios, as shown in Figure 4.5(a). The oscillations in the roll response of the car body with equivalent rigid cargo occur at considerably higher frequencies, ranging from 1.04 *Hz* for 60% fill to about 0.90 *Hz* for 90% fill. These correspond to roll mode frequency of the car body. Although, these frequencies are very close to those of the second slosh mode frequencies, their contributions to the responses of the car with liquid cargo appear to be relatively small.

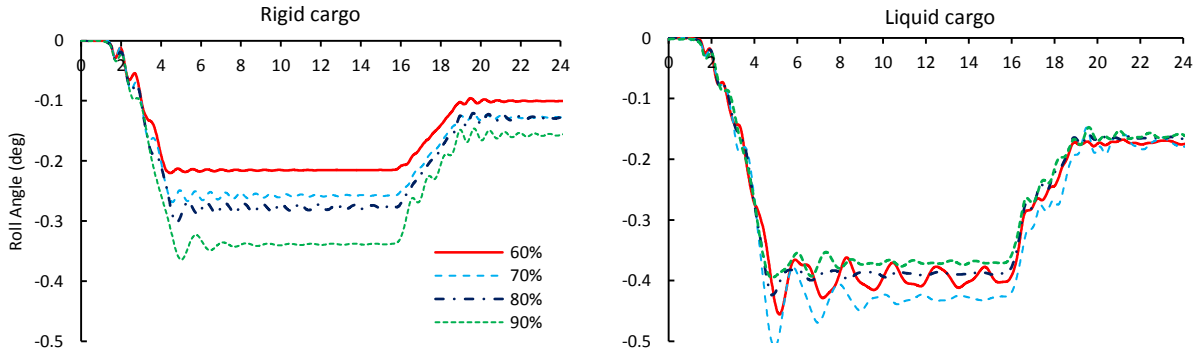

(a) (b)

Figure 4.6: Comparisons of roll angle response of the car with liquid and equivalent rigid cargos during a 600 *m* radius right-handed curve at a speed of 17 *m/s* for different fill ratios: (a) Rigid; and (b) liquid cargos.

The relatively higher roll angle responses of the car body with 60 and 70% liquid fill ratio compared to the 90% fill case is attributed to higher slosh force and moment under lower fill ratios. As an example, Figures 4.7(a) and (b) compare the lateral slosh force $F_S(t)$ and roll moment $M_V(t)$ components attributed to liquid slosh, respectively, for the 60 and 90% fill ratios. The 60% fill ratio causes relatively larger free surface length and its movement, which contributes to considerably higher slosh force and moment compared to the 90% fill, as seen in the figure. Although the *c.g.* height of the 60%-filled car is substantially lower than that of the 90%-filled car, the higher slosh force and moment for the 60% fill ratio yield higher roll angle response of the car during steady curving as shown in Figure 4.6(b).

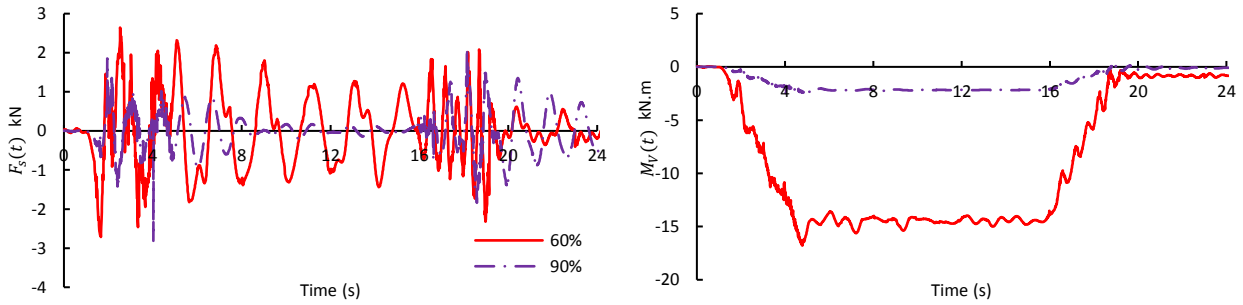

(a) (b)

Figure 4.7: Comparisons of lateral force and roll moment components attributed to fluid slosh for the 60% and 90% fill ratios of the car subject to curving: (a) Lateral force, $F_S(t)$; and (b) Roll moment, $M_V(t)$.

Apart from the higher car body roll, the liquid slosh can also alter the resultant lateral and vertical wheel-rail interface forces. The effect of liquid slosh on the vertical wheel-rail contact force is investigated in terms of the widely used wheel unloading ratio measure, given by:

$$Unlaoding\ ratio = \frac{Q - Q_0}{Q_0} \tag{4.18}$$

Where Q_0 and Q are the static and instantaneous normal forces at the wheel/rail contact, respectively. As an example, Figure 4.8 illustrates variations in unloading ratios of the outer wheel of the leading wheelset, wst_1^l, for different fill ratios, while curving at the constant forward speed of 17 *m/s*. The figure also presents the unloading ratio responses of the car with equivalent rigid cargo. The results suggest that the liquid cargo slosh yields considerably higher unloading of the outer wheel, especially for the 60% fill ratio conditions. This is mostly due to additional roll moment caused by the liquid movement, as defined in Equation (4.12). The results suggest 15% greater unloading of the wheel under 60% fill ratios when compared to that for the equivalent rigid loads. Operations at higher forward speeds may cause even higher unloading of the outer wheel due to higher lateral acceleration of the liquid cargo. The results thus suggest that rigid cargo modeling approach of the liquid cargo cars would lead to under estimation of the unloading ratio responses during curving.

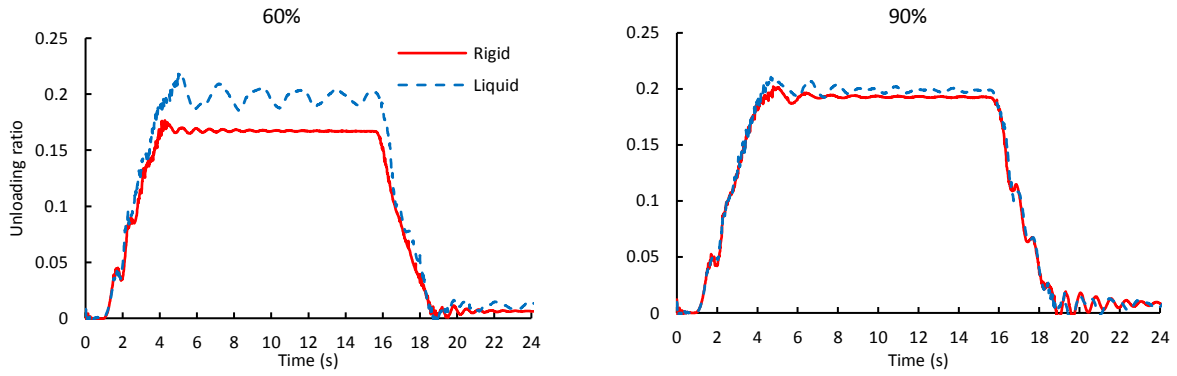

(a) (b)

Figure 4.8: Unloading ratio response of the outer wheel of leading wheelset, wst_1^l, during a 600 *m* right-handed curve at 17 *m/s* forward speed for different fill ratios: a) 60%; and b) 90%.

The variations in the lateral wheel-rail contact force due to liquid slosh are analyzed in terms of derailment criteria or *Y/Q* quotient. The quotient of lateral to vertical forces (*Y/Q*) generally lies around 1.03, for a typical wheel flange angle, $\alpha = 60°$, and wheel-rail friction coefficient, $\mu = 0.25$. A value of 0.86 is considered as the critical derailment ratio considering a safety factor of 1.2, which corresponds to onset of flange climbing over the rail [38]. Figure 4.9 compares the quotient values of the leading wheelset of the car with 60%-filled liquid and equivalent rigid cargos while negotiating the curve at a forward speed of 20 *m/s*. The figures show comparable trends in *Y/Q* ratios of the inside and outside wheels for both types of cargos, although the liquid cargo yields slightly higher ratios for both wheels. The quotient values, however, are well below the critical derailment ratio, which suggests that liquid slosh does not constitute as an essential factor in view of the flange climbing.

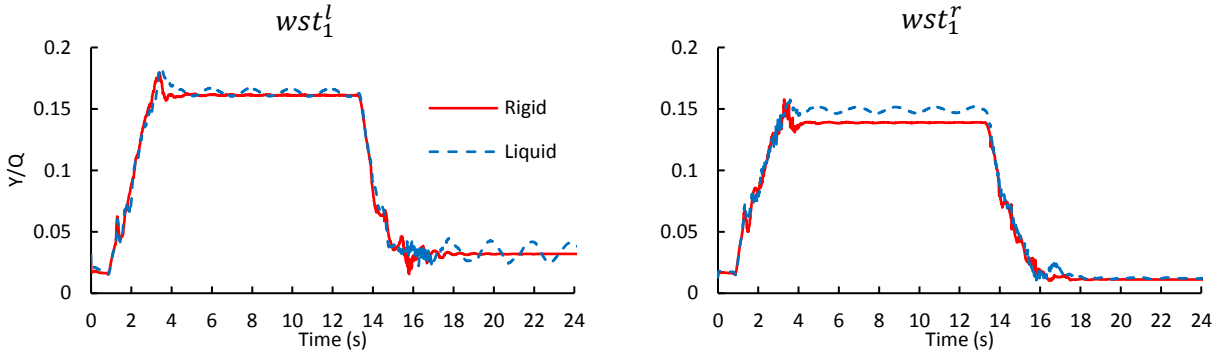

(a) (b)

Figure 4.9: Comparisons of derailment ratios of the leading wheelset of the car with 60%-filled liquid and equivalent rigid cargos while negotiating the 600 *m* radius curve at the speed of 20 *m/s*:(a) outer wheel, wst_1^l and (b) inner wheel, wst_1^r.

The wheel-rail contact forces are greatly influenced by the super-elevation of the track. The effect of liquid slosh force and moment on the unloading ratio, car lateral displacement and derailment ratio responses are investigating during curving on a track with 0.0736 *m* super-elevation. Curving on the chosen super-elevated track corresponds to a balance speed of 17 *m/s*. The results are obtained for different fill ratios and forward speeds, ranging from 15 to 20 *m/s*. As an example, Figure 4.10 compares the unloading responses of the outer wheel of the leading wheelset of the car with 60-filled liquid and equivalent rigid cargos at different speeds. The comparisons suggest relatively small effect of the liquid slosh, irrespective of the forward speed, although the effect is evident when $v > v_{bal}$. The unloading responses of the liquid cargo car, however, exhibit notable oscillations predominant in the vicinity of the fundamental slosh frequency. The results show lower peak unloading responses during the transient segments of the curve compared to those obtained for the non-elevated track (Figure 4.8). Furthermore, the super-elevation of the outer rail leads to substantially lower load transfer during the steady section of the curve.

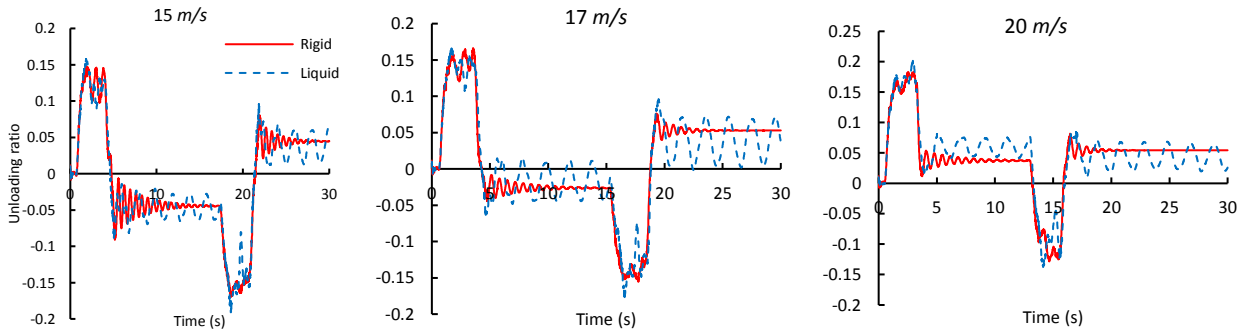

(a) (b) (c)

Figure 4.10: Comparisons of the unloading ratio responses of the outer wheel of the leading wheelset, wst_1^l, of the car with 60%-filled liquid and equivalent rigid cargos during super-elevated curve at different speeds: (a) 15 *m/s*; (b) 17 *m/s*; and (c) 20 *m/s*.

The liquid slosh, however, presents a more pronounced effect on the lateral displacement response of the car body *c.g.* with respect to track centerline, as seen in Figure 4.11. The figure presents the lateral displacement responses of the car with 60%-filled liquid and equivalent rigid cargos, while curving the elevated track at three different speeds. At $v < v_{bal}$, the lateral slosh force and roll moment contribute to substantially higher lateral dispalcement and thus higher inward leaning of the car when compared to the rigid cargo car. As the speed exceeds the balance speed, the lateral movement of rigid cargo car causes it to lean outwards, as seen in Figure 4.11(c), which has also

been reported in [131]. The liquid cargo car, however, continues to lean inward due to actions of the lateral slosh force and roll moment. The results also show notable offset in the responses of the rigid cargo car, as it exits the constant radius segment of the elveated track, which is likely cause by clearances in the wheel-rail interface and stick-slip friction forces in the suspension components of the bogies. The effect is more pronounced at the higher speed (v>v_{bal}), as shown in Figure 4.11(c). The magnitude of this offset is negligible for the liquid cargo car, which is likely due to the lateral slosh force that serves as a self-aligning force for centering of the car as it exits the curve. The liquid slosh, however, causes oscillations of the car body about the centreline of the track near the fundamental slosh frequency, as seen in Figure 4.11.

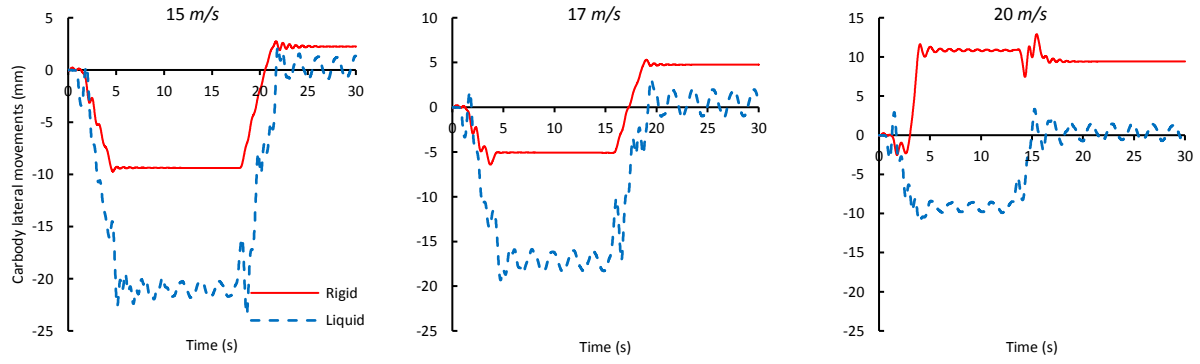

(a) (b) (c)

Figure 4.11: Lateral displacement responses of the 60%-filled liquid and equivalent rigid cargo cars with respect to track centerline while negotiating the 600 *m* radius super-elevated curve at different speeds: (a) 15 *m/s*; (b) 17 *m/s*; and (c) 20 *m/s*.

Figure 4.12 compares the derailment ratio of the leading wheelset of the 60%-filled liquid and rigid cargo cars negotiated the elevated curved track at different speeds. The liquid slosh contributes to higher values of the quotient compared to the rigid cargo, especially at speeds up to v_{bal}. The tendency of the liquid cargo to lean the vehicle toward inside of the curve leads to unloading of the outer wheel of wheelset, wst_1^l, and higher derailment quotient. The effect of liquid slosh, however, vanishes as the speed exceed v_{bal}, and response approaches to that obtained for the track with zero elevation (Figure 4.9(a)). The oscillation frequency of the *Y/Q* quotient during the steady and exit section of the curve is in vicinity of fundamental natural frequency of the 60% filled tank.

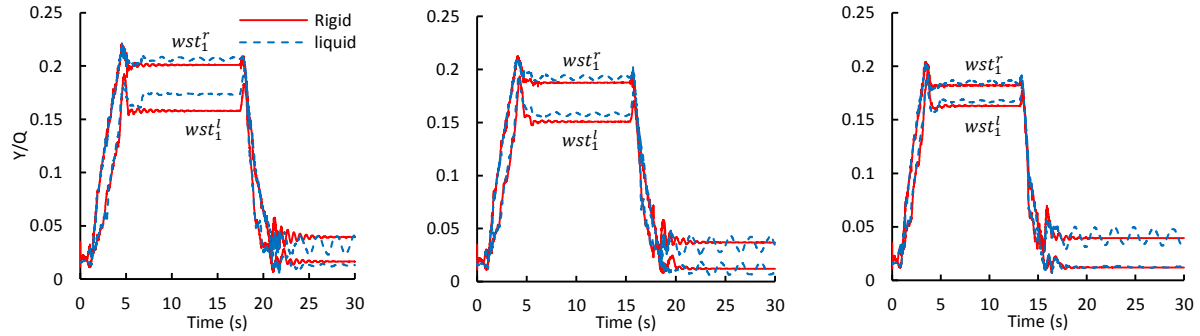

Figure 4.12: Derailment ratio values of the leading wheelset of the 60%-filled liquid and equivalent rigid cargo cars while negotiating the 600 *m* radius super-elevated curve at different speeds: (a) 15 *m/s*; (b) 17 *m/s*; and (c) 20 *m/s*.

4.4.3 Liquid cargo sloshing and overturning

The results obtained during curving maneuver suggest that neglecting the liquid slosh effect could lead to underestimations of the dynamic response, especially the unloading ratio. The reported studies of partly-filled road tankers have shown significant effects of cargo slosh on overturning risk of the vehicle [7, 98, 126]. The rollover potential of a vehicle is mostly assessed in terms of lateral acceleration threshold during steady curving and lateral load transfer ratio (LTR) during path-change maneuvers. The lateral acceleration threshold could be described as the acceleration magnitude leading to loss of wheel-rail contact during curving. Simulations are performed under increasing values of constant speeds to determine the magnitude of lateral acceleration leading to loss of wheel-rail contact during non-elevated curving (Section 4.3) for fill heights ranging from 40 to 97%. Figure 4.13 compares the lateral acceleration threshold values of the liquid cargo car with those of the corresponding equivalent rigid cargos for range of fill conditions. The results show opposing trends for the liquid and rigid cargo cars. In case of the rigid cargo, a lower fill condition yields higher overturning limit due to lower *c.g.* height. The liquid cargo, on the other hand, yields lower acceleration threshold for lower fill compared to the higher fill. This is due to higher lateral load shift and roll moment associated with greater movement of liquid free surface under lower fill heights. For fill levels, exceeding 90%, the overturning limit of the liquid cargo car approaches that of the equivalent rigid cargo car, near 2.4 m/s^2. This represents a critical forward speed of about 38 *m/s* on a 600 *m* radius curve. For the 40% fill condition, the critical speed reduces to about 35.5 *m/s*. The results suggest that lack of consideration of the slosh effect could yield

overestimation of the lateral acceleration threshold and critical overturning speed by nearly 50% and 25%, respectively, for the 40%-filled tank car.

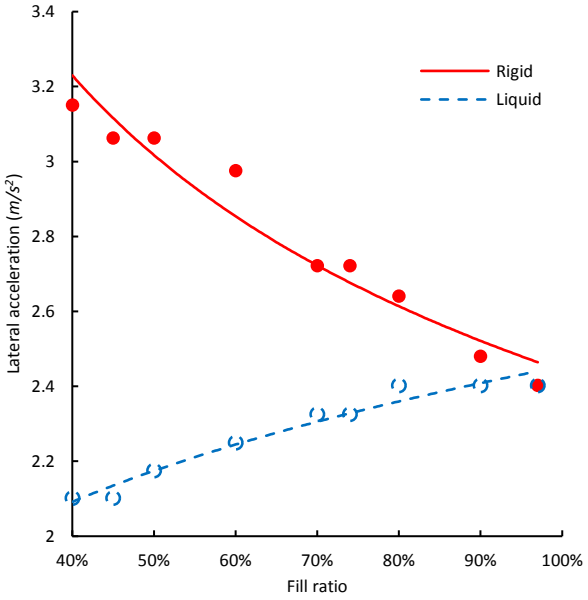

Figure 4.13: Comparison of critical performance measures of the liquid and equivalent rigid cargos in different filled conditions in terms of lateral acceleration threshold in curving.

4.5 Conclusions

A comprehensive coupled fluid-railway car model is developed to investigate the effects of fluid slosh in partially filled tank during different curve passing manoeuvres. The Freight tanker car with two three-piece bogie is modelled as multibody dynamic system with 114 DoF. The characteristics of freight car suspension and connections between car body and bogie is developed with careful attention to detail including multi-directional spring forces, contacts between suspension wedge and bogie frames, and side bearing contacts. Linear fluid slosh model with four anti-symmetric natural mode shapes of a partially filled tanker is shown to be adequate for fill levels in the range of 40 to 97%. The coupled dynamic model is realized by co-simulation of the linear slosh model and the multi-body tank car model. The approach is found to be adequate and highly computing efficient. The slosh model can be extended to other tank configurations with and without baffles, and without imposing high computational demand such as in the case of *CFD* models. The results from the present investigation reveal that for a curving manoeuvre, the fluid slosh effect of 60 to 70% fill level can lead to car roll angles that are more than twice that of equivalent rigid cargo. The comparison of derailment quotient (*Y/Q* ratio) consistently show slightly higher value due to fluid slosh during curving. The magnitude is however significantly lower than critical for the curving maneuver considered. Liquid slosh dynamics is essential to predict the limit as they are significantly lower when compared with those of rigid cargo simulations. It should be pointed out that the present investigation considers the track to be free of any defects or unevenness. In the presence of track disturbance, the response to a maneuver can be further deteriorated due to fluid slosh and may be of interest in further studies. The proposed liquid slosh model could also be used for more computational demanding analyses like wheel-rail wear or rolling contact fatigue test.

CHAPTER 5

Investigation of coupled railway tank car dynamics and liquid cargo response subject to switch passing maneuver

5.1 Introduction

Transportation of crude oil and other hazardous materials (HAZMAT) via rail and road modes constitutes important economic and employment factors in North America. Although the bulk of crude oil is transported via pipelines, the transportation by the railways has been increasing since 2009, which peaked in 2013 to about 16 000 carloads in Canada and over 400 000 in the United States [132]. The unpressurized US DOT-111 (CTC-111 A in Canada) tank cars accounted a major number of the tank cars used in North America. The circular cross-section tanks employed in these cars are designed with a minimum shell thickness of 11.1 *mm* and maximum capacity of up to 130 000 liters [133, 134]. Such tanks are prone to rupture in the event of an accident, which may cause catastrophic damages to the environment and property in commerce apart from human fatalities. Following the Lac-Megantic accident [135], railway authorities have defined alternate new regulations, namely TP14877 [136-138], to enhance operational safety performance of tank cars. The standard proposed design modifications for DOT-111 tanks and new tank design, denoted as TC-117 for transportation of flammable cargo, which requires minimum shell thickness of 14.3 *mm* together with electronically controlled pneumatic (*ECP*) brakes to limit the longitudinal forces developed during braking [138].

Despite the extensive interest in structural aspects of tank car, limited studies are reported on effects of liquid cargo movements on dynamics of railway vehicles. The partially filled conditions in the transportation of railway tank cars could be observed due to variations in density of different liquid products or limitation of the maximum load of specific tracks. The additional force and moments of liquid cargo due to directional accelerations of tank car could change the dynamic response of the vehicle in different maneuvers. The movements of liquid cargo in its container, known as sloshing, has been the subject of a number of extensive studies in road [*e.g.*, 99], aerospace [*e.g.*, 65], and marine [*e.g.*, 126] transport systems. Deferent methods for liquid cargo slosh analysis could be summarized as simple quasi-static liquid motion [7], mechanical analogs of the moving cargo [87], and linear and nonlinear fluid slosh methods [64, 84]. Some of these

methods have been employed for analyses of liquid cargo slosh effects in railway cars during curving and braking, as summarized in Table 5.1.

Mechanical-equivalent models, as most applied slosh model in railway dynamics, are presented in different models such as pendulum and mass-spring-damper [87, 95, 126]. The equivalent liquid slosh models are able to represent the fundamental lateral or longitudinal slosh frequencies of a partially filled horizontal tanker while their application for coupled conditions like braking in curve is questionable. Convenient integration of the equivalent mechanical models to multi-body dynamic (*MBD*) models is the considerable advantage of the method for vehicle dynamic studies. Most of studies on liquid cargo effects in railway dynamics are focused on the response of the vehicle in curving maneuvers. The underestimation of the roll response of the system with equivalent rigid model is reported where considerable load shift is generated due to liquid slosh. Di Gialleonardo *et al.* [94] established a slosh model as uncoupled equivalent mechanism of lateral mass-springs that equally spaced along the tank. The model incorporates the response of liquid slosh subject to yaw excitation. The liquid slosh was observed to generate higher unloading and derailment ratio, subject to an s-shape curve negotiation.

Table 5.1: Liquid slosh analysis methods used in reported studies in railway dynamics

Reference	**Vehicle model**	**Slosh model**	**Analyses objectives**
Khandelwal and Nigam [91]	Pitch plane model of a tank car	Equivalent mechanical model for rectangular tank in longitudinal direction	Simulation of braking/acceleration on an irregular track
Bogomaz [92]	Three-dimensional (3D) model of a tank car	Spherical pendulum model based on solutions of the boundary value problem	Curving simulation on a track with irregular
Vera *et al.* [95]	3D nonlinear model 4-wagon model	Lateral Pendulum that validated with 2D *CFD* results.	Simulation of a s-curve negotiation
Younesian *et al.* [3]	3D nonlinear model	Longitudinal mass-spring for different fill condition and fluid density.	Derailment and load shift analysis during brake in a curve
Di Gialleonado *et al.* [94]	3D nonlinear model	Lateral mass-spring model that validated by 2D *CFD* results	Dynamic load transfer and derailment for different analyses for different fill conditions
Hazrati *et al.* [34, 96]	3D nonlinear model	Trammel pendulum for different fill ratio and fluid density	Hunting and derailment analyses
Wang *et al.* [123]	3D nonlinear model	Continuum-based liquid sloshing in rectangular tank	Load shift and inertia effects of liquid cargo on dynamic responses under a s-shape track
Shi *et al.* [5]	3D nonlinear model	Absolute nodal coordinate formulation (ANCF) of liquid cargo	Curving and braking studies (high computational demand)

Reported studies on curving or braking analyses of railway tank cars have mostly employed mechanical-equivalent models of fluid slosh such as pendulum and mass-spring-damper models, generally identified through linear slosh analyses [87, 95, 126]. Such equivalent slosh models are limited to one-dimensional slosh corresponding to fundamental mode frequencies of a partially filled horizontal tanker in the lateral or longitudinal direction, while their applications under multiple axis excitations encountered during braking and curving are questionable. The mechanical equivalent models of slosh, however, can be conveniently integrated to multi-body dynamic (*MBD*) models of the vehicle, which permit analysis of the coupled cargo-vehicle system in a computationally efficient manner. Most of the studies on liquid cargo effects in railway dynamics are focused on the response of the vehicle during curving maneuvers. These have shown considerable load shifts due to liquid slosh [96, 131]. It has been reported that equivalent mechanical slosh models underestimate the roll response of the vehicle [5]. Di Gialleonardo *et al.* [94] employed multiple equally spaced but uncoupled lateral mass-spring models to study fluid slosh along the tank length under a yaw excitation. The liquid slosh was observed to generate higher unloading and derailment ratio of the tank car during an s-shape curve negotiation.

As an alternative to the equivalent mechanical analogous of liquid movement, computational fluid dynamic (*CFD*) methods have been widely used for analysis of transient liquid slosh, although a number of these focus on non-circular cross-section and baffled tanks [63, 65, 139]. A number of studies on partly-filled road containers have employed *CFD* methods, which are known to impose extensive computational demands [5, 123]. Shi *et al.* [5] proposed a continuum based fluid constitutive model coupled with a fluid-tank contact algorithm. The model was used to evaluate the tank car responses during curving and electronically-controlled pneumatic (*ECP*) braking tests. The proposed method also poses considerable computational demand similar to the *CFD* methods.

Alternatively, linear slosh theory has been widely applied to study fluid slosh in storage tanks and road containers in a computationally efficient manner assuming inviscid and irrotational flows [99, 126]**.** Through comparisons of linear and nonlinear liquid slosh responses in a partly-filled horizontal cylindrical container, it has been shown that the linear theory can yield accurate predictions of the slosh forces and moments under excitations encountered during typical vehicle maneuvers [13]. The linear theory, however, underestimates the resonant slosh, when separation of the free surface occurs. The linear slosh theory has been applied for predicting slosh modes, and force responses in partly-filled arbitrary cross-section tanks with and without baffles of varying

geometry [6, 98]. The linear slosh model can also be easily integrated to the *MBD* models of the vehicle as in case of the mechanical equivalent models. Furthermore, unlike the mechanical models, the linear slosh theory permits analyses of three-dimensional slosh encountered during simultaneous braking and curving in a highly efficient manner [129].

As stated above, the majority of the reported studies on railway tank cars are focused on analyses of slosh effects during curving, which generally yields relatively gradual and smooth variations in acceleration excitation. Studies reported the influences of fluid slosh on road tankers have shown that considerably more severe effect under transient type of excitations encountered during path-change operations [6, 99]. The switch-passing maneuver in railway vehicles represents a transient excitation, where the magnitude of lateral acceleration may vary rapidly [140]. Furthermore, during a switch-passing maneuver, the railway car undergoes considerable lateral movement, which gives rise to substantial variations in the wheel-rail contact forces that have been associated with more significant derailment potential [141, 142]. The force arising from the wheel-rail contact, including the flange contact, during a switching maneuver constitute relatively higher-frequency excitation for the liquid cargo. The cargo movement under the rapidly varying lateral acceleration during switching may also contribute to variations in the wheel-rail contact forces. Moreover, the residual free surface oscillations may serve as continued disturbances to the system even after passing the switch. A study of liquid cargo movements caused by excitation encountered during a switch-passing maneuver and their effects on dynamic responses of the tank car is thus important in seeking guidance for safer operating conditions and maintenance of the switch segments.

In this study, the liquid slosh within a partly-filled railway tank is analyzed using a linear slosh model. A comprehensive nonlinear multi-body dynamic model of a tank car is formulated in the *Universal Mechanism* (UM) software [110, 124]. The vehicle model comprises the nonlinear damping and stiffness properties generated by friction wedges in the secondary suspension of the bogie. The effects of liquid sloshing on the dynamic response of the vehicle in a switch-passing maneuver are evaluated through co-simulations of the vehicle and liquid cargo models considering different fill conditions. The response characteristics of the partly-filled tank car are compared with those of the car with an equivalent rigid cargo in order to illustrate adverse effects of liquid cargo slosh on the directional performance of the railway vehicle during a switch-passing maneuver. The simulations are performed to evaluate contributions of the dynamic liquid slosh to different

performance indices, namely, derailment quotient, car body roll and lateral dynamic load applied to the track. The critical speeds corresponding to wheel-rail separation during the switch-passing maneuver are further identified as a function of the liquid cargo fill height using different slosh models.

5.2 Model formulations

5.2.1 Multi-body dynamic model of the tank car

The multi-body dynamic (*MBD*) model of the railway tank car with three-piece freight bogies is formulated in *Universal Mechanism* (*UM*) software. The model incorporates friction forces in different suspension components of the bogie and the interface between bogie and the car body, which resulted in a relatively complex *MBD* model of the car with 114 degrees of freedom (DoF). The model has been described in details in [28]. Briefly, the vehicle model employs comprehensive representations of the friction forces due to suspension wedges, and interactions of the car body with the center plate and side bearings.

The friction wedges together with the secondary suspension of the bogie were modeled as multi-directional stiffness and damping elements considering the contact forces and friction, as shown in Figure 5.1. For this purpose, an array of point-plane contact elements were formulated to derive frictional forces due to relative motions of the wedges with respect to the side frame and the bolster. A methodology for identifying the model parameters has been described in [28, 35, 96]. The point-plane contact approach could efficiently estimate the resultant friction moments developed at the center plates and side bearings under relative rotations of the contacting bodies encountered during curving or switch-passing maneuvers. The variations in interactions between the car body and the center plate (bogie) under varying loads could also be described accurately using this modeling approach. The dynamic model of rail vehicle is thus considered appropriate for simulation of dynamic respond of the vehicle subject to the disturbance of liquid slosh movements, where instantaneous load transfer may vary performance of the bogie and suspension system considerably.

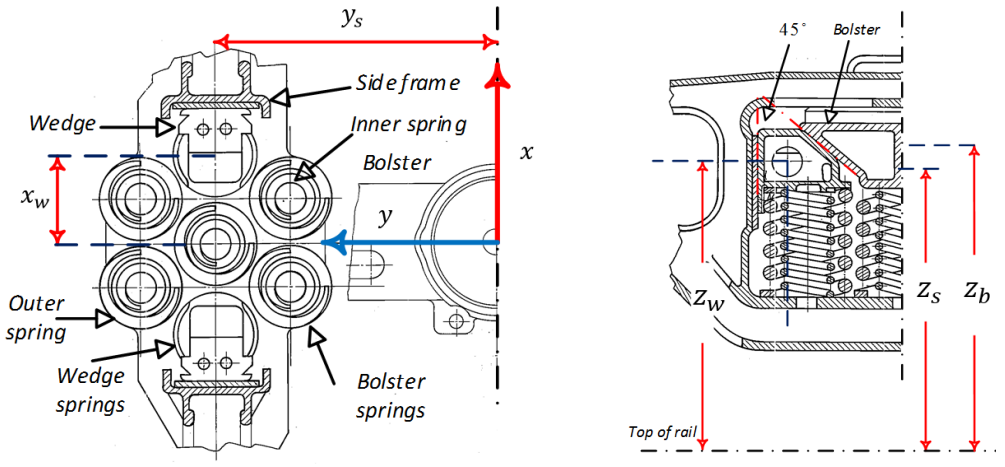

(a) (b)

Figure 5.1: (a) Top view and (b) side view of the friction wedge suspension [28, 35]. (a) top view of wedge and spring group suspension (b) side view of the wedge suspension.

Table 5.2 summarizes the inertial and geometric parameters of the simulated model components, namely, the wheelset, bolster, side-frame, wedges and car body with empty tank. The table also lists coordinates of mass centers of the side frame (y_s, z_s) and wedges (x_w, y_w, z_w) and height of mass center of the fully loaded tank with respect to the top of the rail (z_{tank}).

Table 5.2: Simulation parameters of multibody dynamic of the tank car [109-111, 143].

Component	Mass (kg)	I_x ($kg \times m^2$)	I_y ($kg \times m^2$)	I_z ($kg \times m^2$)	Additional Geometric parameters
Wheelset	1,500	925	200	925	Wheel gauge = 1.500 m Wheel base = 1.850 m Wheel diameter = 0.950 m
Bolster	596	323	7.25	326.3	z_b = 0.653 m (Loaded)
Side-frame	526.3	13.6	175	161.8	y_s = ± 0.978 m z_s = 0.515 m
Wedge	21.6	0.080	0.103	0.102	x_w = ± 0.335 m y_w = ± 0.978 m z_w = 0.555 m *empty* z_w = 0.515 m *loaded*
Car body	12,400	21,840	74,785	87,666	Bogie to bogie distance = 9.130 m z_{tank} = 1.386 m (Loaded)

A multi-directional wheel/rail contact model is further used in the vehicle model to determine the contact forces and moments as functions of the translational and rotational motions of the wheelset, including the flange contact. For this purpose, The Kalker's *FastSim* algorithm [104] is applied to determine the creep forces and moment at the wheel/rail interface considering an elliptical contact patch.

5.2.2 Liquid slosh model

A two-dimensional linear slosh model is formulated to study the liquid cargo free surface movement, dynamic load shift, and lateral force and roll moment caused by lateral acceleration and roll motion of the tank that may be encountered during a switch-passing maneuver. For this purpose, a partially filled cylindrical tank of radius R is considered with the tank-fixed coordinate system (y,z) located at the geometric center of tank, O, as shown in Figure 5.2(a). The fill height H determines the tank wetted surface, S_w, and length of the free surface ($2y_0$). z_0 defines the free surface height with respect to the geometric center of the tank. Figure 5.2(b) illustrates the free surface motion when the tank surface is subjected to a lateral acceleration $\ddot{Y}(t)$ at the geometric center of the tank and roll angle of the car body $\theta(t)$.

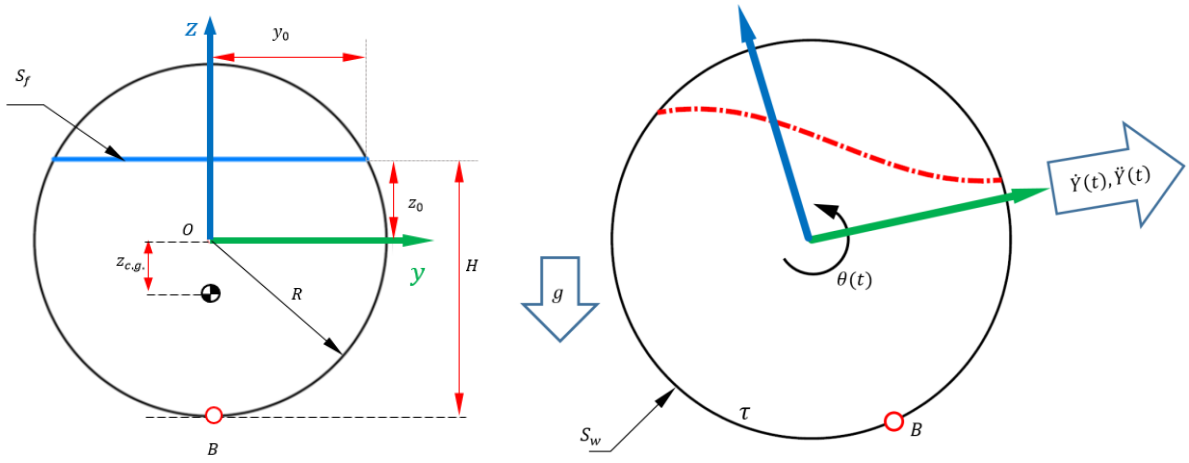

(a) (b)

Figure 5.2: (a) Circular cross-section tank with liquid free surface; and (b) two-dimensional motion of the liquid free surface.

The equation of motion of the liquid is formulated considering incompressible and irrotational flow in the form of the Laplace equation, as:

$$\nabla^2\Phi = \nabla^2(\Phi_R + \Phi_S) = 0 \qquad \text{in} \quad \tau \tag{5.1}$$

where Φ_R and Φ_S are two components of the velocity potential corresponding to the rigid body motion of the liquid cargo and its motion relative to the tank in the liquid domain, τ.

Based on the multimodal method [126], the potential Φ_S attributed to liquid slosh can be expressed as a function of the lateral and vertical motions of the liquid (*y,z*) through superposition of natural modes, φ_i, expressed in the generalized coordinates, γ_i:

$$\Phi_S(y,z,t) = \sum_{i=1}^{\infty} \gamma_i(t)\varphi_i(y,z) \tag{5.2}$$

Substituting the above equation into the free-surface boundary condition results in the following set of ordinary differential equations [64]:

$$\ddot{\gamma}_i + 2\xi_i\sigma_i\dot{\gamma}_i + \sigma_i^2\gamma_i = -\ddot{Y}\lambda_i \qquad \text{on } S_f \tag{5.3}$$

where $\ddot{Y}$ is the time derivative of the effective lateral acceleration acting at the geometric center of the container and σ_i is circular frequency of the liquid oscillations. In the above equation, λ_i is the hydrodynamic coefficient given by:

$$\lambda_i = \frac{\int_{S_f} y\varphi_i dS}{\int_{S_f} (\varphi_i)^2 dS} \tag{5.4}$$

The modal damping coefficients, ξ_i, in Equation (5.3) are estimated considering liquid viscosity, from [78, 99]:

$$\xi_i = \frac{g}{2\sqrt{2}R} v_s^{1/2} \sigma_i^{-5/2} \int_{S_w} \left(\frac{\partial \varphi_i}{\partial s}\right)^2 dS \tag{5.5}$$

where ν_s is the fluid kinematic viscosity and *g* is acceleration due to gravity. Here the natural slosh modes and frequencies are obtained using the Ritz variational method as described in [64]. The solutions of the differential equation (5.3) yield hydrodynamic pressure, $P(y,z,t)$, which directly relates to the slosh force and moment via the linearized Bernoulli's equation [126].

The total lateral force, $F_y(t)$, acting on the container wall, per unit length of the container, is obtained from integration of hydrodynamic pressure over the tank wetted area, S_w, such that:

$$F_y(t) = \int_{S_w} P(y,z,t)dz = F_{y,R}(t) + F_{y,S}(t) \tag{5.6}$$

The resultant lateral force can be expressed in two components, $F_{y,R}$ and $F_{y,S}$, attributed to the rigid body and slosh motions of the liquid, respectively, as:

$$F_{y,R}(t) = -\rho L(\ddot{Y}(t) + \theta(t)g) \int_{S_w} ydz = -M(\ddot{Y}(\mathrm{t}) + \theta(t)g) \tag{5.7}$$

$$F_{y,S}(t) = -\frac{\rho}{g} L \sum_{i=1}^{\infty} \lambda_i \sigma_i^2 \dot{\gamma}_i(\mathrm{t}) \tag{5.8}$$

where M is the total fluid mass in a tank with length L, ρ is fluid mass density and θ is roll angle of the tank. The moment due to liquid cargo motion is evaluated about the base point of tank B (Figure 5.2) by integrating the hydrodynamic pressure over the wetted surface of the tank:

$$M_B(t) = -L \int_{S_w} P(y,z,t)\,[ydy + (R+z)dz] \tag{5.9}$$

The resulting roll moment due to cargo slosh can be defined as summation of three different components associated with the rigid body moment (M_R), moment due to the vertical load transfer (M_V) and the moment due to lateral slosh force (M_s), such that:

$$M_B(t) = M_R(t) + M_V(t) + M_S(t) \tag{5.10}$$

These components are computed from:

$$M_R(t) = \rho L(\ddot{Y}(t) + \theta(t)g) \int_{S_w} y(R+z)dz = M\big(R + z_{c.g.}\big)(\ddot{Y}(t) + \theta(t)g) \tag{5.11}$$

$$M_V(t) = \rho L(\ddot{Y}(t) + \theta(t)g) \int_{S_w} y^2 dy = \frac{2}{3}\rho y_0^3 L(\ddot{Y}(t) + \theta(t)g) \tag{5.12}$$

$$M_S(t) = \frac{\rho L}{g}\, R \sum_{i=1}^{\infty} \lambda_i \sigma_i^2 \dot{\gamma}_i(\mathrm{t}) = R \times F_{y,S}(t) \tag{5.13}$$

where $z_{c.g.}$ in Equation (5.11) is the position of center of gravity for liquid cargo with respect to the geometry center of the tank, point *O*, as shown in Figure 5.2. The $M_V(t)$ can be regarded as the moment due to lateral shift of liquid cargo subject to lateral acceleration and roll motion of the tank car.

5.3 Method of analysis

The differential equations (5.3) can be expressed in the state-space form for a given number of liquid cargo deflection modes, as:

$$\begin{bmatrix} \ddot{\gamma}_1 \\ \vdots \\ \ddot{\gamma}_i \\ \dot{\gamma}_1 \\ \vdots \\ \dot{\gamma}_i \end{bmatrix} = \begin{bmatrix} -2\xi_1\sigma_1 & 0 & 0 & -{\sigma_1}^2 & 0 & 0 \\ 0 & \ddots & 0 & 0 & \ddots & 0 \\ 0 & 0 & -2\xi_i\sigma_i & 0 & 0 & -{\sigma_i}^2 \\ & I_{i\times i} & & & 0_{i\times i} & \end{bmatrix}_{2i\times 2i} \times \begin{bmatrix} \dot{\gamma}_1 \\ \vdots \\ \dot{\gamma}_i \\ \gamma_1 \\ \vdots \\ \gamma_i \end{bmatrix} - \begin{bmatrix} \lambda_1 \\ \vdots \\ \lambda_i \\ 0_{i\times 1} \end{bmatrix} \ddot{Y} \tag{5.14}$$

The subscript i in the above equation denotes the number of modes considered. The solutions of the above differential equations, obtained for a given fill volume (free surface height) and lateral acceleration excitation arising from a switch-passing maneuver, are applied in Equations (5.8) and (5.13) to determine lateral force and roll moment, respectively, due to liquid slosh. The *MBD* model of the car is initially simulated considering the liquid cargo as an equivalent rigid cargo to determine the instantaneous car body roll and lateral acceleration response at the tank's geometric center under the switch-passing maneuver input. This permits to account for the contributions of vertical and lateral inertial forces, $F_z(t)$ and $F_{y,R}(t)$, as well as roll moment, M_R, attributed to rigid body motion of the cargo. The co-simulations of the *MBD* model of the tank car and liquid slosh model were initiated at time $t = 0$, assuming zero initial values for liquid slosh force and moment ($F_{y,S}(t) = 0$; $M_V(t) = 0$) under zero lateral acceleration and roll angle of the tank. The state-space Equation (5.14) were solved in Matlab/Simulink under instantaneous lateral acceleration at the geometric center of tank and roll angle response obtained from the *MBD* model of the tank car. The resulting slosh force and roll moment were subsequently applied to the *MBD* model in *UM* software to compute the car body responses, subject to slosh force $F_{y,S}(t)$ and roll moment $M_V(t)$. These served as inputs applied to the geometric center of the tank in addition to the maneuver input to compute the car body responses at the subsequent instant.

The diameter of the 12 *m* long tank ($2R$) was taken as 2.8 *m*, while the end caps were considered to be flat, assuming negligible contribution of the curved endcaps to the lateral slosh force. The capacity of the tank was 73.85 m^3 with maximum cargo load of 58 550 *kg*, which corresponded to nominal axle load of 210 k*N*. This loading scenario simulated the responses of the tank car with a

constant cargo load irrespective of the fill ratio that may be encountered in a general-purpose tank design transporting liquid products with varying mass density.

The friction coefficient for the multiple contact points between the wheel and rail was considered as 0.25 for the flange and tread regions, as defined in a number of studies [*e.g.*, 38, 96]. Each wheel-rail contact point was divided into 100 cells to identify the creep and stick conditions in addition to the tangential forces using the *FastSim* contact model [104]. The coupled simulations of the *MBD* model of the tank car and liquid cargo model were performed using Park method [117] with time step varying from a minimum of 1×10^{-12} to a maximum of 1 m*s* with an error tolerance of 1×10^{-8}.

The dynamic responses of the partly-filled tank car are likely dependent on both the switch-passing speed and the switch length apart from the fill volume, since these affect the lateral acceleration excitation magnitude and dominant frequency. The dynamic responses of the partially filled tank car are evaluated while passing the divergent route of the 300-1/11 switch at different constant forward speeds in the 15 to 20 *m/s* range. The forward speed in the dynamic simulations is maintained constant to reduce the possibility of longitudinal slosh modes excitation due to longitudinal acceleration. The response characteristics are also evaluated considering a different switch geometry, 200-1/9, which represents a relatively higher magnitude and frequency of excitation [140]. Figure 5.3 illustrates the path followed during a switch-passing maneuver. Table 5.3 summarizes the geometric coordinates of the two switch geometries [110, 144].

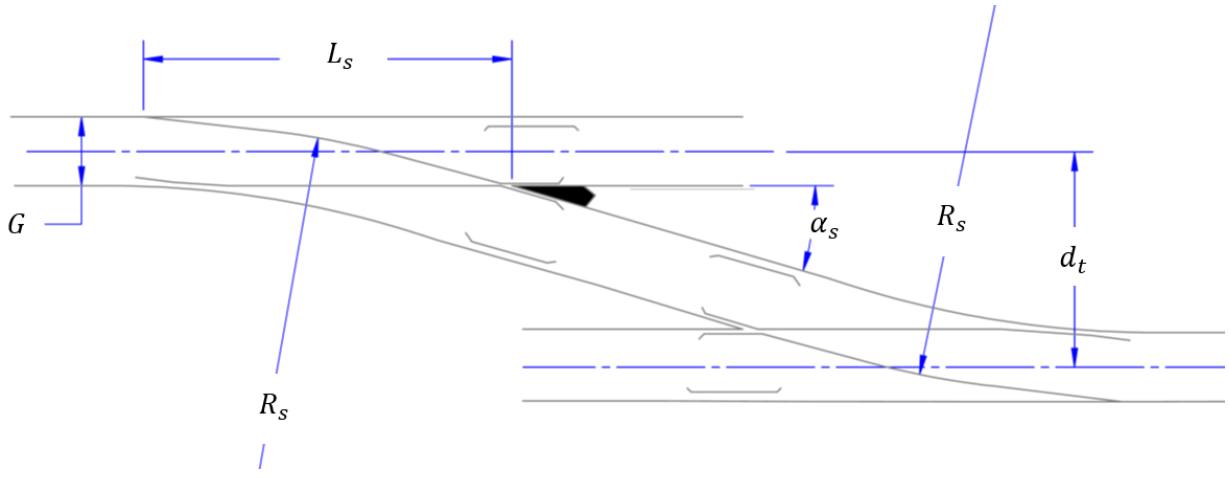

Figure 5.3: The top view of a typical railway switch.

Table 5.3: The values and definition of witch parameters [110].

Switch type	200-1/9	300-1/11		
Parameter	Value	Value	unit	Description
G	1.435	1.435	m	Track gauge
α_s	111.1	90.90	mrad	Switch angle
R_s	200	300	m	Switch major radius
L_s	30.27	33.9	m	Switch length
d_t	5	5	m	Track spacing

The significance of the liquid cargo movements within the tank is evaluated by comparing different dynamic responses of the partly-filled tank car with those of the car with equivalent rigid cargo. Moreover, the critical speeds of the car are evaluated considering the lateral load transfer for both the liquid and equivalent rigid cargo car models.

5.4 Result and discussions

5.4.1 Liquid slosh model validations

The validity of the analytical liquid slosh model is initially examined by comparing the natural slosh frequencies as well as hydrodynamic and damping coefficients with those in the reported studies for a range of fill conditions. It has been reported that the fluid slosh in ground transportation systems of liquid cargo dominates in the low-frequency range, particularly the fundamental mode frequency [64, 98, 99]. The slosh analyses in this study are thus limited to the first four antisymmetric modes for fill ratios ranging from 30 to 90%. Figures 5.4(a) and (b) illustrate natural frequencies and hydrodynamic coefficients corresponding to the first four antisymmetric modes for the entire range of fill ratio and tank geometry presented in Section 5.3 (R=1.4 m; L=12 m). The natural frequencies and hydrodynamic coefficients obtained from the model are in very good agreements with those reported by Faltinsen and Timokha [78]. The natural frequencies corresponding to the selected modes increase monotonically with increasing fill volume, although the rate of increase in the slosh frequencies is higher for fill ratios above 70%. This is due to reduction in the liquid free surface length ($2y_0$) with fill ratio increasing beyond 50%. Moreover, the results in Figure 5.4(b) indicate relatively higher magnitudes of hydrodynamic coefficients in the 50 to 60% fill range for all the modes considered, suggesting relatively higher slosh force. Figure 5.4 (c) presents variations in the values of integral, $\int_{S_w}(\partial\varphi_i/\partial s)^2\,dS$, in Equation (5.5) that relates to effective damping corresponding to each mode for different fill ratios. The results suggest higher damping for the higher antisymmetric modes. Furthermore, the integral value tends to diminish as the fill ratio is increased. The dominant magnitudes of hydrodynamic coefficient for the fundamental mode together with lower damping further stresses the higher significance of the fundamental mode, especially under lower fill ratios, which has been widely considered as the dominant mode in road tankers [64, 98].

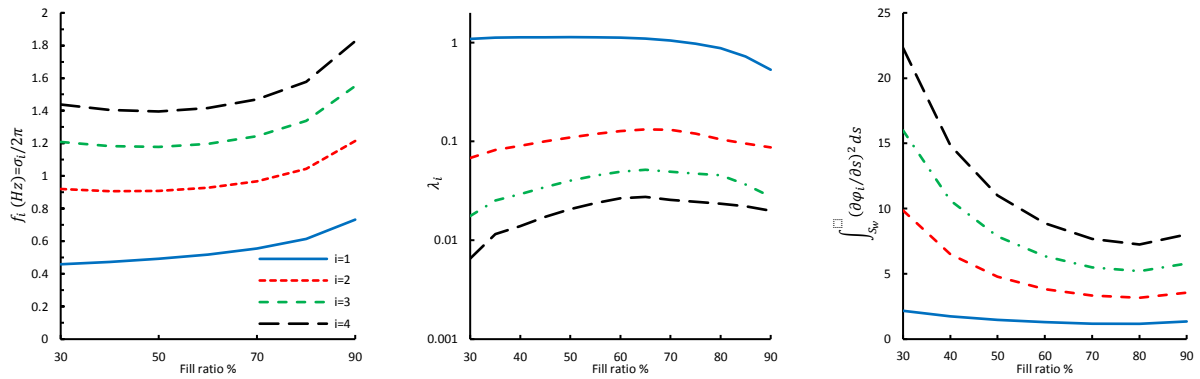

(a) (b) (c)

Figure 5.4: Variations in (a) natural frequencies; (b) hydrodynamic coefficients; and (c) normalized damping coefficient corresponding to lower four antisymmetric modes with the fill ratio.

The validity of the liquid slosh model is further examined by comparing the slosh force response with that obtained from a nonlinear *CFD* slosh model of the partly-filled tank. For this purpose, liquid slosh model is analyzed to compute the lateral slosh force response of the 75%-filled tank car (cargo: water; ρ=998.2 kg/m^3 and $\nu_s = 1.0048 \times 10^{-6}$ m^2/s) under a lateral acceleration excitation encountered during a switch-passing maneuver. The lateral acceleration excitation was obtained through dynamic simulation of the railway tank car model with an equivalent rigid cargo subject to switch-passing maneuver (300-1/11) at a forward speed of 17 *m/s*. The resultant lateral acceleration of car body at the geometric center of the tank is presented in Figure 5.5(a).

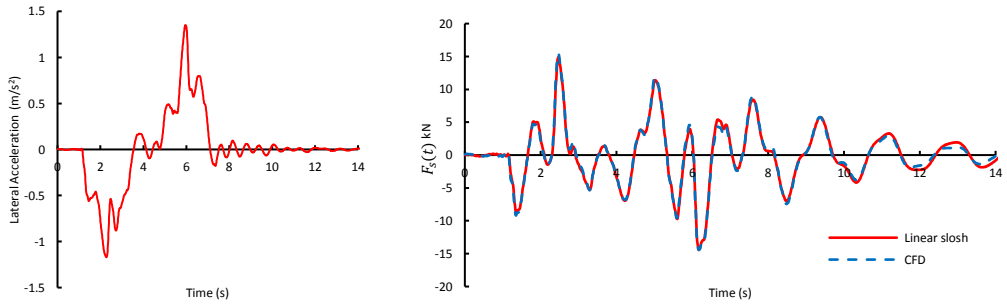

(a) (b)

Figure 5.5: (a) Lateral acceleration of car body passing a 300-1/11 switch at 17 *m/s* speed for 75% fill condition; (b) the variations of liquid slosh, $F_s(t)$, subject to the given excitation with proposed liquid slosh model and alternative *CFD* model.

The lateral force response of the analytical slosh model is obtained by summation of first four antisymmetric modes. A *CFD* model of the tank was also formulated in the Fluent platform, as

described in [84, 129]. The time-histories of the lateral slosh force responses obtained from the analytical and *CFD* models are compared in Figure 5.5(b). Both the models yield nearly identical lateral force response. Both the models also exhibit sustained oscillations in the lateral force even after the acceleration due to switch-passing diminishes (t>8s). The frequency of such free oscillations in slosh force response of both models is nearly 0.6 *Hz*, which is identical to that shown in Figure 5.4(a) for the first antisymmetric mode corresponding to 75% fill ratio. From the results presented in Figures 5.4 and 5.5, it may be concluded that the analytical slosh model, considered in this study, can provide accurate estimation of the slosh response of the partly-filled tank under the lateral acceleration excitation that may be encountered during a switch-passing maneuver. The linear slosh model also yields the response in a highly computationally efficient manner compared to the *CFD* model that poses considerably higher computational cost. The linear slosh model is thus considered to be well suited for dynamic analyses of the coupled tank car and liquid cargo models. Moreover, the linear approach does not require re-computation of the coefficients in the state-space Equations (5.3 and 5.14) at each iteration step and thereby can facilitate real-time co-simulations of the *MBD* model. It should also be noted that these coefficients for an alternate tank geometry of radius $\bar{R}$ can be conveniently estimated from those obtained for the nominal tank radius:

$$\sigma_i^2 \times 1.4 = \overline{\sigma}_i^{\,2} \times \bar{R} \quad \text{and} \quad \lambda_i \times \bar{R} = \overline{\lambda}_i \times 1.4 \tag{5.15}$$

Where $\overline{\sigma}_i$ and $\overline{\lambda}_i$ are the natural frequencies and hydrodynamic coefficient of the tank of radius $\bar{R}$.

5.4.2 Effects of liquid cargo sloshing during switch passing maneuvers

The dynamic responses of the car body coupled with the liquid slosh are evaluated under the lateral acceleration excitations due to the 300-1/11 switch at different forward speeds. The responses obtained for liquid and equivalent rigid cargos are compared to illustrate the effects of liquid slosh when the tank car is partly-filled with a liquid cargo. The roll responses of the tank car body with 60% and 90%-filled liquid and equivalent rigid cargos are compared in Figure 5.6 considering a constant forward speed of 15 *m/s*. The results show considerably higher peak roll angles of the partly-filled tank car when compared to those with the equivalent rigid cargo. The effect of cargo slosh is more pronounced for the 60%-filled tank car compared to the 90%-filled car. The results show that the equivalent rigid cargo consideration of the liquid load will yield considerable underestimation of the car body roll response, especially for the 60% fill condition. The peak roll angle of the 90%-filled liquid tank car is nearly 11% lower than that obtained for the 60% fill condition, even though the cargo *c.g.* height of the 60%-filled tank car is considerably lower compared to the 90% fill condition. The higher roll angle is attributed to larger free surface length for the 60% fill condition compared to the 90%-fill case and thereby higher lateral load shift and roll moment during the switch-passing maneuver. This is also evident from the lower values of the hydrodynamic coefficients obtained for fill ratios exceeding 70%, as presented in Figure 5.4(b). The reduced free surface length of liquid cargo for the 90%-fill condition thus leads to relatively smaller effect of liquid slosh on the roll response. Moreover, the sloshing within the 60%-filled tank yields notable oscillations in roll response near the fundamental slosh frequency (≈0.5 *Hz*) even after passing the switch. Small oscillations are also observed in the response of the rigid cargo car, which occurs in the vicinity of roll mode frequency of the car body, near 1.25 *Hz*.

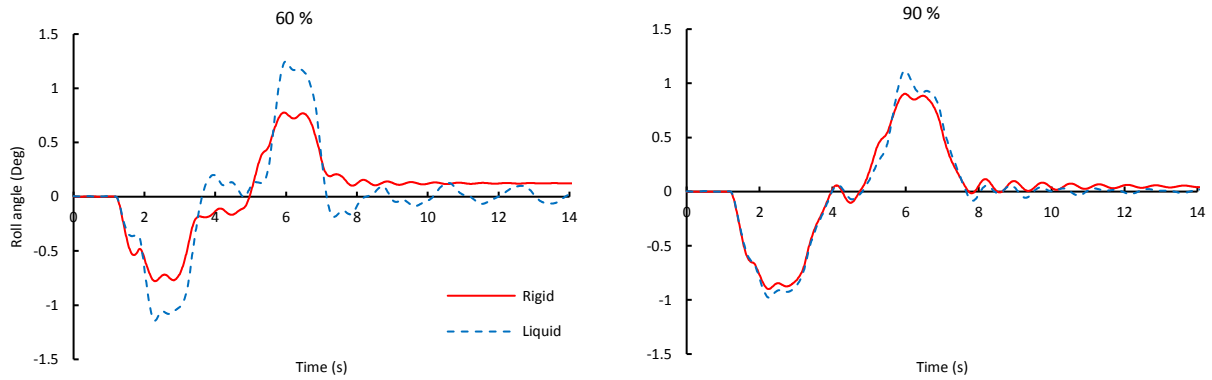

(a) (b)

Figure 5.6: Comparisons of roll angle responses of the car body with liquid and equivalent rigid cargos during a switch passing maneuver at a speed of 15 *m/s* for different fill ratios: (a) 60% and (b) 90%.

The higher peak roll angle response of the liquid cargo car is attributable to contributions of the liquid cargo slosh, particularly the lateral slosh force and roll moment. The lateral slosh force and roll moment, $F_{y,S}(t)$ and $M_V(t)$, responses of the tank car are compared in Figures 5.7(a) and 5.7(b), respectively, for the 60 and 90% fill ratios. It is perhaps worthy to note that the *c.g.* height for the 60%-fill condition is 23% lower than that for the 90%-filled car. Despite the lower *c.g.* position, the relatively larger free surface length in the 60%-filled tank leads to considerably higher slosh force and roll moment, when compared to those for the 90%-filled car. The results also show continued high magnitude oscillations in the lateral force response of the 60%-filled car even after passing the switch, which occur at the fundamental mode frequency of about 0.5 *Hz*. The continued free liquid slosh is due to low damping correspond to the fundamental mode, as seen in Figure 5.4(c).

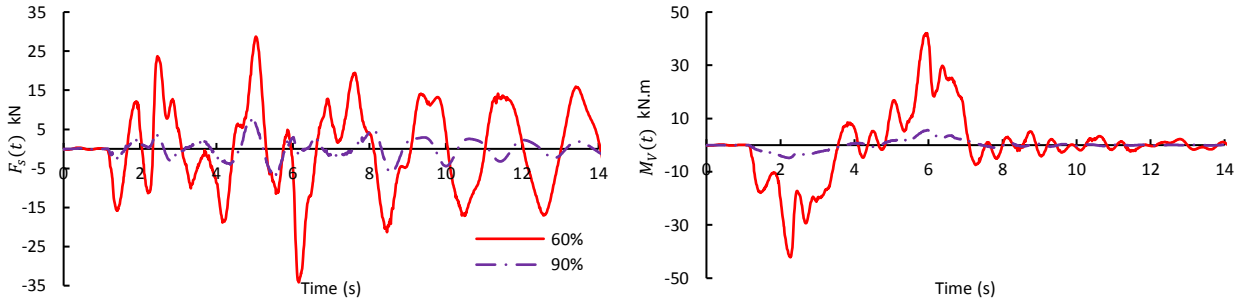

(a) (b)

Figure 5.7: Comparisons of lateral slosh force and roll moment responses of the tank car with 60 and 90% fill ratios while negotiating the 300-1/11 switch at 15 *m/s* forward speed: (a) lateral force, $F_{y,S}(t)$ and (b) roll moment, $M_V(t)$.

The lateral force and roll moment due to cargo slosh also leads to higher lateral force imposed by the wheelsets to the track, as shown in Figure 5.8. The figure compares the variations in wheelset lateral force for the 60%-filled equivalent rigid and liquid cargo tank car models subject to switch-passing maneuver at 17 *m/s*, as an example. The force responses are compared for all the 4 wheelsets, while the notations are shown in Figure 5.8(e). It can be observed that all the wheelsets impose higher peak forces to the track in the presence of liquid slosh. Comparison of responses of the liquid and rigid cargo models show relatively higher significance of the liquid slosh after exiting the switch, which is due to continued free oscillations of the free-surface of the liquid cargo. The oscillations in the lateral wheelset forces of the liquid cargo vehicle dominate near the fundamental mode frequency of 0.5 *Hz*. The rigid cargo vehicle also shows low magnitude oscillations in the lateral force after exciting the switch. The frequency of oscillations is about 1.34 *Hz*, which corresponds to primary hunting frequency of the wheelsets [35]. The magnitude of the oscillatory wheelset lateral force diminishes after a number of oscillations since the forward speed is below the critical hunting speed [28, 35].

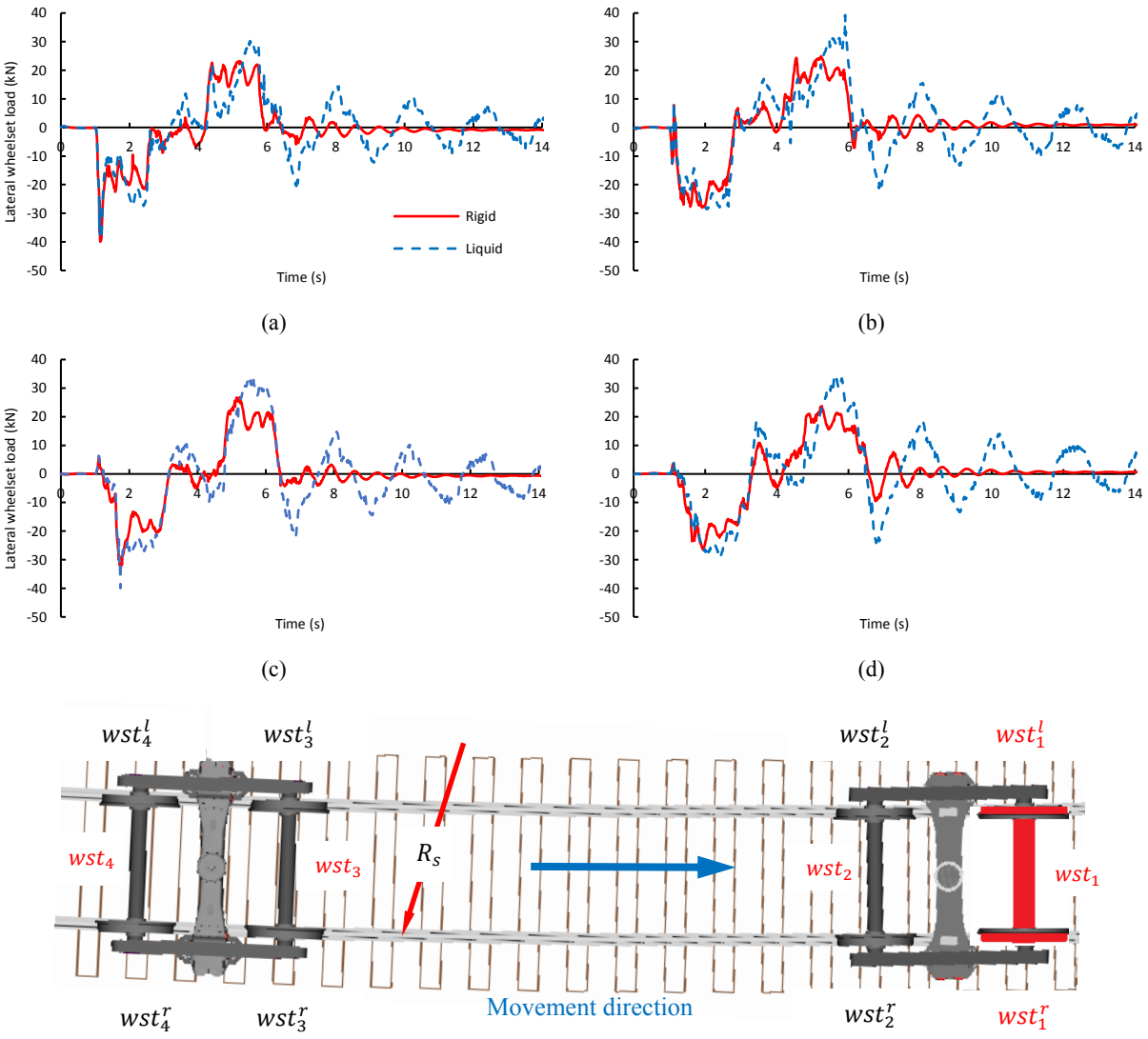

Figure 5.8: Comparisons of wheelset lateral force responses of the tank car with 60%-filled liquid and rigid cargos while passing a 300-1/11 switch at 17 *m/s* forward speed: (a) wst_1; (b) wst_2; (c) wst_3; (d) wst_4; and (e) notations of the wheelsets.

The higher car body roll response in the presence of fluid slosh can also lead to more significant transfer of load across the wheelset, which may affect the normal forces developed at the wheel-rail interfaces. The effect of liquid slosh on the load transfer is evaluated in terms of wheel unloading ratio, $(Q - Q_0)/Q_0$, where Q_0 and Q are the static and instantaneous normal forces at the wheel/rail contact, respectively. As an example, Figure 5.9 compares the unloading ratio responses of the car with 60%-filled liquid and equivalent rigid cargo while passing a 300-1/11 switch. The variations in the unloading ratio are presented for the left-side wheel of the leading

wheelset (wst_1^l) alone subject to switch-passing maneuver at two different forward speeds: 15 and 20 *m/s*. The results show that liquid slosh within the partly-filled tank car could yield 40 and 20% higher peak unloading ratio compared to the equivalent rigid cargo at forward speeds of 15 and 20 *m/s*, respectively. Furthermore, passing the switch at the higher forward speed of 20 *m/s* leads to continued high magnitude oscillations in the unloading ratio after exiting the switch, as seen in Figure 5.9(b). This is due to greater free surface oscillations under relatively higher magnitude lateral acceleration of the car compare to that encountered at the speed of 15 *m/s*. The peak unloading ratio approaches 0.8 in the presence of liquid cargo slosh, while negotiating the switch at the higher speed of 20 *m/s*. The unloading ratio of 0.8 has been termed as a critical value in [52, 57]. The unloading ratio will likely approach or exceed the critical value during switch-passing at a higher speed. Higher speed not only yields higher magnitude of lateral acceleration but also higher frequency of the maneuver-induced excitation, which may lie in the vicinity of the frequency of the fundamental mode of slosh.

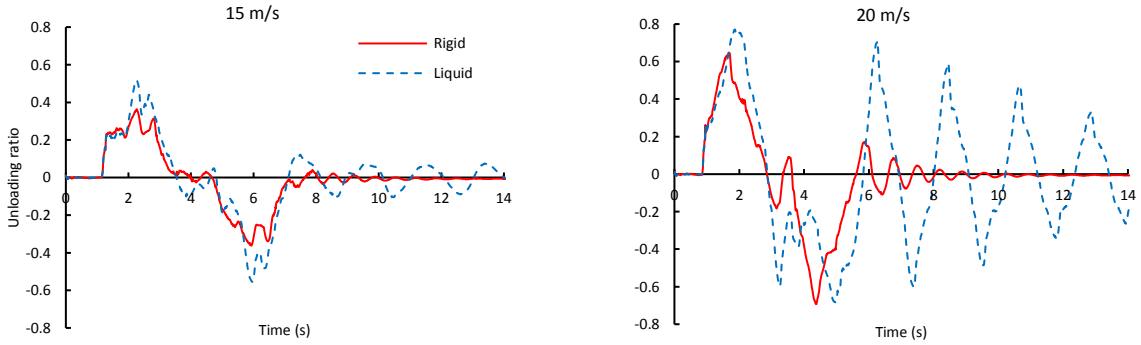

(a) (b)

Figure 5.9: Comparisons of unloading ratio responses of the outer wheel of the leading wheelset, wst_1^l, of the car with 60%-filled liquid and equivalent rigid cargos during passing a 300-1/11 switch at different speeds: (a) 15 *m/s*; and (b) 20 *m/s*.

The effect of liquid cargo movements on the wheel-rail contact force variations is further evaluated in terms of the derailment risk, as the ratio of instantaneous lateral to vertical forces of each wheel-rail interface, (*Y/Q*). This ratio has been reported to occur around 1.03 for the typical wheel flange angle, $\alpha = 60°$, and wheel-rail friction coefficient, $\mu = 0.25$ [38]. The *Y/Q* ratio of 0.86 has been considered as the critical derailment ratio, assuming a safety factor of 1.2, which corresponds to initiation of the flange climbing over the rail [38]. Figure 5.10 illustrates the effect of liquid slosh on variations in *Y/Q* ratio of the wheels of the leading wheelset of the tank car. The results are presented for the 60%-fill liquid and equivalent cargos, while passing the switch at 20 *m/s*. Unlike

the wheel unloading ratio, the quotient values for both types of cargos are well below the critical derailment ratio, which suggests negligible effect of liquid slosh on the flange climb potential during the switch-passing maneuver. A few studies have also reported negligible effects of liquid slosh on vehicle responses during curving [94, 131]. The fluid slosh, however, yields high magnitude oscillations in the *Y/Q* ratio, as observed in the car body roll and unloading ratio responses in Figures 5.6 and 5.9, respectively. The sharp peaks in the *Y/Q* ratio responses, occurring near t=2.4 s and t=5.2 s, correspond to the instants of curvature changes of the switch maneuver.

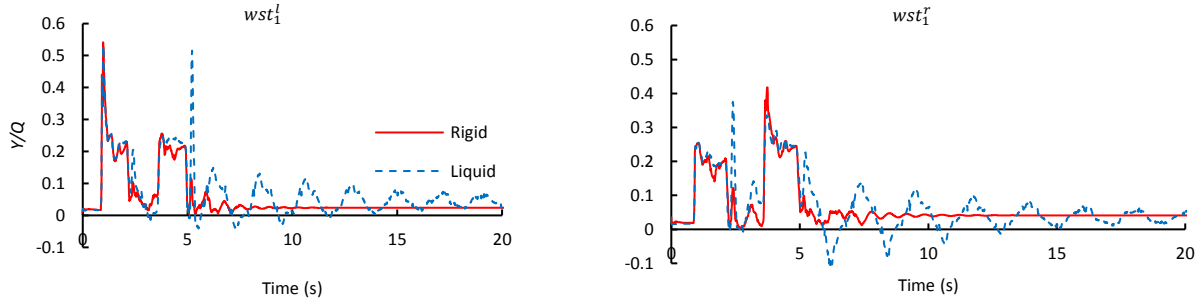

(a) (b)

Figure 5.10: The derailment ratio responses of wheels of the leading wheelset of the car with 60%-filled liquid and equivalent rigid cargos while passing the 300-1/11 switch at the speed of 20 *m/s*: (a) wst_1^l; and (b) wst_1^r.

The effect of liquid slosh on the derailment potential of the partly-filled liquid cargo car is also evaluated using an alternative approach based on the Weinstock ratio [38], which is considered as a less conservative wheel flange climb criterion. The criterion predicts onset of derailment by summing the absolute values of *Y/Q* of the two wheels of the same wheelset. While the *Y/Q* ratio of the flanging wheel is evaluated using the Nadal's equation, the ratio for the non-flanging wheel is described by the friction coefficient between the wheel tread and the rail crown regions with a relatively low contact angle, ranging from 0 to 3°. It has been suggested that the Weinstock criterion based on the summation of the *Y/Q* ratios of the wheelset and the coefficient of friction on the non-flanging wheel tread region (μ_t) can provide a more accurate indication of the impending derailment for small or negative angles of attack. The Weinstock criterion is given as [38]:

$$Weinstock\ creterion = \frac{\left|\frac{Y}{Q}\right|_l + \left|\frac{Y}{Q}\right|_r}{\frac{\tan\beta - \mu}{1 + \mu tan\beta} + \mu_t} < 1 \tag{5.16}$$

The contact angle, β, is the angle between the wheel rail normal force and the track normal plane. Subscripts 'l' and 'r' in the above relation denote left- and right-side wheels, respectively. The Weinstock ratio exceeding 1 has been associated with the onset of the possible flange climb.

Figure 5.11 illustrates variations in the Weinstock ratio computed for critical wheels of the 60%-filled tank car passing the 300-1/11 switch geometry at the constant forward speed of the 17 *m/s*. The results, presented for both the liquid and equivalent rigid cargos, suggest that the Weinstock ratios approach or exceed the critical value for both types of cargos. The Weinstock ratio peaks for the rigid cargo car are slightly higher than those for the liquid cargo. The results in terms of Weinstock ratio confirm that the liquid cargo sloshing does not have a significant role in view of potential flange climb during a switch-passing maneuver.

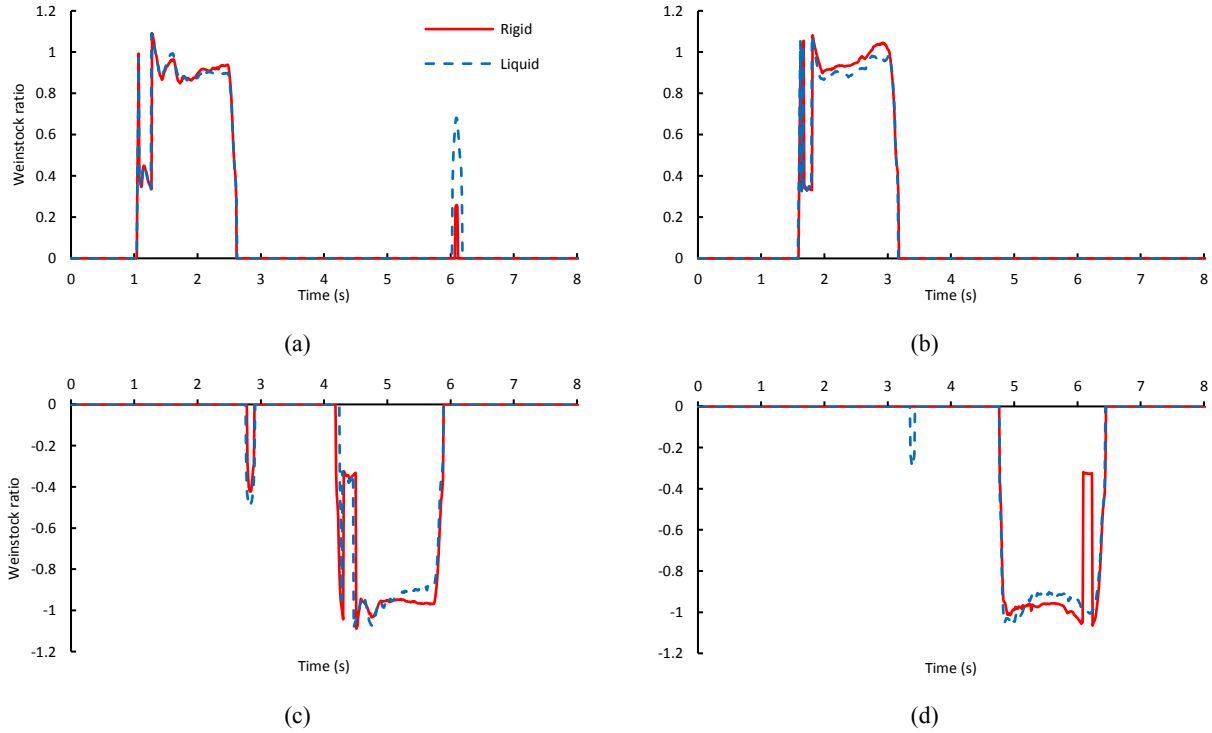

Figure 5.11: Comparisons of Weinstock ratios of different wheelsets of the 60% filled tank car while passing a switch at 17 *m/s* forward speed, (a) wst_1^l, (b) wst_3^l, (c) wst_1^r, (d) wst_3^r.

5.4.3 Critical switch negotiation speeds

The results presented in Figures 5.6 and 5.9 show significant effects of liquid slosh on the roll dynamic and lateral load shift (unloading ratio) characteristics of the car during the switch-passing maneuver. The peak roll angle and unloading ratio responses, however, are strongly related to geometry of the switch and forward speed apart from the liquid cargo fill ratio. Simulations are performed to identify the critical forward speeds while negotiating a switch. The studies reporting dynamics of partly filled road tankers have shown significant effects of liquid cargo movements on the roll stability limits and overturning of the vehicle [7, 98, 126]. The rollover potential of a road vehicle during path change maneuver is generally assessed in terms of lateral load transfer ratio (*LTR*). The *LTR* ratio describes the magnitude of load transfer occurring laterally from inside to the outside tires of the vehicle that may be considered to represent the unloading ratio of a railway car during a switch-passing maneuver. Critical speed while passing a switch is defined as the speed when absolute value of the peak unloading ratio approaches the critical value of 0.8. The critical speeds are evaluated for different fill ratios, ranging from 40 to 97%, and two different switch geometries, namely, 300-1/11 and 200-1/9. The 1/9 switch represents a relatively more severe geometry and would yield higher lateral acceleration excitation to the liquid cargo. Simulations for each fill condition and switch geometry are performed under increasing values of constant forward speed until the critical speed at which peak unloading ratio approaches 0.8.

Figure 5.12 presents critical speeds of the liquid cargo tank car with fill ratio ranging from 40 to 97%, while negotiating the two different switches. The figure also presents the critical speeds obtained for the car with equivalent rigid cargo in the same fill ratio range. The results show opposing trends in critical speeds of the car with increasing fill ratios of the liquid and equivalent rigid cargos. Moreover, the results obtained for both the switch geometries show comparable trends, although the critical speeds obtained for 1/9 switch are considerably lower than those for the 1/11 switch geometry, as it would be expected. For the rigid cargo car subject to both switch geometries, the critical speed increases with decreasing fill ratio due to the resulting lower *c.g.* height. The critical speed obtained for the liquid cargo tank car, however, decreases with decreasing fill ratio despite the lower *c.g.* height of the tank car. This tendency is attributed to higher lateral load shift, lateral force and roll moment caused by enhanced movement of the free surface under lower fill ratios. Such an opposing tendency in the liquid and equivalent rigid cargo vehicles has also been reported in curving responses of tank car [131], and rollover threshold lateral acceleration

responses of the road tankers [98]. Moreover, the critical switch-passing speeds for the liquid cargo car are substantially lower than those of the rigid cargo car, especially for lower fill ratios, irrespective of the considered switch geometry.

For fill ratios exceeding 90%, the critical unloading ratio and thereby the critical switch-passing speed of the liquid cargo car approaches that of the equivalent rigid cargo car. These are obtained as about 19 and 17.75 *m/s*, respectively, for the 1/11 and 1/9 switch geometries. For the partly-filled liquid cargo car, the unloading ratio response is affected by both the cargo *c.g.* height and the cargo movement or the roll moment in an opposing manner. The results suggest a dominant contribution of the *c.g.* height under higher fills (above 80%) and that of the roll moment under lower fill ratios (below 60%). The results also suggest that neglecting the liquid slosh effect in the 40%-filled tank car could yield overestimation of the critical switch-passing speed by nearly 13% and 23% for the 1/11 and 1/9 switch geometries, respectively.

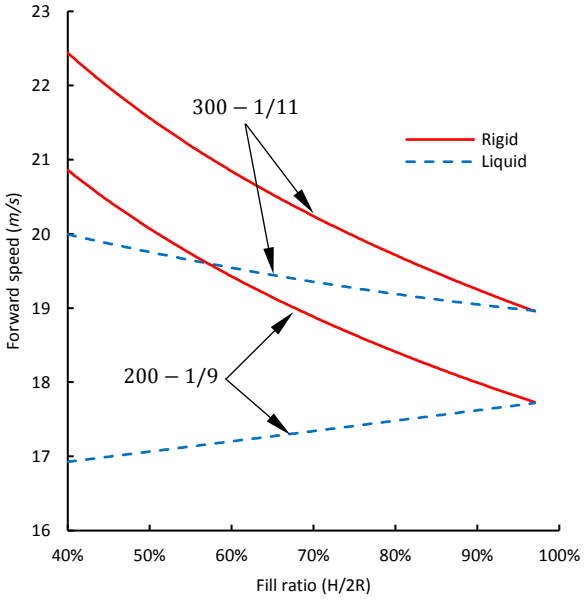

Figure 5.12: Comparisons of critical speeds of the tank car with rigid and liquid cargos in the 40 to 97% fill range, while negotiating two different switch geometries (300-1/11 and 200-1/9).

5.5 Conclusions

The co-simulation of liquid cargo with a multibody dynamic model of a partly filled railway tank car was used to evaluate dynamic response of the coupled system subject to the switch negotiation. It is shown that the linear slosh model involving summation of first four antisymmetric natural modes can provide accurate estimations of the slosh force and roll moment under lateral acceleration excitation encountered during a switch-passing maneuver. Compared to nonlinear computational fluid dynamic (*CFD*) methods, the linear slosh model can be conveniently integrated to the railway car model to perform analyses of the coupled system in a highly efficient manner. The results obtained for the coupled vehicle and liquid slosh model clearly showed strong interactions between the switch-induced transient liquid slosh and vehicle dynamics for partial-fill conditions. The dynamic liquid slosh force and roll moment contributed to notably higher roll angle response of car body and lateral load transfer, especially under the lower fill ratio of 60%. The unloading ratio could approach critical value in the presence of fluid slosh, especially when the fill ratio occurs in the 50-60% range. The lateral force and roll angle responses showed dominant oscillations near the fundamental slosh frequency. The effect of fluid slosh on the car body roll angle and wheelset unloading ratio was observed to diminish with fill ratio above 90%, despite the higher *c.g.*, which was attributed to reduced free surface length under higher fill ratio. The results of the study revealed nearly negligible effect of the fluid slosh on the derailment or flange climb potential during a switch-passing maneuver.

CHAPTER 6

Conclusions and recommendations

The safety concerns related to liquid cargo slosh in road tanker vehicles are widely accepted, yet there has been only a handful of comprehensive study due to complexities and computational demand associated with co-simulation of numerical fluid slosh and vehicle models. For railway tanker vehicles, on the other hand, the possibility of safety hazard from sloshing of liquid cargo and associated forces are relatively new concern stemmed from several catastrophic derailments and tanker spills of dangerous liquid cargo reported in recent years. There has been very limited and simplified preliminary studies that attempt to investigate the effects of liquid cargo slosh in a railway tanker cars. This dissertation research presents a comprehensive method for incorporating the dynamic effect of liquid cargo movements in dynamic analysis of railway tank cars. The developed coupled vehicle/cargo dynamic model incorporates the nonlinearities of the vehicle system and force response of liquid sloshing for different fill conditions. The study examines the effects of liquid slosh on the lateral stability characteristics and the associated critical hunting speed. Further simulations investigate crucial roll response and derailment potentials of the partially filled tank cars subject to curving and track-switch manoeuvers. The significant aspects of the dissertation research and the contributions are highlighted in this section. The following sections outline the major conclusions drawn from this investigation and a list of recommendation for further studies.

6.1 Major contributions and highlights of the dissertation research

- A comprehensive model of a typical freight wagon, which incorporates detail nonlinear characteristics of the secondary suspension system, was developed systematically.
- Highly nonlinear suspension damping properties due to friction wedges used in three-piece bogies were modelled based on points-plane contact method to facilitate parametric study. In comparison to reported methodologies, the proposed method for characterizing the damping properties of the suspension was presented to be highly effective and more importantly, computationally efficient.
- An analytical liquid slosh model based on multimodal approach was formulated and validated to be used for different excitations appropriate for hunting, curving, and switch passing of a typical railway tank car.

- A simplified method to incorporate the effects of liquid sloshing subject to yaw excitation of the tank was developed and validated. The model was essential for meaningful investigation of slosh effect on rail tanker dynamics.
- A method for identification of roll moment of inertia of liquid cargo for different fill ratios was presented for circular cross section tank. The roll moment of inertia of liquid cargo was observed to be lower than equivalent rigid cargo.
- The detailed MBD model of tank car was co-simulated with liquid cargo model to perform different dynamic simulations in a time-efficient manner.
- The effects of liquid cargo sloshing on wheel-rail lateral and vertical forces, the roll angle of car body and different dynamic safety measures are investigated and compared with those predicted for equivalent rigid cargo, as well as simplified pendulum slosh mode.
- The critical speeds of partly filled tank car in terms of hunting, as well as performance limits for curving, and switch passing are identified for different fill conditions.

6.2 Major conclusions

The significant findings and conclusions drawn from the studies are summarized below:

- The MBD simulation of the suspension system of three-piece bogie using proposed method revealed relatively lower damping levels in both the lateral and vertical directions for the unloaded wagon compared to the loaded wagon.
- For lateral stability, a subcritical *Hopf* bifurcation in the responses of the wagon was identified. The sensitivity analysis of the nonlinear system revealed strong dependency of the lateral stability characteristics of the system on both the forward speed and the track disturbance amplitude. Furthermore, at higher forward speeds, the lateral oscillation is observed to be at higher frequency and the magnitude of oscillation limited by the flange is also higher indicating partial wheel climb tendency.
- Among suspension parameters, an increase in the wedge angle yield substantial gain in the critical speed, while increasing the friction coefficient of the contact surfaces resulted in an only marginal increase in the critical speed. Increasing the surface friction, however, could cause more chaotic lateral oscillations of the system at higher speeds. Increasing the preload of the spring on the wedge could further help limit wheelset lateral oscillations leading to higher critical speeds.

- The critical hunting speed of partly loaded wagon was observed to be higher than an empty wagon. The trend was attributed to higher damping characteristics of the suspension system under different loading conditions.
- Linear fluid slosh model with four anti-symmetric natural mode shapes of a partially filled cargo was shown to be adequate for fill levels in the range of 40 to 97%. The approach was found to be accurate and highly computing efficient. The coupled dynamic model was realized by co-simulation of the linear slosh model and the nonlinear multi-body tank car model.
- A very good correlation was observed between the analytical liquid slosh model with reported values and alternative methods in terms of natural frequencies of natural modes of slosh and force response of the slosh model subject to excitations in railway application.
- The roll moment of inertia of the liquid cargo compare to rigid one is shown to be lower as the body can roll with respect to liquid cargo. This in turn effectively contribute as a damper and leads to higher critical hunting speed in high fill conditions of the tank. This effect was observed for fill ratio conditions higher than 80%.
- On the other hand, consideration of liquid cargo with proposed slosh model in partly filled conditions led to lower critical speed compared to the results obtained from frozen and pendulum approaches in moderately filled conditions. The liquid slosh response in partly filled condition tend to eliminate the damping effect of the cargo observed using simple pendulum approach.
- Furthermore, initiation of the yaw oscillations of car body introduced an additional slosh moment and led to lower critical speed in moderated fill conditions.
- The study revealed that for a typical curving maneuver, the fluid slosh effect of 60 to 70% fill level could lead to roll angles of the car body that is more than twice that of equivalent rigid cargo. The comparison of derailment quotient (*Y/Q* ratio) consistently show slightly higher value due to fluid slosh during curving. The magnitude was however significantly lower than critical for the considered geometry of curving manoeuvre.
- The results show that the track super-elevation in a curve tends to reduce the contributions of liquid cargo sloshing while the travelling speed of tank car is close to the balance speed of the curve.

- The curving performance of tank car in partially filled condition is evaluated in terms of unloading ratio, as well as lateral load transfer, derailment quotient and flange climb onset of wheelsets.
- For low to moderate fill levels, the sloshing of liquid cargo reduces the critical speed in view of curving performance. On a 600 *m*-radius curve, the critical speed of the 50% filled tank car can be overestimated by as much as 20% in the event sloshing is not considered.
- The transient liquid sloshing in a switch-passing manoeuvre led to the higher roll angle of car-body, track lateral load, and unloading ratio when compared to rigid cargo. The dynamic response of partly filled tank car, however, indicated that the liquid cargo sloshing did not have a significant effect in view of potential flange climb during a switch-passing manoeuvre. On the other hand, the initiation of free movements of liquid cargo in partly filled condition led to lightly damped lateral oscillation response in the tangent section of the switch.
- The dynamic liquid slosh force and roll moment contributed to notably higher roll angle response of car body and lateral load transfer, especially under the lower fill ratio of 60%. The unloading ratio could approach critical value in the presence of fluid slosh, mainly for the fill ratio in the 50-60% range. The lateral force and roll angle responses showed dominant oscillations near the fundamental slosh frequency.
- The effect of fluid slosh on the car body roll angle and wheelset unloading ratio were observed to diminish with fill ratio above 90%, which was attributed to reduced free surface length under higher fill ratio. The results of the study revealed nearly negligible effect of the liquid sloshing on the derailment or flange climb potential during a switch-passing manoeuvre.
- The critical switch passing speeds of partly filled tanks are identified for two deferent switch geometries and fill condition of liquid cargo from 40% to 97%. For 40% fill condition, the liquid slosh can yield critical speed that is 23% lower than that predicted for rigid cargo.

6.3 Recommendations for future studies

The proposed vehicle/liquid cargo dynamic model can serve as an effective tool for safety assessment and dynamic simulation of railway tank car. The liquid cargo model has been directly integrated to multi-body dynamic model of the railway tank car for coupled simulation. The idea could be extended to other MBD applications like road vehicles. Moreover, the detail model of the suspension system of the three-piece bogie considered in this investigation could also be applied for simulation of a defect in the system as well as improvement of the design. Owing to the high computation efficiency of the liquid model, it is feasible to apply the method for iterative simulations or optimization studies. Particular recommendations for future work may include the following:

- The proposed model of wedges contact could be applied to evaluate the effects of worn wedges and increased clearances, and for identifying optimal wedge design.
- The tuning of the properties of different components of suspension system of three-piece bogie is possible with applied modelling approach.
- The method is capable of simulating highly nonlinear characteristics of the system and can be extended to include other nonlinearities in the system.
- The analytical liquid sloshing model could be applied to different field of transportation like road or tracked vehicles.
- Owing to high computation efficiency of the coupled model, the iterative simulation like wear evolution in wheel and rail profiles are feasible. Moreover, higher lateral and normal load transfer, that stem from liquid sloshing, could lead to possible crack propagation in the different sections of the curve and switch sections of the track. The issue has not yet been addressed in the literature.
- The liquid cargo model could be extended to simulate longitudinal and three-dimensional liquid cargo sloshing. The model then could be coupled with MBD models to evaluate the dynamic response of the partly filled tank car subject to multi-directional time variable acceleration inputs.
- In longitudinal train dynamic analysis, the transient longitudinal liquid slosh could affect the coupling forces and stopping distance. The issue has not been yet investigated in the literature.

References

[1] *Transportation Safety Board of Canada (2014). Statistical Summery-Railway Occurrences.* 2014.

[2] *Rolling Stock: Locomotives and Rail Cars, United States International Trade Commission,*. 2011.

[3] Younesian D, Abedi M and Hazrati Ashtiani I, *Dynamic analysis of a partially filled tanker train travelling on a curved track.* International Journal of Heavy Vehicle Systems, 2010. 17(3): p. 331-358.

[4] Shabana AA, *Nadal's Formula and High Speed Rail Derailments.* Journal of Computational and Nonlinear Dynamics, 2012. 7(4): p. 041003.

[5] Shi H, Wang L, Nicolsen B, and Shabana AA, *Integration of geometry and analysis for the study of liquid sloshing in railroad vehicle dynamics.* Proceedings of the Institution of Mechanical Engineers, Part K: Journal of Multi-body Dynamics, 2017. 231(4): p. 608-629.

[6] Kolaei A, Rakheja S and Richard MJ, *A coupled multimodal and boundary-element method for analysis of anti-slosh effectiveness of partial baffles in a partly-filled container.* Computers & Fluids, 2015. 107: p. 43-58.

[7] Ranganathan R, Rakheja S and Sankar S, *Directional response of a B-train vehicle combination carrying liquid cargo.* Journal of dynamic systems, measurement, and control, 1993. 115(1): p. 133-139.

[8] Rakheja S and Ranganathan R, *Estimation of the rollover threshold of heavy vehicles carrying liquid cargo: a simplified approach.* International Journal of Heavy Vehicle Systems, 1993. 1(1): p. 79-98.

[9] Shabana AA, Zaazaa KE and Sugiyama H, *Railroad vehicle dynamics: A computational approach*. 2010: CRC Press.

[10] Garg VK and Dukkipati RV, *Dynamics of railway vehicle systems*. 1984: Academic Press, New York.

[11] True H, *A method to investigate the nonlinear oscillations of a railway vehicle*, in *Applied Mechanics Rail Transportation Symposium*. 1988.

[12] Polach O, *Comparability of the non-linear and linearized stability assessment during railway vehicle design.* Vehicle System Dynamics, 2006. 44(sup1): p. 129-138.

[13] *49CFR238, (2003). FRA regulations, Title 49: Transportation, Part 238 – Passenger Equipment Safety Standards, Revised 1 October 2003. Federal Railroad Administration*.

[14] *UIC Code 518, Testing and approval of railway vehicles from the point of view of their dynamic behaviour – safety – track fatigue – ride quality*. 2003: Paris.

[15] *BS EN 14 363. Railway applications – testing for the acceptance of running characteristics of railway vehicles – testing of running behaviour and stationary tests*. 2005, CEN: Brussels.

[16] *UIC519: Method for determining the equivalent conicity*. 2004, International Union of Railways: Paris.

[17] Wrang M, Li M, Sundvall P, and Jahlenius Å, *Assessing wheel-rail contact conditions based on in-service values of equivalent conicity and radial steering index*, in *IAVSD Symposium*. 2009: Stockholm.

[18] Huilgol R, *Hopf-Friedrichs Bifurcation and Hunting of a Railway Axle.* Quarterly of Applied Mathematics, 1978. 36(1): p. 85-94.

[19] True H, *Some Recent Developments in Nonlinear Railway Vehicle Dynamics.* Mathematical Research, 1993. 72: p. 129-130.

[20] Polach O, *On Non-Linear Methods of Bogie Stability Assessment Using Computer Simulations.* Proceedings of the Institution of Mechanical Engineers, Part F: Journal Of Rail And Rapid Transit, 2006. 220(1): p. 13-27.
[21] Yang S and Chen E, *The Hopf Bifurcation in a Railway Bogie with Hysteretic Nonlinearity.* Journal of the China Railway Society, 1993. 15(4).
[22] Wickens A, *Comparative Stability of Bogie Vehicles With Passive and Active Guidance as Influenced by Friction and Traction.* Vehicle System Dynamics, 2009. 47(9): p. 1137-1146.
[23] Wu Q, Cole C, Spiryagin M, and Sun YQ, *A review of dynamics modelling of friction wedge suspensions.* Vehicle System Dynamics, 2014. 52(11): p. 1389-1415.
[24] Gardner JF and Cusumano JP. *Dynamic models of friction wedge dampers*. in *Railroad Conference, 1997., Proceedings of the 1997 IEEE/ASME Joint*. 1997. IEEE.
[25] Hazrati Ashtiani I, Rakheja S, Ahmed AKW, and Zhang J, *Hunting analysis of a partially-filled railway tank car*, in *2015 Joint Rail Conference*. 2015, American Society of Mechanical Engineers: San Jose, CA. p. V001T10A003-V001T10A003.
[26] Orlova A and Romen Y, *Refining the wedge friction damper of three-piece freight bogies.* Vehicle System Dynamics, 2008. 46(S1): p. 445-455.
[27] Iwnicki S, Stichel S, Orlova A, and Hecht M, *Dynamics of railway freight vehicles.* Vehicle system dynamics, 2015. 53(7): p. 995-1033.
[28] Hazrati Ashtiani I, *Optimization of secondary suspension of three-piece bogie with bevelled friction wedge geometry.* International Journal of Rail Transportation, 2017. 5(4): p. 213-228.
[29] Harder RF. *Dynamic modeling and simulation of three-piece freight vehicle suspensions with nonlinear frictional behaviour using adams/rail*. in *IEEE/ASME Joint Rail Conference*. 2001. IEEE.
[30] Klauser PE. *Modeling Friction Wedges: Part II—An Improved Model*. in *ASME International Mechanical Engineering Congress and Exposition*. 2004.
[31] Xia F, *Modelling of a Two-Dimensional Coulomb Friction Oscillator.* Journal of Sound and Vibration, 2003. 265(5): p. 1063-1074.
[32] Kaiser AB, Cusumano J and Gardner J, *Modeling and dynamics of friction wedge dampers in railroad freight trucks.* Vehicle System Dynamics, 2002. 38(1): p. 55-82.
[33] Steets J, Chan B and Sandu C. *A multibody dynamics approach to friction wedge modeling for freight train suspensions*. in *ASME/IEEE 2007 Joint Rail Conference and Internal Combustion Engine Division Spring Technical Conference*. 2007. American Society of Mechanical Engineers.
[34] Hazrati Ashtiani I, Ahmed AKW, Rakheja S, and Zhang J, *Hunting characteristics of a freight car in presence of secondary suspension non-smooth contact dynamics*, in *IMECE2014*. 2014, ASME: Montreal, Canada.
[35] Hazrati Ashtiani I, Rakheja S and Ahmed AKW, *Influence of friction wedge characteristics on lateral response and hunting of freight wagons with three-piece bogies.* Proceedings of the Institution of Mechanical Engineers, Part F: Journal of Rail and Rapid Transit, 2016. 231(8): p. 877-891.
[36] Shabana AA, Tobaa M, Sugiyama H, and Zaazaa KE, *On the computer formulations of the wheel/rail contact problem.* Nonlinear Dynamics, 2005. 40(2): p. 169-193.
[37] Shabana AA, Zaazaa KE, Escalona JL, and Sany JR, *Development of elastic force model for wheel/rail contact problems.* Journal of sound and vibration, 2004. 269(1-2): p. 295-325.
[38] Iwnicki S, *Handbook of railway vehicle dynamics*. 2006: CRC press.

[39] Sugiyama H and Suda Y, *On the contact search algorithms for wheel/rail contact problems.* Journal of Computational and Nonlinear Dynamics, 2009. 4(4): p. 041001.
[40] Vollebregt E, Iwnicki S, Xie G, and Shackleton P, *Assessing the accuracy of different simplified frictional rolling contact algorithms.* Vehicle System Dynamics, 2012. 50(1): p. 1-17.
[41] Sugiyama H, Araki K and Suda Y, *On-line and off-line wheel/rail contact algorithm in the analysis of multibody railroad vehicle systems.* Journal of mechanical science and technology, 2009. 23(4): p. 991-996.
[42] Carter F. *On the action of a locomotive driving wheel*. in *Proc. R. Soc. Lond. A*. 1926. The Royal Society.
[43] Alonso A and Giménez J, *Tangential problem solution for non-elliptical contact areas with the FastSim algorithm.* Vehicle System Dynamics, 2007. 45(4): p. 341-357.
[44] Vermeulen P and Johnson K, *Contact of nonspherical elastic bodies transmitting tangential forces.* Journal of Applied Mechanics, 1964. 31: p. 338.
[45] Kalker JJ, *Three-dimensional elastic bodies in rolling contact*. Vol. 2. 2013: Springer Science & Business Media.
[46] Giménez J, Alonso A and Gómez* E, *Introduction of a friction coefficient dependent on the slip in the FastSim algorithm.* Vehicle System Dynamics, 2005. 43(4): p. 233-244.
[47] Piotrowski J and Kik W, *A simplified model of wheel/rail contact mechanics for non-Hertzian problems and its application in rail vehicle dynamic simulations*. Vehicle System Dynamics, 2008. 46(1-2): p. 27-48.
[48] Shen Z and Li Z, *A fast non-steady state creep force model based on the simplified theory.* Wear, 1996. 191(1-2): p. 242-244.
[49] Alonso A and Giménez J, *Non-steady state modelling of wheel-rail contact problem for the dynamic simulation of railway vehicles.* Vehicle System Dynamics, 2008. 46(3): p. 179-196.
[50] True H and Kaas-Petersen C, *A bifurcation analysis of nonlinear oscillations in railway vehicles.* Vehicle System Dynamics, 1983. 12(1-3): p. 5-6.
[51] Spinola Barbosa R, *A 3D contact force safety criterion for flange climb derailment of a railway wheel.* Vehicle System Dynamics, 2004. 42(5): p. 289-300.
[52] Wilson N, Fries R, Witte M, Haigermoser A, Wrang M, Evans J, and Orlova A, *Assessment of safety against derailment using simulations and vehicle acceptance tests: a worldwide comparison of state-of-the-art assessment methods.* Vehicle System Dynamics, 2011. 49(7): p. 1113-1157.
[53] Cheng Y-C and Hsu C-T, *Hunting stability and derailment analysis of a car model of a railway vehicle system.* Proceedings of the Institution of Mechanical Engineers, Part F: Journal of Rail and Rapid Transit, 2012. 226(2): p. 187-202.
[54] Jun X and Qingyuan Z, *A study on mechanical mechanism of train derailment and preventive measures for derailment.* Vehicle System Dynamics, 2005. 43(2): p. 121-147.
[55] Xiang J, Zeng Q and Lou P, *Transverse vibration of train-bridge and train-track time varying system and the theory of random energy analysis for train derailment.* Vehicle System Dynamics, 2004. 41(2): p. 129-155.
[56] Blader F, *A review of literature and methodologies in the study of derailments caused by excessive forces at the wheel/rail interface*. 1990: Association of American Railroads, Research & Test Department.

[57] ČSN E, *14363: 2006 Railway applications – Testing for the acceptance of running characteristics of railway vehicles – Testing of running behaviour and stationary tests*, in *Czech Institute for Normalisation* 2006.
[58] *AAR Mechanical Division M1001 AAR manual of standards and recommended practices*, in *Section C-Part II*. 1993.
[59] Braghin F, Bruni S and Diana G, *Experimental and numerical investigation on the derailment of a railway wheelset with solid axle.* Vehicle System Dynamics, 2006. 44(4): p. 305-325.
[60] Bauer HF, *On the Destabilizing Effect of Liquids in Various Vehicles (part 1).* Vehicle system dynamics, 1972. 1(3-4): p. 227-260.
[61] Zhao W, Yang J and Hu Z, *Effects of sloshing on the global motion responses of FLNG.* Ships and Offshore Structures, 2013. 8(2): p. 111-122.
[62] Kim Y, Nam B, Kim D, and Kim Y, *Study on coupling effects of ship motion and sloshing.* Ocean Engineering, 2007. 34(16): p. 2176-2187.
[63] D'Alenssandro V. 2012. *Modeling of tank vehicle dynamics by fluid sloshing coupled simulation.* Italy.
[64] Kolaei A, Rakheja S and Richard MJ, *Range of applicability of the linear fluid slosh theory for predicting transient lateral slosh and roll stability of tank vehicles.* Journal of Sound and Vibration, 2014. 333(1): p. 263-282.
[65] Ibrahim RA, *Liquid sloshing dynamics: theory and applications*. 2005: Cambridge University Press.
[66] Rakheja S, Sankar S and Ranganathan R, *Roll plane analysis of articulated tank vehicles during steady turning.* Vehicle System Dynamics, 1988. 17(1-2): p. 81-104.
[67] Ibrahim RA, Pilipchuk V and Ikeda T, *Recent advances in liquid sloshing dynamics.* Applied Mechanics Reviews, 2001. 54(2): p. 133-199.
[68] Popov G, Sankar S and Sankar T, *Shape optimization of elliptical road containers due to liquid load in steady-state turning.* Vehicle system dynamics, 1996. 25(3): p. 203-221.
[69] Zhanqi W, Rakheja S and Cunzhen S, *Influence of partition location on the braking performance of a partially-filled tank truck*. 1995, SAE Technical Paper.
[70] Kang X. 2001. *Optimal tank design and directional dynamic analysis of liquid cargo vehicles under steering and braking.* Concordia University.
[71] Modaressi-Tehrani K, Rakheja S and Sedaghati R, *Analysis of the overturning moment caused by transient liquid slosh inside a partly filled moving tank.* Proceedings of the Institution of Mechanical Engineers, Part D: Journal of Automobile Engineering, 2006. 220(3): p. 289-301.
[72] Yan G, Rakheja S and Siddiqui K, *Analysis of transient fluid slosh in partly-filled tanks with and without baffles: Part 1–model validation.* International Journal of Heavy Vehicle Systems, 2010. 17(3): p. 359-379.
[73] Romero J, Ramírez O, Fortanell J, Martínez M, and Lozano A, *Analysis of lateral sloshing forces within road containers with high fill levels.* Proceedings of the Institution of Mechanical Engineers, Part D: Journal of Automobile Engineering, 2006. 220(3): p. 303-312.
[74] Dodge F, *The new" Dynamic Behavior of Liquids in Moving Containers," 2000.* Southwest Research Institute, San Antonio, TX.
[75] McCarty JL and Stephens DG, *Investigation of the natural frequencies of fluids in spherical and cylindrical tanks*. 1960: National Aeronautics and Space Administration.

[76] Hasheminejad SM and Mohammadi M, *Effect of anti-slosh baffles on free liquid oscillations in partially filled horizontal circular tanks.* Ocean Engineering, 2011. 38(1): p. 49-62.
[77] Hasheminejad SM and Aghabeigi M, *Liquid sloshing in half-full horizontal elliptical tanks.* Journal of sound and vibration, 2009. 324(1): p. 332-349.
[78] Faltinsen OM and Timokha AN, *A multimodal method for liquid sloshing in a two-dimensional circular tank.* Journal of Fluid Mechanics, 2010. 665: p. 457-479.
[79] Zang Y, Xue S and Kurita S, *A boundary element method and spectral analysis model for small‐amplitude viscous fluid sloshing in couple with structural vibrations.* International journal for numerical methods in fluids, 2000. 32(1): p. 69-83.
[80] Firouz‐Abadi R, Haddadpour H, Noorian M, and Ghasemi M, *A 3D BEM model for liquid sloshing in baffled tanks.* International journal for numerical methods in engineering, 2008. 76(9): p. 1419-1433.
[81] Rebouillat S and Liksonov D, *Fluid–structure interaction in partially filled liquid containers: a comparative review of numerical approaches.* Computers & Fluids, 2010. 39(5): p. 739-746.
[82] Fleissner F, Lehnart A and Eberhard P, *Dynamic simulation of sloshing fluid and granular cargo in transport vehicles.* Vehicle System Dynamics, 2010. 48(1): p. 3-15.
[83] Popov G, Sankar S, Sankar T, and Vatistas G, *Dynamics of liquid sloshing in horizontal cylindrical road containers.* Proceedings of the Institution of Mechanical Engineers, Part C: Journal of Mechanical Engineering Science, 1993. 207(6): p. 399-406.
[84] Modaressi-Tehrani K, Rakheja S and Stiharu I, *Three-dimensional analysis of transient slosh within a partly-filled tank equipped with baffles.* Vehicle System Dynamics, 2007. 45(6): p. 525-548.
[85] Ranganathan R, Ying Y and Miles J, *Analysis of fluid slosh in partially filled tanks and their impact on the directional response of tank vehicles.* 1993.
[86] Ranganathan R, Ying Y and Miles J, *Development of a mechanical analogy model to predict the dynamic behavior of liquids in partially filled tank vehicles*. 1994, SAE Technical Paper.
[87] Salem M, Mucino V, Saunders E, and Gautam M, *Lateral sloshing in partially filled elliptical tanker trucks using a trammel pendulum.* International Journal of Heavy Vehicle Systems, 2009. 16(1): p. 207-224.
[88] Abramson HN, *The dynamic behavior of liquids in moving containers. NASA SP-106.* NASA Special Publication, 1966. 106.
[89] Roberts JR and Chen P-Y, *Slosh design handbook I.* Vol. 406. 1966: National Aeronautics and Space Administration.
[90] Budiansky B, *Sloshing of liquids in circular canals and spherical tanks*. 1958, DTIC Document.
[91] Khandelwal R and Nigam N, *Digital simulation of the dynamic response of a vehicle carrying liquid cargo on a random uneven surface.* Vehicle System Dynamics, 1982. 11(4): p. 195-214.
[92] Bogomaz G, Markova O and Chernomashentseva YG, *Mathematical modelling of vibrations and loading of railway tanks taking into account the liquid cargo mobility.* Vehicle System Dynamics, 1998. 30(3-4): p. 285-294.
[93] Ranganathan R, Rakheja S and Sankar S, *Influence of liquid load shift on the dynamic response of articulated tank vehicles.* Vehicle System Dynamics, 1990. 19(4): p. 177-200.
[94] Di Gialleonardo E, Premoli A, Gallazzi S, and Bruni S, *Sloshing effects and running safety in railway freight vehicles.* Vehicle System Dynamics, 2013. 51(10): p. 1640-1654.

[95] Vera C, Paulin J, Suarez B, and Gutiérrez M, *Simulation of freight trains equipped with partially filled tank containers and related resonance phenomenon.* Proceedings of the Institution of Mechanical Engineers, Part F: Journal of Rail and Rapid Transit, 2005. 219(4): p. 245-259.
[96] Hazrati Ashtiani I, Rakheja S and Ahmed AKW, *Hunting and derailment analyses of a partly-filled railway tanker*, in *International Heavy Haul Association Conference*. 2015: Pert, Australia.
[97] Yan G, Siddiqui K, Rakheja S, and Modaressi K, *Transient fluid slosh and its effect on the rollover-threshold analysis of partially filled conical and circular tank trucks.* International journal of heavy vehicle systems, 2005. 12(4): p. 323-343.
[98] Kolaei A, Rakheja S and Richard MJ, *Effects of tank cross-section on dynamic fluid slosh loads and roll stability of a partly-filled tank truck.* European Journal of Mechanics-B/Fluids, 2014. 46: p. 46-58.
[99] Kolaei A, Hazrati Ashtiani I, Abedi M, and Rakheja S, *Application of linear slosh theory on stability of the B-train combination*, in *24th International Symposium on Dynamics of Vehicles on Roads and Tracks (IAVSD 2015)*. 2015: Graz, Austria.
[100] Wu X and Chi M, *Parameters study of Hopf bifurcation in railway vehicle system.* Journal of Computational and Nonlinear Dynamics, 2015. 10(3): p. 031012.
[101] Ahmadian M and Yang S, *Hopf bifurcation and hunting behavior in a rail wheelset with flange contact.* Nonlinear Dynamics, 1998. 15(1): p. 15-30.
[102] Chengrong H and Feisheng Z, *The numerical bifurcation method of nonlinear lateral stability analysis of a locomotive.* Vehicle System Dynamics, 1994. 23(S1): p. 234-245.
[103] True H, Engsig-Karup AP and Bigoni D, *On the numerical and computational aspects of non-smoothnesses that occur in railway vehicle dynamics.* Mathematics and Computers in Simulation, 2014. 95: p. 78-97.
[104] Kalker J, *A fast algorithm for the simplified theory of rolling contact.* Vehicle System Dynamics, 1982. 11(1): p. 1-13.
[105] Gao X-j, True H and Li Y-h, *Lateral dynamic features of a railway vehicle.* Proceedings of the Institution of Mechanical Engineers, Part F: Journal of Rail and Rapid Transit, 2015.
[106] Molatefi H, Hecht M and Kadivar M, *Effect of suspension system in the lateral stability of railway freight trucks.* Proceedings of the Institution of Mechanical Engineers, Part F: Journal of Rail and Rapid Transit, 2007. 221(3): p. 399-407.
[107] Molatefi H, Hecht M and Kadivar MH, *Critical Speed and Limit Cycles in The Empty Y25-Freight Wagon.* Proceedings of the Institution of Mechanical Engineers, Part F: Journal of Rail and Rapid Transit, 2006. 220(4): p. 347-359.
[108] Ballew BS. 2008. *Advanced Multibody Dynamics Modeling of the Freight Train Truck System.* Ph. D. thesis, Virginia Polytechnic Institute and State University.
[109] Xia F and True H, *The Dynamics of the Three-Piece-Freight Truck.* Vehicle System Dynamics, 2004. 41: p. 212-221.
[110] *UM 7.0, Universal Mechanism Software*. 2014.
[111] Ghazavi MR and Taki M, *Dynamic simulations of the freight three-piece bogie motion in curve.* Vehicle System Dynamics, 2008. 46(10): p. 955-973.
[112] Zhai W and Wang K, *Lateral hunting stability of railway vehicles running on elastic track structures.* Journal of Computational and Nonlinear Dynamics, 2010. 5(4): p. 041009.
[113] Sauvage G, *Determining the Characteristics of Helical Springs for Application in Suspensions of Railway Vehicles.* Vehicle System Dynamics, 1984. 13(1): p. 19-41.

[114] Pogorelov D, Simonov V, Kovalev R, Yazykov V, and Lysikov N. *Simulation of freight car dynamics: mathematical models, safety, wear*. in *The 2nd International Conference on Recent Advances in Railway Engineering. Tehran: Iran University of Science and Technology*. 2009.
[115] Sun YQ and Cole C, *Finite Element Modeling and Analysis of Friction-Wedge Dampers During Suspension Pitch Modes.* Journal of Vibration and Acoustics, 2008. 130(2): p. 021003.
[116] Sun YQ and Cole C, *Vertical dynamic behavior of three-piece bogie suspensions with two types of friction wedge.* Multibody System Dynamics, 2008. 19(4): p. 365-382.
[117] Park K, *An improved stiffly stable method for direct integration of nonlinear structural dynamic equations.* Journal of Applied Mechanics, 1975. 42(2): p. 464-470.
[118] Huang C, Zeng J and Liang S, *Carbody hunting investigation of a high speed passenger car.* Journal of Mechanical Science and Technology, 2013. 27(8): p. 2283-2292.
[119] Stichel S, *Limit cycle behaviour and chaotic motions of two-axle freight wagons with friction damping.* Multibody System Dynamics, 2002. 8(3): p. 243-255.
[120] Polach O and Kaiser I, *Comparison of methods analyzing bifurcation and hunting of complex rail vehicle models.* Journal of Computational and Nonlinear Dynamics, 2012. 7(4): p. 041005.
[121] True H, *Multiple attractors and critical parameters and how to find them numerically: the right, the wrong and the gambling way.* Vehicle System Dynamics, 2013. 51(3): p. 443-459.
[122] Kaas-Petersen C and True H, *Periodic, biperiodic and chaotic dynamical behaviour of railway vehicles.* Vehicle System Dynamics, 1986. 15(sup1): p. 208-221.
[123] Wang L, Octavio JRJ, Wei C, and Shabana AA, *Low order continuum-based liquid sloshing formulation for vehicle system dynamics.* Journal of Computational and Nonlinear Dynamics, 2015. 10(2): p. 021022.
[124] Kovalev R, Lysikov N, Mikheev G, Pogorelov D, Simonov V, Yazykov V, Zakharov S, Zharov I, Goryacheva I, and Soshenkov S, *Freight car models and their computer-aided dynamic analysis.* Multibody System Dynamics, 2009. 22(4): p. 399-423.
[125] Wu Q, Sun Y, Spiryagin M, and Cole C, *Methodology to optimize wedge suspensions of three-piece bogies of railway vehicles.* Journal of Vibration and Control, 2016: p. 1077546316645698.
[126] Faltinsen OM and Timokha AN, *Sloshing*. 2009: Cambridge University Press.
[127] Kolaei A. 2014. *Dynamic Liquid Slosh in Moving Containers.* PhD, Concordia University
[128] Hazrati Ashtiani I and Abedi M, *Effects of Liquid Cargo on Lateral Stability of B-Train Combination*. 2014, SAE International.
[129] Kolaei A, Rakheja S and Richard MJ, *Three-dimensional dynamic liquid slosh in partially-filled horizontal tanks subject to simultaneous longitudinal and lateral excitations.* European Journal of Mechanics-B/Fluids, 2015. 53: p. 251-263.
[130] McIver P, *Sloshing frequencies for cylindrical and spherical containers filled to an arbitrary depth.* Journal of Fluid Mechanics, 1989. 201: p. 243-257.
[131] Hazrati Ashtiani I, Rakheja S and Ahmed AKW, *Effects of coupled liquid cargo sloshing on roll response of partly filled railway tank cars.* Vehicle System Dynamics, 2018. Under review.

[132] Cairns M. *Crude oil by rail: parts I and II potential for the movement of Alberta oil sands crude oil and related products by Canadian railways*. in *Halifax, NS: Canadian Transportation Research Forum (CTRF)*. 2013.
[133] Liu X, Liu C and Hong Y, *Analysis of multiple tank car releases in train accidents.* Accident Analysis & Prevention, 2017. 107: p. 164-172.
[134] Elkins A, *Field guide to tank cars, third edition*. 2017, Association of American Railroads.
[135] *Transportation Safety Board of Canada, Runaway and Main-Track Derailment, Montreal, Maine & Atlantic Railway, Freight train MMA-002 Mile 0.23, Sherbrooke Subdivision LAC-Megantic, Quebec 06 July 2013, Railway Investigation Report R13D0054*.
[136] Communities SR, *Environmental risks of hazardous goods transported by rail.* 2015.
[137] *Railroads and chemicals.* 2017, Association of American Railroads.
[138] TP14877E TCS, *Containers for transport of dangerous goods by rail*. 2013.
[139] Ibrahim RA, *Road Tanker Dynamics Interacting with Liquid Sloshing Dynamics*, in *Recent Trends in Applied Nonlinear Mechanics and Physics*. 2018, Springer. p. 1-47.
[140] Blanco-Saura AE, Velarte-González JL, Ribes-Llario F, and Real-Herráiz JI, *Study of the dynamic vehicle-track interaction in a railway turnout.* Multibody System Dynamics, 2017: p. 1-16.
[141] Kassa E and Nielsen JC, *Dynamic interaction between train and railway turnout: full-scale field test and validation of simulation models.* Vehicle System Dynamics, 2008. 46(S1): p. 521-534.
[142] Skrypnyk R, Nielsen JC, Ekh M, and Pålsson BA, *Metamodelling of wheel–rail normal contact in railway crossings with elasto-plastic material behaviour.* Engineering with Computers, 2018: p. 1-17.
[143] Zhai W, Wang K and Cai C, *Fundamentals of vehicle–track coupled dynamics.* Vehicle System Dynamics, 2009. 47(11): p. 1349-1376.
[144] EN B, *Railway applications – track – switches and crossings – Part 9: layouts. BS EN 13232-9*. 2006.